Ink flow within the screen-printing process.

Fox, Ian James

University of Wales Swansea

Ink Flow Within The Screen-Printing Process

By

Ian James Fox B.Eng. (Hons.), M.Phil.

Thesis submitted to the University of Wales Swansea in fulfilment of the requirements for the degree of Doctor of Philosophy.

University of Wales Swansea

July 2002

Summary

Screen-printing is one of the oldest printing processes, yet its market share remains very limited due to its slower printing speeds compared to the other available processes. This is mainly because of the reciprocating motion of the squeegee upon the printing screen. In order for screen-printing to become more competitive, the concept of a high-speed continuous belt screen-printing press was developed. However, this will produce an increase in squeegee wear and friction of the squeegee upon the screen. For this reason, this work investigated the use of a roller squeegee that could rotate across the screen.

It has been proven that screen-printing with a roller squeegee can be successfully achieved. Additionally, in terms of density and tone gain, these images were comparable to those produced with traditional blade squeegees.

A numerical model has been developed to simulate the characteristics that will be encountered within the ink film when printing with a roller squeegee. Numerical simulations were run where the settings corresponded to the parameters utilised in experimental trials. Here, it was discovered that an increase in squeegee diameter will increase the ink film on the squeegee and will also increase the contact width of the screen upon the substrate. This will have the effect of increasing the pumping capacity of the squeegee, which will therefore increase the ink deposit. This was confirmed in the experimental trials.

It was also shown that the locking of the squeegee increased the shear mechanism within the ink film, resulting in a reduction in the ink viscosity within the nip contact region. This had the effect of reducing the ink film thickness on the squeegee, which reduces the pumping capacity of the squeegee, thus producing a reduced ink deposit.

Additionally, this work is the first method that has been able to estimate the height of the ink deposit for a range of halftone open areas where the results correspond almost identically to the actual printed heights of the prints obtained in experimental studies.

This work has improved the fundamental understanding of the mechanics and the process physics within the ink transfer mechanism in the screen-printing process. Use of experimental and numerical models has resulted in new theories being developed that will further the knowledge of the process.

This has led to the design and manufacture of a high-speed rotary screen-printing press that will enable high-speed, continuous screen-printing.

Declaration

This work has not previously been accepted in substance for any degree and is not being concurrently submitted in candidature for any degree.

*Signed*_____*(Candidate)*

Date: July, 2002.

Statement 1

This thesis is a result of my own investigations, except where otherwise stated. Other sources are acknowledged giving explicit references. A bibliography is appended at the end of the thesis.

*Signed*_____*(Candidate)*

Date: July, 2002.

Statement 2

I hereby give consent for my thesis, if accepted, to be available for photocopying and for inter-library loan, and for the title and the summary to be made available to outside organisations.

*Signed*_____*(Candidate)*

Date: July, 2002.

Acknowledgements

I would like to take this opportunity to thank all the people that have helped me throughout the period of this work. In particular I would like to show my appreciation to my supervisors, Prof. David Gethin and Dr. Tim Claypole for their help and guidance. I must also thank the other members of the Welsh Centre for Printing and Coating that have helped me through this work. Amongst others, two of these include Dr. Eifion Jewell for his knowledge of screen-printing, although I would like to point out to Eifion that the light at the end of the tunnel did not turn out to be an oncoming train, and Dr. Mark Bohan for his valuable computer programming knowledge.

In addition, I would like to thank the technicians from the workshop, in particular Steve Jones and Clive Francis for their valuable advice and characteristic abuse. I would also like to thank the industrial members of the high-speed belt screen-printing project that made this project possible, turning it from a conceptual sketch to a working printing-press. These include Brian Hardwick (AMTRI), Allen Bullock (AMTRI), Phil Sholl (AMTRI), Richard Hall (Timsons Ltd.) and John Jefferis (Timsons Ltd. *Retired*)

Finally, I would like to thank my family and friends for their friendship, help and ongoing support.

Thanks !

Contents

Chapter 5. Numerical Model Development and Investigation

Figures

Chapter 1. Introduction

Chapter 2. Literature Review

Chapter 3. Initial Experimental Study

Chapter 4. Secondary Experimental Study

Chapter 5. Numerical Model Development and Investigation

Chapter 6. High-Speed Belt Screen-Printing Press

Tables

Nomenclature

b_i	Body force within boundary domain
b_k	Body forces within boundary domain
B_h	Hertzian contact width
c_{lk}^{i}	Corner factor for the boundary integral equation
d	Mesh fibre diameter
E	Modulus of elasticity
$f(v)$	Ink flow velocity through screen
F_0	Integral in pressure equation
F_1	Integral in pressure equation
G	Shear modulus in Kelvin solution
h	Film thickness
h_0	Engagement of rollers at $x=0$
k	Viscosity constant
m	Dynamic viscosity
mr	Mesh ruling
MOA	Mesh open area
n	Viscosity index
n_{ij}	Direction cosine of the normal with respect to the x axis
p	Pressure
p_{ij}	Force component
$\overline{p_{ij}}$	Force constraints
p_k	Force intensity for the boundary integral equation
p_{lk}^{*}	Force component to the Kelvin solution
POA	Percentage of open area
r	Radius of stencil opening
r_i	Projection of point i
r_k	Projection of point k
R	Equivalent radius
t	Time n at point x
$u(x)$	Surface indentation

u_{ij} Displacement component

$\overline{u_{ij}}$ Displacement constraints

u_k Displacement for the boundary integral equation

u_{lk}^* Displacement component to the Kelvin solution

U_1 Squeegee rotational velocity

U_2 Press bed velocity

v Flow velocity through screen

$\bar{v}$ Mean flow velocity through screen

$v(z)$ Fluid velocity profile

α Dimensionless screen open area

β Actual open area within printing screen

δ_l^i Direc delta function

$\tilde{\delta}_{lk}$ Kronecker delta

ε_{ij} Strain field component

ϕ Permeability

Γ Boundary surface

$\dot{\gamma}$ Shear rate

η Viscosity

λ Lame's constant

$\hat{\lambda}$ Lame's constant

μ Apparent viscosity

ρ Density

σ Stress

σ_{ij} Stress field component

τ Shear stress

υ Poisson ratio

Ω Boundary domain

Chapter 1

Introduction

1 Introduction

In 1998, it was estimated that there were over 10,000 printing companies in the United Kingdom, with a total turnover in excess of £8.6 billion. The main market share of this industry can be divided into six volume printing processes. These are offset lithographic, rotogravure, screen-printing, flexographic, letterpress and digital, Figure 1.1 [1].

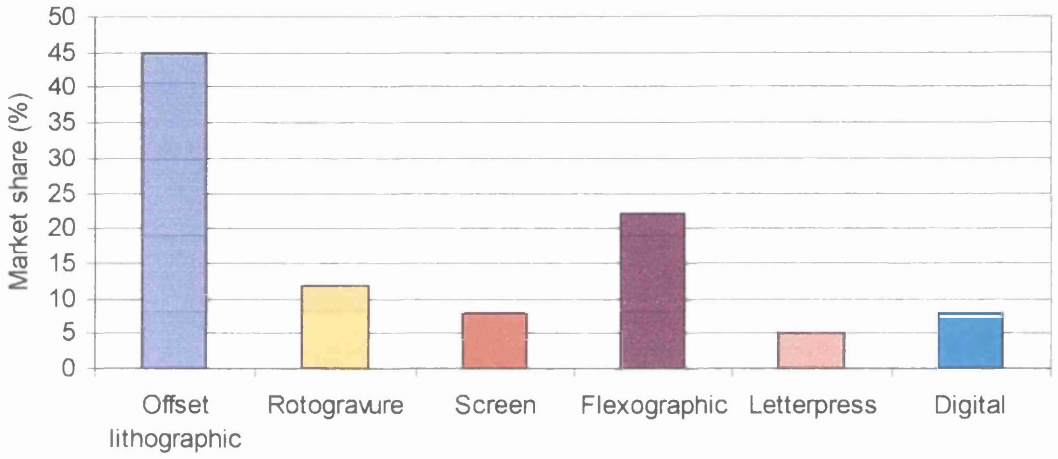

Figure 1.1 Market Share of the Six Main Printing Processes.

As shown, screen-printing only accounts for a small proportion of the printing market, despite the fact that it is one of the oldest printing processes. This is mainly due to the slower printing speeds and until recently, the lack of understanding of the impact of process parameters. Although screen-printing has its disadvantages, it also has many advantages making it the most versatile printing process. Screen-printing is the only process that is used to produce electronic circuits and sensors and can produce the largest colour gamut with ink deposits up to 300μm, where the other process are restricted to approximately 5μm. It is also capable of printing onto different substrates from textiles to glass. In order for screen-printing to become more competitive, the process needs to be developed and the printing speed needs to be increased to be more in-line with the other printing processes. This will also allow screen-printing to be integrated with the other print processes, making it a much more attractive process.

1.1 High Volume Rotational Printing Processes

Rotogravure, lithographic, flexographic and letterpress are all rotational printing systems and consequently print at much higher speeds than screen-printing. A schematic representation of each of these processes can be seen in Figure 1.2, where a brief description of each process is then given.

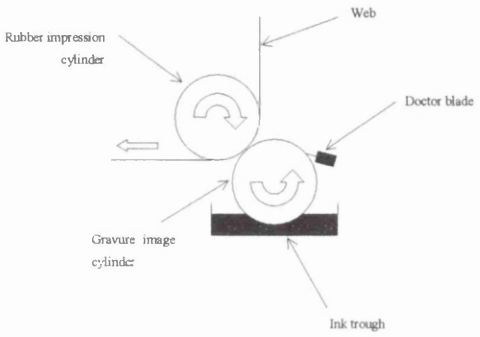

Rotogravure Station

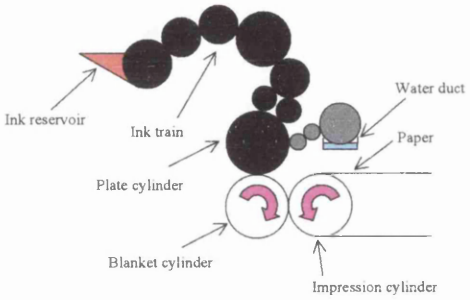

Lithographic Station

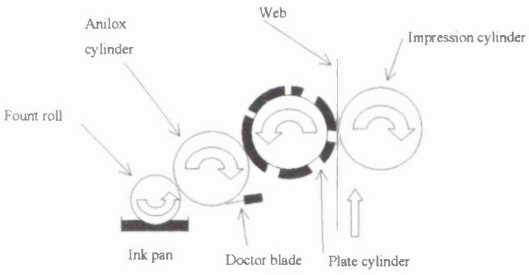

Flexographic Station

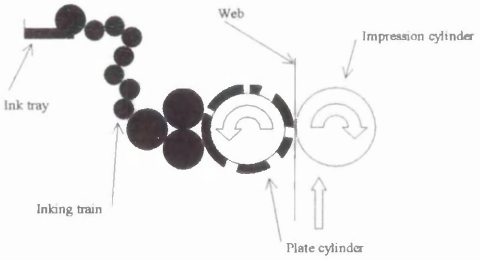

Letterpress Station

Figure 1.2 Schematic of Rotational Printing Stations

Rotogravure is the fastest of all of the printing processes and is capable of printing in excess of 1,000 metres per minute, producing prints of exceptionally high quality and accuracy. This makes it an ideal process to print long runs such as catalogues, magazines, wrapping paper, books, etc. The image is transferred to the substrate via a gravure cylinder that has a series of cells that are etched or engraved onto the cylinder surface to form the image area. These cells are filled with ink by rotating the cylinder in a trough, or by spraying the ink onto the cylinder surface. A rigid plastic or steel doctor blade is then used to remove the excess ink from the cylinder surface, leaving

only the ink in the cells. The ink is then transferred to the substrate by rotating the gravure cylinder against the substrate and the impression roller.

Lithographic or offset printing is a high speed, high resolution printing process mainly used for printing onto paper, card, plastics and for printing books and posters. The plate cylinder is designed to accept ink onto the image areas of the plate and to accept water onto the non-image areas of the plate. First of all the water is applied to the printing plate by a series of rollers and wets the hydrophilic regions. Ink is then applied to the plate and can only adhere to the hydrophobic regions due to the water on the non-image areas. The ink is then transferred to the substrate via the blanket cylinder [2].

Whereas rotogravure uses an engraved surface to hold the required ink, flexography works in the opposite way, where the ink is deposited on the raised sections of a flexographic printing plate. The plate cylinder is then brought into contact with the substrate where the ink is removed from the raised sections of the plate. Flexography is normally used for printing packaging or labelling products, printing at speeds of over 200 metres a minute.

Letterpress printing works in the same way as flexographic printing, except the printing plates are made of a much harder material. This means that higher printing pressures within the nip junction are needed, which result in poor quality halftones. This makes the process suitable for printing books, newspaper and labels.

Each of these processes is capable of printing at high speed from 200 metres a minute, up to 1000 metres a minute. A high-speed screen-printing press also needs to be capable of printing at speeds that approach this level to allow integration between the processes. This has provided the motivation for undertaking this project since it will develop the basic understanding that is required to design a high-speed screen-printing press.

1.2 Screen-Printing

Screen-printing presses can be categorised into three basic configurations. These are flatbed, cylindrical and rotary screen-printing presses, where each of these are discussed individually in the next section.

1.2.1 Flatbed Screen-Printing

Compared to the other printing processes, flatbed screen-printing is a very slow process, printing at a maximum speed of approximately 60 metres per minute with a state of the art machine, which is limited due to the reciprocating nature of the squeegee. The process works by tightly stretching a fine mesh, either synthetic or wire gauze, over a rigid frame to produce the printing screen. A photo emulsion is then applied to the screen, where a positive of the required image is placed on the screen and then exposed to a light source. The positive is then removed and the unexposed areas of the screen are washed away, leaving the exposed area of the screen covering the mesh. During press operation, ink is applied to the screen surface and the traversing action of the squeegee forces the ink through the open areas of the screen and onto the substrate, Figure 1.3, producing ink deposits of between 5μm and 300μm [3].

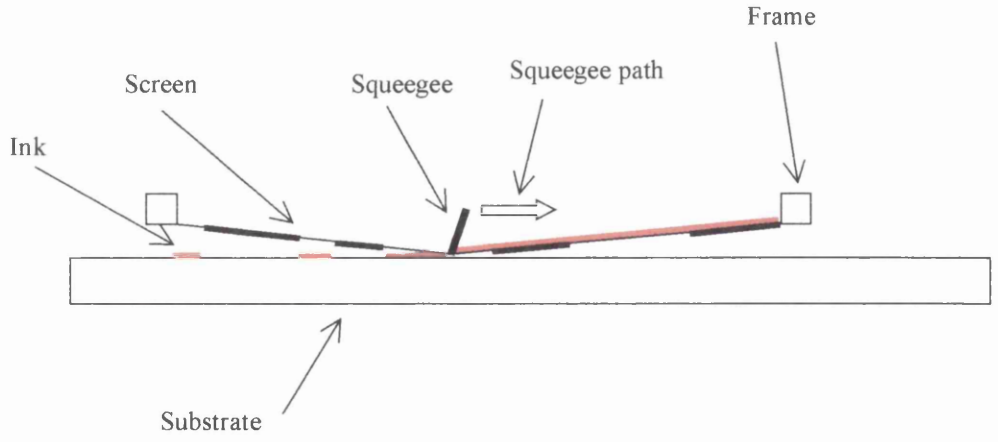

Figure 1.3 Flatbed Screen-Printing Station

1.2.2 Cylindrical Screen-Printing

Cylindrical screen-printing works in a similar way to flatbed screen-printing, except the squeegee is stationary and does not traverse across the screen surface. Instead of the squeegee moving, the screen and the substrate move, Figure 1.4. This has the same effect as a moving squeegee, but due to the different configuration, allows slightly higher printing speeds than that with a flatbed press. However, the process is again limited by the acceleration/deceleration but has the advantage of improved substrate handling in comparison to the flatbed press design.

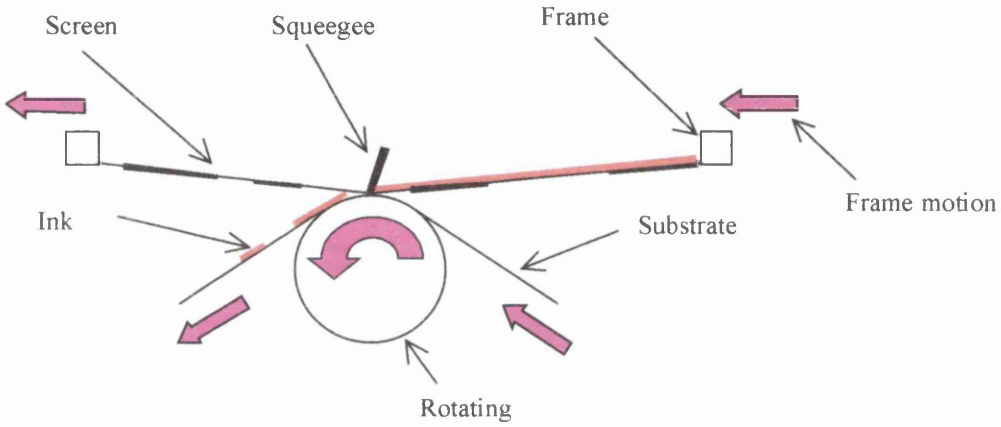

Figure 1.4 Cylindrical Screen-Printing Station

1.2.3 Rotary Screen-Printing

This variant of screen-printing is used for printing at higher speeds, where speeds of around 125m/min are achievable [4]. Compared with traditional screen-printing, rotary screen-printing is a relatively new concept. The process works by having a rotary screen to form a drum. This is commonly constructed from elecro-deposited nickel, with the chosen printing design stencilled onto the screen to create the open printing area. The printing ink is then placed into the centre of the screen drum, where it then rotates with the stationary squeegee blade forcing the ink through the open areas of the screen, Figure 1.5. Due to the rotating action of the rotary screen, there is no need for a return stroke of the squeegee or the screen, thus continuous printing is achievable making it suitable for printing wall paper and textiles. However, rotary screen-printing is not capable of the resolution that is required of high quality printing in the graphics and industrial sector.

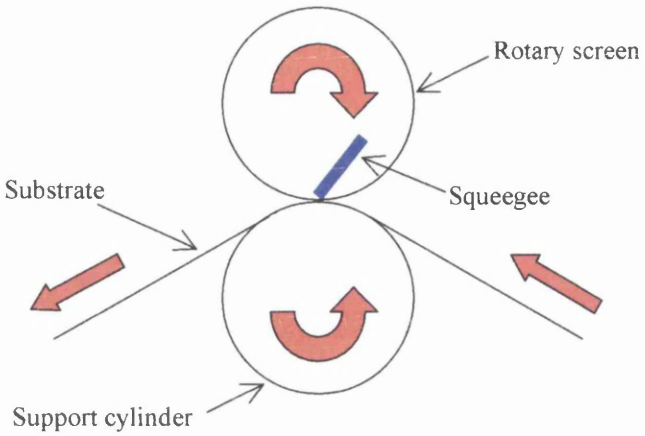

Figure 1.5 Rotary Screen-printing Station

1.3 Screen-Printing Components

Since this thesis will focus on the screen-printing process, this section sets out a brief description of the main components used in traditional screen-printing. This has been included to ensure a common understanding of the process shown in Figure 1.3 and Figure 1.4.

1.3.1 Squeegee

The squeegee has three main functions. These are to fill the mesh with ink, to keep the mesh in contact with the substrate and to remove the excess ink from the screen after the printing stroke. Typically, they are manufactured from polyurethane and range in hardness values from approximately 60 to 90 Shore A, more commonly described as soft, medium or hard squeegees. Squeegee blades can also be constructed from more than one type of material. These can be reinforced with fibreglass, partly steel backed, fully steel backed or made from more than one type of polyurethane. The different construction of the squeegee, along with a selection of profiles available is shown in Figure 1.6. Together, the variation of squeegee profile and the squeegee angle setting on the press allows for a wide range of printing characteristics depending upon the required job specification.

Figure 1.6 Squeegee Profiles

1.3.2 Printing Screen

The printing screen consists of three separate components. These are the frame, the stencil and the mesh. The frame is usually constructed from aluminium due to its light weight and rigidity. The mesh comprises either stainless steel or polyester fibres, where the open areas allow the ink to flow though the mesh and onto the substrate. Stainless steel mesh is generally used where high precision is required due to its low deformation. Additionally, they posses a higher open area than the equivalent polyester mesh, allowing a greater amount of ink to be transferred. The disadvantage of stainless steel mesh is that the low deformation properties mean that they are delicate and easily damaged and they cost substantially more than the more durable polyester mesh. The stencil determines where the ink can flow through the mesh. This is produced using a coating process or applied as a film held by capillary action. Indirect capillary stencils produce the best quality images due to the stencil being exposed before it is applied to the mesh, thus, minimising mesh interference effects on the image exposure. The stencil forms a gasket with the substrate under the pressure applied by the squeegee. The quality of the print depends on many factors including mesh resolution and the screen resolution, along with the quality of the seal produced by the gasket effect [5].

1.3.3 Substrate

Due to the flexible nature of the squeegee and the printing mesh, it is possible to screen-print onto a wide range of substrates. This includes printing onto bottles, paper, card, plastic, textiles, glass and ceramics. The choice of substrate greatly affects the quality of the printed image as some substrates will absorb the deposited ink and other substrates will fail to absorb the ink at all.

1.3.4 Ink

The type of ink used in screen-printing is highly dependent upon the final properties required of the printed product and the substrate adhesion characteristics. Depending upon the type of ink used, there are two different methods used to dry the ink after it has been transferred to the substrate. These are by evaporation or by exposure to ultra violet radiation. Both of these ink types can be water-based or solvent-based, where solvent-based UV inks are more commonly known as conventional UV inks. The viscosity of each ink can be reduced with the addition of the appropriate solution. However, the viscosity of conventional UV inks cannot be reduced, as this will affect its drying properties. Due to the rapid evaporation of solvent in the solvent-based inks, there is a risk that the ink will dry in the printing screen before it has been transferred to the substrate, preventing areas within the screen from being printed. This can be avoided by using a mesh that contains fewer threads per cm, which will increase the ink volume in the mesh and therefore increase the drying time. A summary of the recommended mesh types for the corresponding ink types can be seen in Table 1.1 [6].

Ink type	Threads/cm	Thread diameter (μm)
Solvent-based	120-165	27, 31 & 34
Conventional UV	140-180	27, 31 & 34
Water-based	140-180	27 & 31

Table 1.1 Mesh Structure for Corresponding Ink Type [6]

1.4 High-Speed Belt Screen-Printing Press Concept

Due to the reciprocating nature of the squeegee system used in traditional screen-printing, the maximum printing speed is limited and printing is only achieved when the squeegee is travelling in one direction. This problem has been overcome with the advent of rotary screen-printing machines, which print in a continuous cycle. However, the print resolution of rotary screen-printing is restricted and is insufficient for high quality graphical and industrial printing. For this reason, a preliminary design of a high-speed belt screen-printing press has been established that will enable high resolution, high-speed screen-printing to be achieved at more than twice the rate of a traditional screen-printing press.

A project proposal was submitted to the EPSRC in 1997 [7] for the design and manufacture of such a press including development of the underpinning science. The project included a number of companies as suppliers to the screen-printing industry as well as a machinery designer and manufacturer.

The original design concept consisted of a flexible belt screen in the form of a conveyor belt, with an automated ink delivery and removal system located at either side of the squeegee station, Figure 1.7. This will enable continuous screen-printing without the squeegee having to traverse back across the print screen. Due to the increase in print speed, it was believed that traditional blade squeegees would be subject to excessive wear and an increase in friction. For this reason, the use of a rotating roller squeegee needed to be considered.

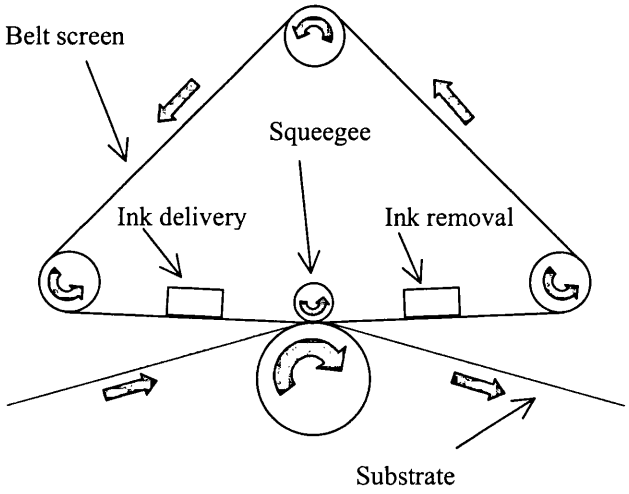

Figure 1.7 Schematic of High-Speed Belt Screen-Printing Press

Specific details of the press design, ranging from the development of the original design to the final manufactured prototype press, are set out in Chapter 6.

Due to the novel design of the high-speed belt screen-printing press, the printing characteristics and the knowledge obtained within traditional screen-printing may not necessarily be applicable. Additionally, there is little information on the ink transfer mechanism through the printing screen, which will ultimately influence the print

quality. For these reasons, a number of fundamental studies were undertaken to underpin the final design set out in Chapter 6

1.5 Thesis Objectives

The objectives of this thesis are to carry out a series of experiments and numerical simulations to investigate the behaviour of components within the belt screen press. Primarily, this will focus on the use of a roller squeegee to effect the ink transfer on the high-speed belt screen-printing press.

The thesis is set out in the following format;

- Chapter 2- A literature review into the relevant screen-printing topics.
- Chapter 3- This chapter describes a preliminary investigation into screen-printing with a roller squeegee where specific areas are highlighted that could cause the roller squeegee to fail to print successfully.
- Chapter 4- Following on from the information obtained in the preliminary investigation, a further more comprehensive study is undertaken into the process parameters of the roller squeegee.
- Chapter 5- Using a numerical model, the experimental studies carried out in the previous chapters are simulated to give a further insight into the behaviour of the ink in the nip contact region. These results are then correlated to the prints produced in the experimental studies.
- Chapter 6- The final design of the high-speed belt screen-printing press is shown in this chapter along with the practical issues and developments associated with such a press.
- Chapter 7- Conclusion, recommendations and further work.

This presentation will fulfil the aims and objectives of the work that are as follows;

- To develop a further understanding of graphics screen-printing with a roller squeegee. This will result in a reduction in squeegee wear and will allow continuous printing with the high-speed belt screen-printing press.
- To produce a numerical model to calculate the hydrodynamic characteristics within the nip contact region of the squeegee when using Newtonian and non-Newtonian fluids. This will also allow the impact of the squeegee deformation to

be studied as a result of the hydrodynamic pressure, thus gaining a further understanding of the process.

- To highlight the practical issues and developments of the high-speed belt screen-printing press.
- Using the knowledge gained from the previous studies, to design an appropriate squeegee for the high-speed belt screen-printing press and to therefore, predict the resultant print characteristics.

Chapter 2

Literature Review

2 Literature Review

2.1 Introduction

This chapter reviews previously published papers that have a direct relevance to the high-speed belt screen-printing press. The reviewed work focuses upon the technical aspects within each subject heading. This concentrates mainly on work published in the open literature. However, where it is essential, reference is made to scientific work reported internally where client confidentiality allows this.

During the review, it was found that the studies predominantly focused upon three main areas. These are indicated in Figure 2.1 and comprise of the ink roll in front of the squeegee (region I), the ink injection into the mesh (region II), and the ink release from the screen to the substrate (region III).

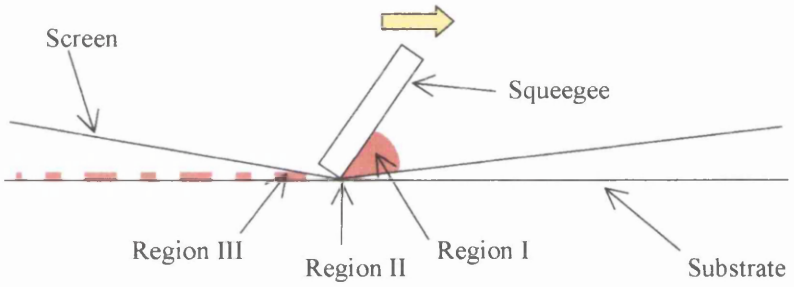

Figure 2.1 Regions of Ink Transfer Within the Screen-Printing Process

Consequently, the review is divided into the following sections, where the studies within each section are presented in chronological order.

- Investigation into the technical aspects of the relevant screen-printing components.
- The study of the physical ink flow in regions I, II, III.
- A review of process modelling within the three aforementioned regions. Further relevant process modelling studies are then presented in this section.
- High speed rotary screen-printing.

2.2 Screen-Printing Components

Compared to the other industrial printing processes, screen-printing possesses the fewest components, yet each of the components is critical to the process. This section reviews the relevant work that has been carried out into the main screen-printing components.

2.2.1 Mesh

The majority of research on mesh has focused upon stretching, with no scientific studies carried out on the effect of the mesh upon image reproduction. It is well documented that mesh stretching is a vital component in the screen-printing process, although it is only recently that modelling of the mesh stretching process has been investigated.

The importance of mesh stretching was highlighted in a report by the Screen Printing Technical Foundation, which stated that there were over seventy variables in screen-printing that were accounted for by the mesh stretching process [8]. This is an area that has been investigated extensively, with one of the most relevant articles produced by *Anderson et al* [9], where a concise review of previous work into mesh stretching is given. The work describes an experimental and numerical investigation into the tensioning characteristics of a polymeric mesh. It shows that there is a relaxation mechanism within the screen that cannot be completely attributed to creep, but may be affected by filament deformation. A finite element model of the tensioning system was also developed that was used to predict the stretching displacements and the effective stresses that are generated within the screen during the screen stretching procedure. This highlighted regions of high local stress, together with the development of an effective strategy for mesh stretching.

The mesh can be constructed from either stainless steel or polyester. The main advantages of using stainless steel meshes as oppose to polyester meshes are that the open area for stainless steel mesh is greater, allowing an increased amount of ink to flow through the screen [10]. This is particularly important when producing printed circuit boards, but less important in the graphics arts industry. Additionally, stainless steel meshes can withstand higher mesh tension, resulting in less image distortion.

However, the disadvantages of a stainless steel mesh are the increase in costs and the fragile nature of the screens, which are easily dented and damaged.

2.2.2 Stencil

Although the stencil is a key component in determining the quality of the print and the ink film thickness, very few technical articles are available, with the majority being published in the trade press. Predominantly, stencils can be either capillary film (indirect) or direct emulsions, where the thickness of the stencil and the profile of the stencil ultimately govern the thickness and the quality of the ink deposit. Generally, capillary films produce higher quality images [11] as the thickness of the capillary film is pre-determined and there is little variation in the stencil deposit throughout the screen. However, the disadvantages in capillary films are the cost incurred, which can be an order of magnitude higher than direct emulsions.

2.2.3 Imaging

The transfer of the image to the stencil is achieved via the film positive and its exposure to the ultra violet light source. Therefore, the resolution of the positive has a great influence upon the image to be printed and although nearly two thirds of the stencil defects are attributed to the film positives [12] there are no relevant technical studies in this field. However, the mesh ruling should be approximately twice that of the screen ruling of the positive to ensure good shadow definition [10].

2.2.4 Novel Screens

Generally, polyester is the favoured material for screen construction. However, several different materials have been investigated as an alternative, with a mesh manufacturer recently claiming to produce a polyester mesh that is stronger than stainless steel [13]. In 1992, a patent for the use of a laser to ablate holes in a thin non-woven sheet of nylon or polyester to produce a screen was filed [14]. However, the idea was never developed any further and its suitability remains unknown. Additionally, laser ablation has been successfully achieved with relation to disposable and digital screens, although its printability was not thoroughly investigated and the work was not presented fully in the public domain [7].

2.2.5 Squeegee

In the screen-printing process, the squeegee is one of the most influential components yet very few articles describing systematic scientific investigations have been published. This section of the review will mainly focus upon the impact of squeegees on printing performance and the different types of squeegees employed.

For graphic arts printing, blade squeegees are the most common form available and are usually constructed from polyurethane or synthetic rubber where a sharp squeegee edge is desirable. However, blunted or intentionally rounded squeegees can be used for thick ink film application as they also fail to remove all of the ink from the screen. Any ink remaining on the screen after the print stroke is then available to be drawn through the screen and onto the substrate [6] [15].

Jewell et al [16] carried out a study on polyurethane squeegees focusing on the relationship between squeegee hardness, profile, set angle and pressure on ink transfer and tonal reproduction. It was highlighted that the most dominating factor in determining ink transfer is the squeegee contact angle, where the smaller the contact angle, the higher the tone gain. This was found to be the case for eight different types of squeegees, with the more flexible squeegees having the greatest effect on tone gain due to its increase in deflection. It has also been suggested that if a soft squeegee is used, the ink is pressed onto a greater area of the substrate due to the increase in contact area created by the deformation of the squeegee. Therefore, this will result in an increase in ink deposit [6]. This is also the case when blunt or rounded squeegees are used [17].

Barden [18] recently completed a study upon the effect of squeegees on printed images. In this work, it was stated that softer squeegees produce a higher ink film thickness than harder squeegees and also, as the squeegee angle becomes closer to the horizontal, the ink film thickness increases. This was postulated to be as a result of the squeegee deformation, but this was not proven theoretically.

In addition to conventional blade squeegees, screen-printing with roller squeegees is also possible, although there is very little published work into this area. *Anderson* [19] used a roller squeegee that was free to rotate on a flat bed screen printing press.

During normal operation, using a water-based UV ink, the squeegee failed to rotate and skidded across the screen, producing slurred dots and heavy ink deposits. Trials were then carried out with the ink thinned with 10% water on a cylinder printing press. Under these circumstances, the squeegee rotated successfully, producing high ink densities at slower printing speeds, with a clear print with high ink deposits.

For rotary printing of fabrics and for producing printed circuit boards, stainless steel and nickel squeegees are sometimes used [20] [21]. However, where high ink deposits are required, such as in printing fabrics, magnetic rolling rod squeegees can be used, Figure 2.2. These novel squeegees move across the printing screen, driven by an electromagnet positioned under the blanket. This is also used to control the squeegee pressure [22]. This type of squeegee is also used in rotary screen printing machines, where the diameter of the rod is usually small enough to allow the ink to flow over and round the squeegee. For higher ink penetration, such as printing carpets, double roller squeegee systems can be used where the squeegee pressure and reciprocating movement is also controlled with electromagnets. Two rollers are used so as to confine the ink and are typically 80mm diameter. The penetration of the ink is accomplished by the pressure wedge in the ink trapped between the two rollers as it moves across the screen. The electromagnets produce sufficient force on the carpet surface to cause pile deformation for longer pile carpets, with more than one squeegee stroke sometimes needed at a normal printing speed of 5m/min. Double blade squeegee systems are also used to aid ink penetration using a reservoir of ink confined between the two squeegee blades, Figure 2.2. A vacuum is then applied underneath the print bed to pull the ink through the carpet.

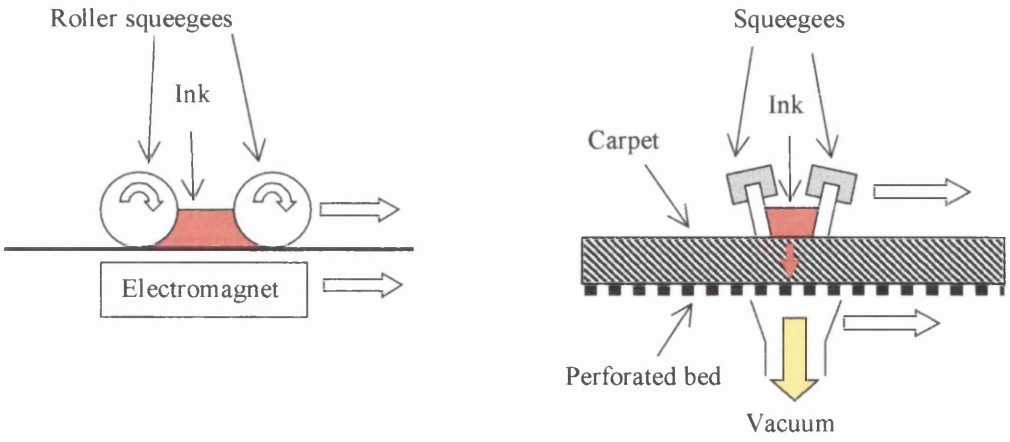

Figure 2.2 Double Roller and Double Blade Squeegee System

Although there are different types of squeegee employed in the screen-printing process, blade squeegees dominate the graphics area, with other types of squeegee used for higher ink coverage applications.

2.3 Ink Flow in the Screen-Printing Process

As previously mentioned, the flow of ink in the screen-printing process can be divided into three distinct regions. The aim of this section is to identify the flow characteristics within these regions, where the reviews have then been itemised in chronological order.

2.3.1 Region I

There has been little experimental work carried out into the study of the ink roll ahead of the squeegee. However, an experimental and theoretical investigation into the transfer process in solder paste screen-printing has been undertaken by *Owczarek and Howland* in 1990 [23] [24]. This included a consideration of the bow wave region and it was suggested that three main areas of flow exist. A number of different flow patterns are suggested at various different stages within the print stroke. These were partly deduced by analysing the shape of the bow wave that was obtained by stopping and raising the squeegee during the stroke. The squeegee deflection was then approximated, which was then used in conjunction with the volume of ink within the mesh open area and the equivalent open area height, to obtain an expression for the thickness of paste beneath the squeegee. This was then related to the thickness of the paste deposit.

Some years later, a similar experiment to this was then carried out by *Nikel* [25] to measure the squeegee deflection by printing a fast curing paste instead of an ink. As the squeegee traversed the printing screen, the squeegee was brought to a standstill. The paste was then allowed to cure with the set ink roll moulded into the shape of the squeegee deflection. The results highlighted a strong interaction between the squeegee pressure and the squeegee deflection, with an increase in pressure resulting in a reduction in squeegee angle. However, it is not known what effect the paste will have upon the squeegee deflection compared to that created by ink, but this work did emphasise the importance of modelling the squeegee as deformable rather than treating it as a rigid component.

2.3.2 Region II

As far as the author is aware, to date there is no published literature on the physical flow of ink through the screen and onto the substrate, with the work that has been carried out into this field being through process modelling. Therefore, this work is reviewed in the process modelling section.

2.3.3 Region III

The majority of work into the ink release from the screen to the substrate was carried out between approximately fifteen to thirty years ago. In the early seventies, *Riemer* [26] suggested that the transfer of ink from screen to substrate is based on the fact that the adhesion of the ink to the substrate is sufficient to break the ink from the screen. An equation was derived that enabled the calculation of the force required such that various screens can be lifted from a printed substrate, which as the author states, should produce a better understanding of the deposition process. The equation is based on the theory of the deflection of a two dimensional rope under a given load, where the screen is assumed to be the dominating factor.

A decade after this work was published *Messerschmitt* [27] attempted to explain how the ink is passed through an open mesh, when the squeegee presses the ink into the mesh. The idea of adhesion between the substrate and the ink is dispelled due to the mesh having a much greater surface area contacting the ink than the area of the substrate to be printed. However, when a small force is applied against the adhesive

force, flow will be induced in the ink, although this will not be enough to break the adhesion, as shown in Figure 2.3. This creates a shearing force within the ink which causes a break in cohesion of the ink and not in its adhesion to the mesh or the substrate. This causes the ink to split, leaving an ink layer on the surface of the mesh and on the surface of the substrate.

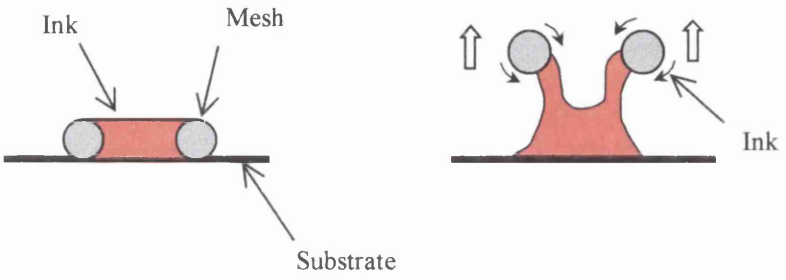

Figure 2.3 Ink Movement Within a Mesh Opening

In contrast to this early work by *Messerschmitt*, several years later *Riemer* [28] published work stating that the ink is forced from the mesh onto the substrate by a pressure differential between the top and the bottom of the mesh. When the screen is removed from the substrate surface, a vacuum is created underneath the wires of the mesh. This vacuum then draws the ink out of the mesh and onto the substrate. A schematic of this phenomenon is shown in Figure 2.4. However, this has not been proved in the paper, and as *Messerschmitt* [27] states, this theory has one major flaw, it is possible to screen print in a vacuum

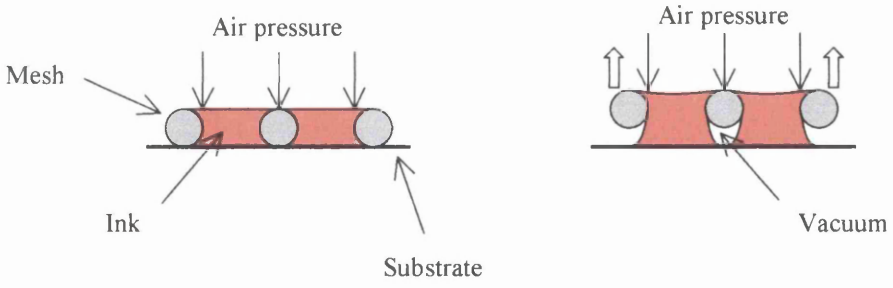

Figure 2.4 Vacuum Under Mesh Created During Snap Off

Riemer [29] then focused upon all three aforementioned regions of ink transfer. The ink flow in front of the squeegee, the injection of the ink into the screen and the ink

release from the screen to the substrate. It is suggested that the ink roll that is formed in front of the squeegee acts as a hydraulic pump, forcing the ink into the screen by a pressure mechanism. It has been shown that when particles flow though small tubes, such as the mesh openings in the screen, collisions occur between the particles and the tube walls. These solid particles are deflected towards the centre of the hole, which creates a film layer on the surface of the wires. *Riemer* [30] estimated that this accounted for 25% to 30% of the total mesh volume and acts as a lubrication layer for the movement of particles through the mesh, Figure 2.5. This hypothesis was proved by measuring the solid content of the residue left on the mesh and this was found to be significantly lower than that of the unused ink. It is also believed that without this lubrication layer, printing will not be successful which is why several printing strokes are required before satisfactory results are obtained.

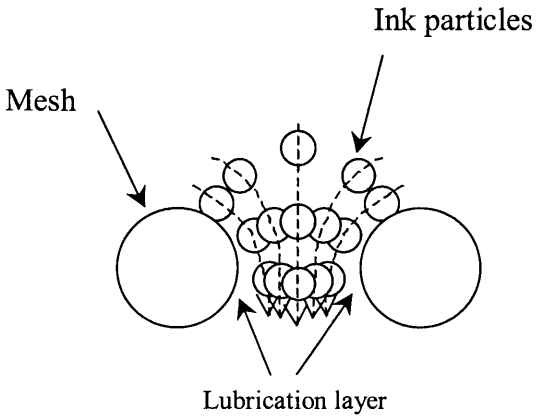

Figure 2.5 Ink Particle Deflection

2.4 Process Modelling

In an attempt to further understand the screen-printing mechanism, a number of studies have focused upon modelling the process, the majority of which have been in electronics application. This next section highlights some of the more relevant papers that have been published.

2.4.1 Region I

The majority of work into modelling the bow wave was carried out in the 1980's and 1990's. In the mid 1980's *Riemer* [31] carried out a theoretical study into the effect of the hydraulic pressure, created by the squeegee, upon the thickness of the ink that is transferred onto the substrate. The work is based on the Navier-Stokes differential equation and was simplified by assuming creeping flow, with the forces acting on the fluid (gravity, inertia and body forces) being negligible compared to the viscous stresses. Streamline patterns within the ink roll were then developed in conjunction with Taylor's solution, where the squeegee was then set to various angles. These were then analysed to derive a correlation between the print parameters and the pressure within the ink roll. It was found that high levels of hydraulic pressure, created by the ink roll in front of the squeegee, lift the squeegee causing ink cut-off at a higher level. Therefore, it was stated that any parameter that increases the hydrodynamic pressure would also increase the ink deposit by either lifting or deflecting the squeegee angle. However, the major problem with this work is that Taylor's equation does not incorporate the ink flow through the screen to the substrate [32].

Riemer [30] then furthered his work into predicting the streamline patterns in conjunction with developing a theoretical model to calculate the hydrodynamic pressure at any point along the squeegee edge, Equation 2.1. The terms that related to the relatively small forces acting on the fluid, such as gravity, centrifugal force and inertia were neglected, so that only viscous forces and a pressure drop remained in the equation. However, in theory this equation will produce infinite pressure at the squeegee point as the pressure is calculated using the reciprocal of the distance from the squeegee. The analysis was then used to show that reducing the squeegee angle would reduce the velocity of the ink, which will therefore increase the ink pressure. It was then shown that the position of lowest ink velocity arises near to the point of contact between the screen and the squeegee, thus producing the highest ink pressure, forcing the ink through the screen at this point, Figure 2.6. This work also assumes a rigid squeegee with a perfect seal at the screen.

$$P_L = \frac{2Sin^2\alpha}{\alpha^2 - Sin^2\alpha}\mu U\frac{1}{L}$$ Equation 2.1

Where:

P = Hydrostatic pressure

L = Distance from contact point

U = Squeegee speed

α = Squeegee angle

μ = Ink viscosity

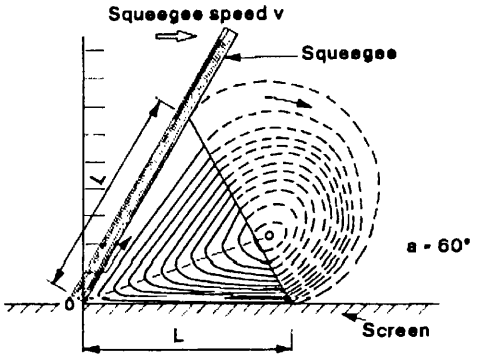

Figure 2.6 Streamline Patterns Predicted by Riemer [30] [31]

A recently published paper by *Glinski et al* [33] used computational fluid dynamics (CFD) to simulate the bulk motion of solder paste ahead of a moving squeegee, Figure 2.7. Newtonian pressure distributions were then obtained and evaluated against *Riemer's* work [30], where the results correlated well due to using similar boundary conditions and Newtonian fluid properties. It is stated that the most crucial factor governing the filling of the screen is the region close to the squeegee tip. Here, the pressure will be infinite due to the pressure being calculated using the reciprocal of the distance from the tip. However, *Glinski et al* mentioned that this cannot be the case in reality and that the pressure must be dissipated by the forcing of paste underneath the blade or squeegee. The non-Newtonian results proved that the majority of the ink roll moves at a relatively slow pace and at high viscosity, with a much less viscous layer adjacent to the stencil and the blade surfaces, in agreement with previous work carried out some years earlier [34]. The main limitations with this paper are that the squeegee removes all of the paste from the screen surface and the

ink is not transferred through the screen. Additionally, the squeegee is assumed to be rigid with a single point contact on the screen.

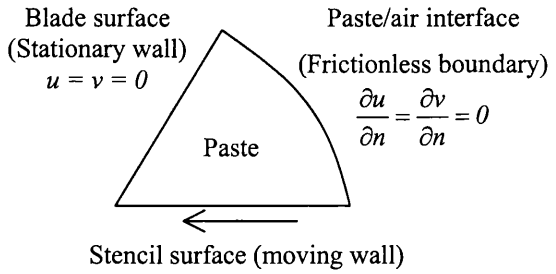

Figure 2.7 Boundary Conditions

An experimental and numerical study into the ink roll in front of a squeegee has been undertaken by *Jewell and Claypole* [35]. The numerical approach was also similar to *Glinski's* and modelled the squeegee as being rigid, removing all of the ink from the surface of the printing screen. However, in an attempt to simulate the nip contact gap between the squeegee and the screen more accurately, the squeegee was displaced above the screen, although ink was prevented from flowing through this gap by boundary condition prescription. A number of squeegee angles, nip gaps, ink viscosities (Newtonian and non-Newtonian) and different sizes of ink roll were investigated. Again, it was found that the maximum pressure occurs at the squeegee tip with the ink viscosity and nip gap having the greatest effect. The pressure within the ink roll was found to be negligible, with the size of the ink roll having no effect on the pressure at the squeegee tip. This was then verified experimentally where increasing quantities of ink were added to the screen to increase the size of the ink roll and this was found to have a negligible effect on the tone gain or solid density. Although this work highlights some important aspects, such as minimum pressure within the ink roll, it still fails to approach fundamental issues such as squeegee deformation, ink flow through the screen and ink remaining on the screen after the print stroke.

2.4.2 Region II

Huner [36] also modelled the stream functions within the ink roll ahead of a rigid squeegee as it slides over a plate, but applied a point sink at the tip of a squeegee, thus allowing the ink to flow through the nip junction. Although this work produces physically reasonable flow patterns that are more feasible than *Riemer's* [30] [31], it also utilises a rigid squeegee blade, Figure 2.8.

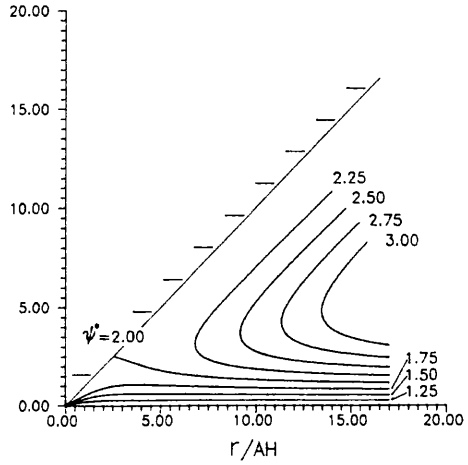

Figure 2.8 Streamlines For a Wedge Angle of 45° [36]

Where:

ψ = Stream function

r = Distance from tip

A = Porosity of screen

H = Thickness of screen

Although *Riemer* [28] previously stated that the vacuum under the meshes produces ink transfer, a tacky adhesion has been shown to be present by *Banks and Mills* [37] which aids the ink transfer and was discovered almost three decades earlier. This tacky adhesion has been shown to be a result of the mesh fibres lifting away from the substrate. From these two factors of ink transfer, *Riemer* considers the most significant transfer mechanism to be the pressure differential. Using a modification of the Hagen-Poiseuille Law, Equation 2.2, and modelling each mesh as a short piece of pipe, a correlation between the maximum allowable squeegee speed and the ink viscosity were plotted. However, the application of this equation was found to be

limited, as the results contradict the experience of print quality and were only applicable to a squeegee at the centre of the print stroke.

$$\mu V \leq \frac{1}{128}\frac{D^2}{d}\left(\frac{S-B}{a}\right)Pa \qquad \text{Equation 2.2}$$

Where:

D = Diameter of mesh opening
M = Mesh count per unit length
d = Wire diameter
L = Thickness of fabric = $2d$
v = snap off velocity
V = Squeegee speed
a = Snap-off distance
S = Screen size
B = Length of printed pattern
Pa = Atmospheric pressure

The quantity of ink transferred in the screen-printing process was investigated further by *Rangchi et al* [38] over fifteen years ago. Theoretical considerations were based on the squeegee speed, squeegee angle, ink viscosity and the screen properties, with the flow assumed to be Newtonian for mathematical simplicity. A formula for the ink film thickness was then derived but was found to be independent of the squeegee speed and the fluid viscosity with a dependency on squeegee angle and the screen parameters.

In order to model the ink flow through a screen, previous researchers have modelled meshes as a matrix of capillaries. However in 1989, *Huner* [39], argued that as printing screens are examples of monofilament monoporous cloths, they should be modelled as anisotropic porous media, which satisfy Darcy's law and not modelled as a matrix of capillaries. This is because a matrix of capillaries does not observe the correct wetting and de-wetting responses, the flow resistance is not accurately predicted and the possibility of flow within the plane of the fabric is not accounted for. The paper also states that the ink movement through the screen is a result of the bearing effect ahead of the squeegee tip, as well as the peeling of the screen in the breakaway region.

The coating thickness that is deposited from a coating blade system was then estimated by *Huner* [32] using the generated pressure distribution within the fluid. The blade is assumed to be a vertically orientated rigid chisel, modelled as a slipper bearing where the blade is at a set height from the substrate surface as to produce a coating layer. This model is then applied to a squeegee within the screen-printing process, where the thickness of the screen is represented by the blade height above the substrate in the coating blade model, thus allowing ink to flow underneath the squeegee. However, this investigation neglects the presence of the screen and assumes a low mesh count with a high open area whilst using a rigid squeegee with a sharp point.

Later work by *Huner* [40] investigated the flow of Newtonian ink within the plane of the printing screen during a screen-printing stroke. General expressions for the pressure beneath the squeegee and for the volume of ink passing underneath the squeegee tip were developed, although squeegee deformation was ignored. The effect of the speed of the squeegee was also discussed explaining that at low speeds, the ink only spreads across the surface of the screen. Increasing the speed causes the pressure underneath the squeegee to increase, until the speed increases such that the peak pressure beneath the squeegee exceeds the wetting resistance of the screen. At which point, the screen mesh floods and fills with ink. A further increase in speed results in the point of injection of the ink moving away from the squeegee tip.

More recent work by *Anderson et al* [41] used previously calculated squeegee deformations [47] to develop a non-Newtonian model to represent the transfer of ink through a porous screen in the screen-printing process. The model treats the ink beneath the squeegee as a hydrodynamic film thus allowing ink to flow underneath the squeegee, with the ink viscosity modelled using a power law equation. The governing equation for the pressure within the ink film was expressed as [42];

$$\frac{dp}{dx}\left[G\frac{dp}{dx}\right] = U\frac{dh}{dx} + U\frac{dF}{dx} - f(v) \qquad \text{Equation 2.3}$$

Where;

$$G = \int_0^h \frac{y}{\mu}(y - F)dy \qquad F = \frac{F_1}{F_0} \qquad F_1 = \int_0^h \frac{y}{\mu}dy \qquad F_0 = \int_0^h \frac{1}{\eta}dy$$

With the flow through the screen represented by;

$$f(v) = \frac{\alpha\pi R^2}{8\mu}\frac{dp}{dy} \qquad \text{Equation 2.4}$$

Where;

h = Local film thickness
p = Film pressure
x,y = Cartesian co-ordinates
U = Sliding velocity
R = Screen capillary radius
α = Dimensionless screen open area
μ = Ink dynamic viscosity

The model highlighted that the variation in viscosity in the nip contact region was substantial and that shear thinning greatly affected the pressures that were generated. However, the variation in the power law index had minimal effect upon the flow rate through the screen. The screen open area was shown to have a large influence upon the pressure that is generated within the nip, with an increase in open area resulting in a reduction in pressure. Although this work utilises the calculated squeegee deformations, the paper still fails to include the effect that the pressure generation within the ink film has upon the deformation of the squeegee.

2.4.3 Region III

One of the most recent studies on the ink release from the screen to the substrate was carried out by *Abbott et al* [43]. A mathematical model was used to calculate the volume of liquid removed from a mesh and onto a substrate. It is based on the assumption that the free energy surface effects dominate, and that the printed liquid is pulled out of the mesh, rather than flowing out of the mesh. The main assumptions were that the liquid is incompressible, body forces are neglected, slip does not occur on the boundary surfaces, inertia effects are negligible and the squeegee tip is sharp and rigid, removing all of the ink from the screen surface. The model is two-dimensional and uses both Newtonian and non-Newtonian liquids and works by

application of the *Landau Levich* equations. These equations are based on the dragging of a liquid out of a pool by an ascending solid surface [44]. Through its application, it is possible to calculate the liquid left on the screen after it has been removed from the substrate. This then allows the liquid transfer to be calculated. The results obtained from the model were then compared with a number of experimental data. It was found that the ink deposits were in good agreement over a wide range of mesh counts.

2.4.4 Squeegee Deformation Models

In the early 1990's a study by *Huner* [45] modelled the macro squeegee deformation as a rigidly clamped, cantilevered plate loaded at its tip by a concentrated force from a combination of the contact force and the fluid pressure generated by a Newtonian liquid. The curvature and the bending moment of the plate were estimated using a simple beam bending equation. This was calculated using all components of moments produced by the normal and the tangential forces acting upon the blade. These included the reaction of the squeegee on the screen, frictional drag at the squeegee tip and the normal and tangential fluid stresses acting on the squeegee face, with the predominant forces being the contact force at the squeegee tip and the fluid pressure. The press was treated as the equivalent of a slider bearing with a porous walled stator with the analysis carried out in the lubrication limit using the *Morgan-Cameron* approximation. This approximation is used in the analysis of bearings with a porous stator backed by a solid wall, where the pressure gradient normal to the surface of the stator is neglected and by symmetry there is no pressure gradient in the direction of the bearing width [46]. With the squeegee shape having been calculated, the ink flow in the breakaway region was established. However, an analytical solution was not available but ratios of when the elastic forces were dominant and then when the fluid forces were dominant were established. When the elastic stresses are dominant, the ink flow in the breakaway region is independent of the ink viscosity and the squeegee speed, whilst being insensitive to squeegee pressure and squeegee angle. When the fluid stresses are dominant, hydroplaning can occur where the ink flow at the breakaway region is a function of the viscosity and the squeegee speed.

A more recent paper by *Anderson et al* [47], concentrates upon the importance of understanding the squeegee deflection and local tip deformation. This was facilitated

through using finite element analysis. A number of different squeegee configurations were investigated including reinforcing the squeegee with a rigid steel backing. For a standard squeegee, it was found that the vertical load results in a rounding of the squeegee edge and horizontal drag component causes a further localised deformation, Figure 2.9. For the steel-backed squeegee, the squeegee is only subjected to a rounding of the squeegee tip, where it is then stated that it will be more conducive to promoting ink flow through the screen, Figure 2.10. Although this paper emphasises the change is squeegee geometry when subject to loading, it fails to explore the effect that the hydrodynamic pressure has upon squeegee deformation through direct coupling with the fluid phase analysis.

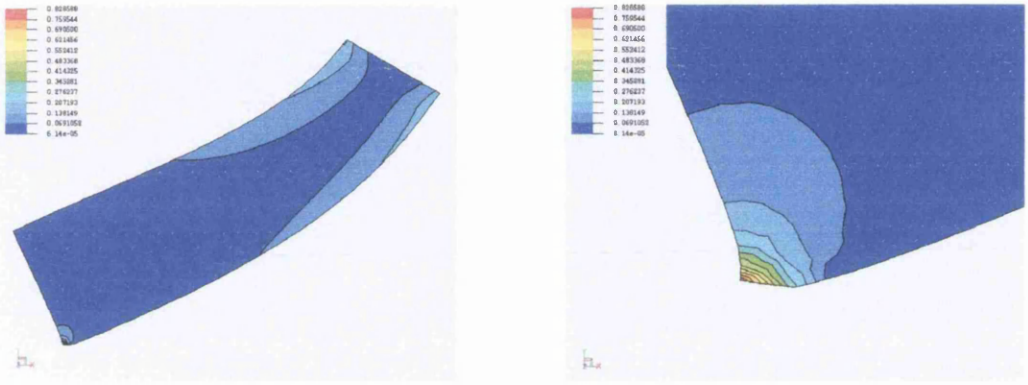

Figure 2.9 Squeegee Deformation When Subject to Vertical and Horizontal Loading

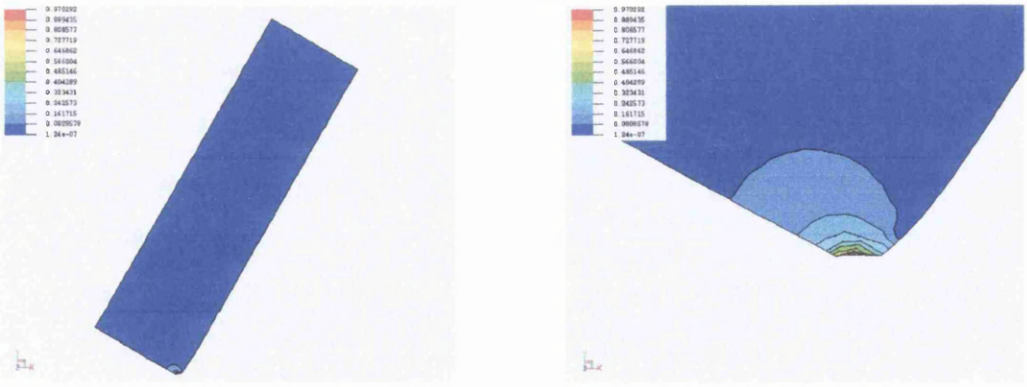

Figure 2.10 Steel-backed Squeegee Deformation When Subject to Vertical and Horizontal Loading

2.4.5 Applicable Numerical Models to the Screen-Print Process

In many printing and coating processes, the coating fluid is often transferred to the substrate via a number of rollers that form a train to accurately meter and distribute the fluid. These trains are constructed from a series of rubber coated and steel rollers and are usually positioned so that the elastomer surface of the rubber roller deforms against the steel roller. Therefore, the behaviour of the rollers will greatly influence the metering of the coating fluid, in a similar manner to the impact of the deformation of a squeegee upon the ink transfer mechanism. The coupling of deformation and fluid flow imposes the need to iterate between the fluid and the roller deformation for Soft Elasto Hydrodynamic Lubrication (SEHL) analysis and was highlighted by *Cudworth* [48] over twenty years ago. However, this has only been applied to printing and coating applications in recent years. A dimensionless analysis into roller trains was carried out by *Xue et al* [49], where the fluid film thickness on the surface of the rollers, the roller deformation and the pressure profiles were evaluated for a broad range of different scenarios using a Newtonian fluid. The Reynolds equation was transformed into a form of boundary integral equation and the surface deformation was solved by a boundary element method. As a result of large roller deformations, the resultant film thickness on the rollers were relatively large, with the speed having a significant effect. It was also found that an increase in the Poisson's ratio produces a smaller film thickness, highlighting the effect of the roller properties and fluid pressure upon the surface deformation.

Using a similar numerical approach to the work by *Xue et al* [49], *Bohan et al* [50] furthered this work using a Newtonian fluid to compare experimental and numerical investigation into the behaviour at the nip junction of a roller train. The experimental results showed that the level of the engagement is directly proportional to the increase in pressure. The pressure distributions were then compared to previous work [51], where the general form and magnitude were similar, with the numerical results also in good agreement. In addition, an increase in the rubber modulus resulted in a reduction in film thickness, although the pressure profiles remained similar due to the model using a constant loading.

Although various models can be used to predict the ink flow through a screen, flow through membranes has been extensively researched [52] [53]. This flow can be likened

to flow through a porous printing screen, although the membrane openings are small in comparison to the screen openings. A two-dimensional finite difference numerical solution of the Navier-Stokes, continuity and convection diffusion equations has been recently used to predict the permeation rate of cross-flow diffusion of a colloidal suspension by *Bowen and Williams* [54]. This is show schematically in Figure 2.11. The model allows the effects of the variation of the osmotic pressure (the pressure required to prevent passage through the membrane), diffusion coefficient and the viscosity to be studied. Good agreement between theoretical predictions and experimental cross-filtration were obtained with the model showing that the effects of the viscosity and the variable diffusion coefficient were significant and comparable in magnitude.

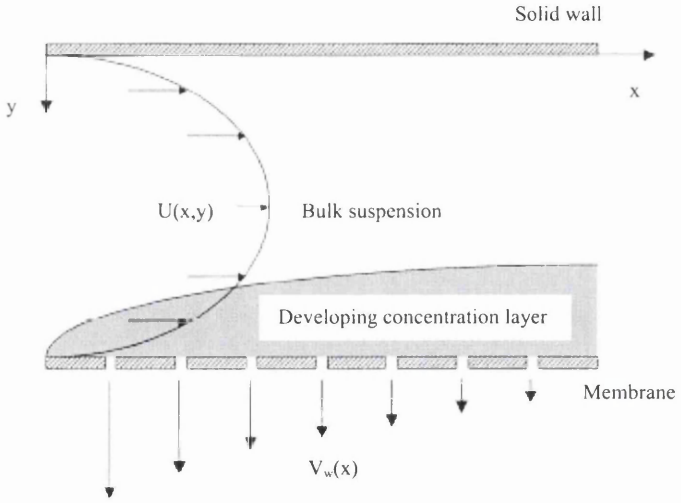

Figure 2.11 Schematic Representation of Ultra-filtration Through One Wall in a Flat Plate System

There have been a number of studies carried out into modelling the screen-printing process, although the majority of them omit significant facts and contain simplifying assumptions. However, it is widely believed that the ink is transferred through the screen either by the pressure differential created within the bow wave of the fluid, or by the pressure differential directly beneath the squeegee tip. The work on modelling roller trains has a significant resemblance to screen-printing as it models the pressure generated within a number of rollers, whilst taking into account the effect of the hydrodynamic pressure upon the roller deformation. Although this has not been directly applied to the screen-printing process, it is a vital aspect of the mechanism

that has yet to be researched, leaving a substantial area for further work and investigation.

2.5 Rotary Screen-Printing

Although the conception of rotary screen-printing came about over 50 years ago [20], there has been minimal published work into this field. This is mainly because of the difficulty in making a mesh system that may be incorporated readily into the concept. The current manufacture method uses an electro-deposition technique to build a nickel mesh, but this is susceptible to damage and the process is only suitable to a small niche market. However, this next section discusses the most relevant papers that have been published into this field. For reference, a schematic of a rotary screen-printing press can be seen in Figure 2.12.

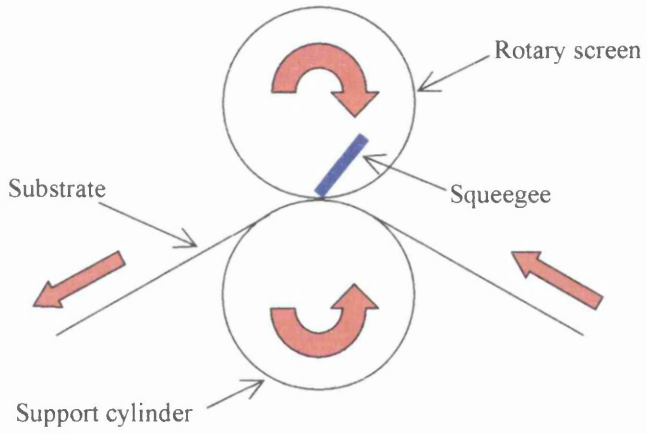

Figure 2.12 Schematic of Rotary Screen-Printing Press

Several different types of squeegee systems have been developed for use in rotary screen-printing [22]. The first types of squeegees that were used were constructed from rubber but the rubber wore quickly and the drag of the squeegee inside the screen caused the screen to distort. This then led to flexible stainless steel blades, which were more resistant to wear. Generally, the supply of ink is automatic, where the ink is pumped into the interior of the rotary screen by flexible tubes. This ensures an even ink distribution, where the exact quantity of ink can be monitored with electric or pneumatic level detection probes [20].

A study by *Hawkyard and Miah* [55] has been carried out into the press parameters of rotary screen-printing with a roller squeegee. The main parameters that have been investigated are the effect of the squeegee angle (in this case the squeegee diameter), the base length of the pressure zone, screen deformation, the shape of the screen holes, rheology of ink and the penetration of the ink into the fabric. It is suggested that the base length, described as the distance within the paste wedge where there is significant hydrodynamic pressure, is closely connected with the effective squeegee angle. This can be seen to increase as the angle between the squeegee and the screen decreases. It is also highlighted that a roller squeegee will produce a greater hydrodynamic pressure than that of a squeegee blade. This is due to the roller squeegee system having two moving surfaces as oppose to one moving surface acting on the ink, Figure 2.13.

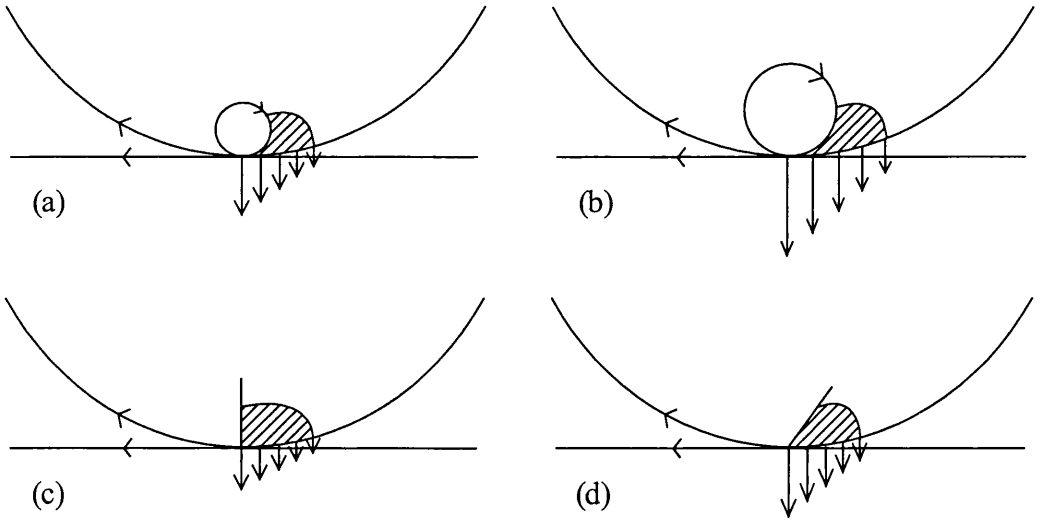

(a) Roller squeegee, small diameter
(b) Roller squeegee, large diameter
(c) Blade squeegee, large squeegee angle
(d) Blade squeegee, small squeegee angle

Figure 2.13 Schematic of Pressure Profiles For Blade and Rod Squeegees

The type of roller squeegee that was used was a steel rolling rod squeegee where the squeegee pressure is determined by applying a magnetic field to the squeegee. It was found that rod squeegees having a diameter greater than 25mm caused sufficient screen deformation as to damage the nickel screens. Amongst the results that were discovered, which generally corresponded to conventional screen printing methods, it was found that a higher volume of ink penetrated the fabric where a higher magnetic

field was applied, or a larger squeegee diameter was used. This was postulated to be caused by the fabric compressing and therefore the ink passing a shorter distance through the interstices of the fabric. Additionally, larger diameter squeegees increase the contact time and contact width, resulting in greater ink deposits. It was shown experimentally that the volume of ink applied decreases sharply with an increase in printing speed when using smaller diameter squeegees and low magnet settings with a viscous printing ink. Whereas when using a larger diameter squeegee and high magnet settings with a low viscosity ink there is very little decrease in the volume of ink applied.

The advantages and disadvantages of rotary screen-printing have been published in a paper by *Scott* [56]. The advantages that were highlighted are that rotary screens are relatively cheap, easy to handle and easy to store. In addition, the specific aesthetic characteristics and qualities of traditional screen-printing are available, such as thick ink film coverage and the printing of high contrast colours. Short runs can also be accommodated economically when design changes are very frequent. The disadvantages of rotary screen-printing were stated as being that the screens are prone to damage, high material costs and that the printing of tones is not of a particular high quality. Additionally, the screen diameter dictates the repeat length of the image. Two different types of printing screen were discussed. The main differences between these two types of screen being that the holes in a galvano screen vary in shape and size and make up the design that is to be printed. Whereas the holes in a lacquer screen are the same throughout and form a regular mesh across the whole surface. It was also stated that increasing the blade length and pressure, or decreasing the blade angle and thickness would produce higher ink deposits.

Compared to flatbed and cylindrical screen-printing, rotary screen-printing is capable of printing in a continuous cycle. Thus, a reciprocating motion of the squeegee or the press bed is not required, resulting in higher printing speeds. This has also resulted in the advent of roller squeegees to minimise the squeegee wear that is encountered with the increased speeds. However, it must also be noted that flexible stainless steel blades can also be used, which are more resistant to wear.

2.6 Closure

This chapter has reviewed the relevant literature in relation to the screen-printing process. Traditionally, screen-printing has been a relatively slow printing process, although rotary screen-printing has meant that production speeds can be increased. However, as stated in this chapter rotary screen-printing has several disadvantages. This has resulted in an opening for a high-speed, increased print resolution printing press, whose image size is not dictated within the realms of that of rotary screen-printing.

Although there are several different types of squeegees used in screen-printing, it is widely believed that the only type of squeegee suitable for graphic art printing is the traditional polyurethane squeegee, where the more rounded the squeegee, the higher the ink deposit. Consequently, the majority of the work into modelling the screen-printing process has focused upon rigid squeegees with a sharp, single point, with the pressure within the ink having no impact on squeegee deformation. However, there have been studies carried out into the calculation of the pressure generated between two rollers in the coating process where the fluid pressure greatly affects the roller geometry, although this work has mainly focused upon Newtonian fluids. Overall, the review has shown that the screen-printing process, although well established, remains a process that still requires a great deal further work and investigation to drive towards higher speed application.

For these reason, the concept of belt screen screen-printing press will be investigated within this work and will mainly focus upon the development of a novel squeegee system that is capable of printing at high speeds. Additionally, subjects such as ink delivery, ink removal and the belt screen development issues will be discussed where appropriate.

As a consequence of the literature review, the overall aims of this study are as follows;

- To develop a further understanding of graphics screen-printing with a roller squeegee. This will result in a reduction in squeegee wear and will allow continuous printing with the high-speed belt screen-printing press.

- To produce a numerical model to calculate the hydrodynamic characteristics within the nip contact region of the squeegee when using Newtonian and non-Newtonian fluids. This will also allow the impact of the squeegee deformation to be studied as a result of the hydrodynamic pressure, thus gaining a further understanding of the process.
- To highlight the practical issues and developments of the high-speed belt screen-printing press.
- Using the knowledge gained from the previous studies, to design an appropriate squeegee for the high-speed belt screen-printing press and to therefore, predict the resultant print characteristics.

Chapter 3

Initial Experimental Study

3 Initial Experimental Study

3.1 Introduction

The purpose of this chapter is to describe the experimental equipment and procedures that were adopted to explore screen-printing with a roller squeegee. The experimental techniques employed include flatbed screen-printing trials with a traditional squeegee blade and roller squeegees. The following sections will describe the test set-up and procedure. This will lead to an initial assessment of the roller squeegee.

3.2 Print Trial Experimental Equipment

3.2.1 Screen-Printing Press

The type of press used throughout this work is a small format, single station, Fleischle flatbed screen-printing press, Figure 3.1. The press is a manual front loading design and comprises the usual features for flowcoat and squeegee mounting. It is capable of accepting a range of substrates from film to glass and has the facility for printing at different squeegee downforce and speed.

Figure 3.1 Fleischle Flatbed Screen-Printing Press

The printing speed can be set on a dial from a 0 to 10, where a setting of 10 corresponds to a linear speed of approximately $0.8ms^{-1}$ over the printing area. The squeegee pressure is regulated by a manually operated air valve that allows a maximum pressure of 4.5b to be applied to the actuators at either end of the squeegee mounting bar. Details of the press loading calibrations can be found in Appendix C.

3.2.2 Roller Squeegee

Anderson's [19] early work into graphical printing with a roller squeegee stated that successful printing depended upon the complete rolling action of the squeegee. For this reason, the design of the roller squeegee incorporated a motor to positively drive it, where the speed of this motor is adjustable to allow for different printing speeds. The motor was sufficiently small to be mounted on the squeegee holder, whilst delivering enough torque to rotate the squeegee during the print stroke. The motor selected has a maximum torque of 0.12Nm, with the speed being controlled by a variable power supply. The drive was transferred to the squeegee by a toothed belt where the tension can be adjusted by the vertical movement of the motor. The motor was rated using predicted squeegee drag force, roller radius and speed. It was chosen to ensure a rolling action, not to apply a level of control to achieve rolling/sliding action since this requires a more advanced control system and was not warranted at this stage.

To explore the impact of different roller squeegees, two diameters were manufactured, notably 30mm and 50mm, the largest diameter being dictated by the space available on the press, Figure 3.2.

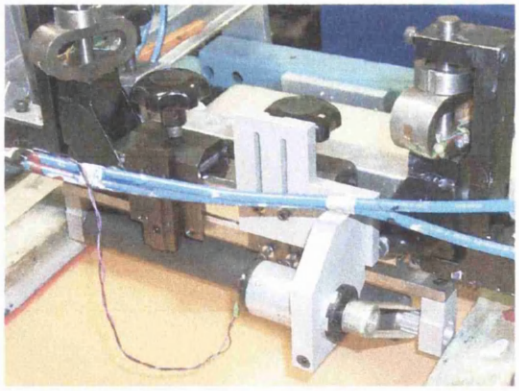

Figure 3.2 Roller Squeegee and Drive Mechanism on Flat-bed Press

The rollers were covered with rubber of 70 Shore A hardness and a thickness of 6mm and were finished by grinding to a surface finish of 3.00Ra, as measured with a white light interferometer [57]. This particular grade of rubber was used as it is the same as that of a medium squeegee blade that is most commonly used in graphic art screen-printing. The roller squeegee was attached to the existing squeegee bar with the

squeegee holder modified to accommodate the drive motor with adjustable positioning for alignment and belt tension, shown in Figure 3.3.

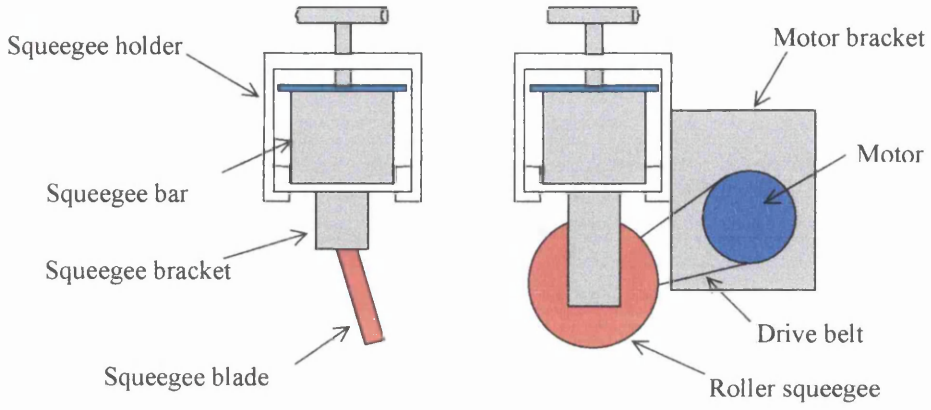

Figure 3.3 Schematic of Blade Squeegee and Roller Squeegee Fixture

3.2.3 Flowcoat

Due to the reciprocating motion of the squeegee in traditional screen-printing presses, there is a need to redistribute the ink across the screen surface ready for the next print stroke. This is achieved by a flowcoat (sometimes called flood bar or doctor blade), which is situated parallel to the squeegee and spreads the ink back over the screen on the return stroke. For this experimental work on the flatbed screen-printing press, the flowcoat was used to perform the task of distributing the ink across the printing screen, where the speed, angle and the height of the flowcoat remained constant. This was considered to be adequate since *Jewell and Claypole* [58] showed that flowcoat settings have very little effect on print quality and can be considered secondary.

3.2.4 Printing Screen

The printing frames used in these experiments were aluminium with internal dimensions of 525mm by 398mm. To assess the impact of prints produced from screens of different mesh counts, two screens were prepared. The first from 120 and the second using 150 threads per cm mesh of 34μm thread diameter (denoted as 120-34 and 150-34), with the image layouts depicted in Figure 3.4 (i) and (ii) respectively. However, the work in this chapter focuses on the screen using 120-34 mesh since the initial trials were printed with this screen.

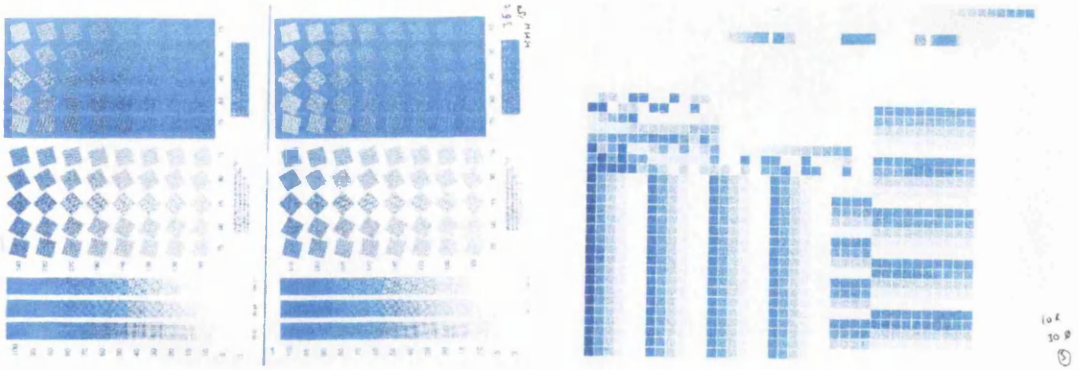

(i) 120-34 (ii) 150-34

Figure 3.4 Image Layout For Roller Squeegee Print Trials

The printed image areas were created with a CAP-CP capillary stencil, chosen for its exceptionally thin profile and low Ra value, giving the ability to produce high accuracy prints. The printed image for the 120-34 screen comprised a number of tonal gradations ranging from 3% to 100%. To allow the effect of line rulings to be explored, the open areas were set to line rulings of 85lpi, 100lpi and 120lpi. In addition, for the study of fine line reproduction, a series of lines set at various orientations were produced.

For the 150-34 screen, a series of similar gradations were positioned over the printing area at a line ruling of 100lpi. This stencil was prepared to allow for further trials into four colour reproduction with the roller squeegee. However, for this preliminary study only the gradation in the centre of the print was analysed with a single print colour, as the aim of this work was to investigate the primary characteristics of roller squeegee printing.

In order to achieve optimum printing screens, the screens were constructed in accordance with the findings from *Andersons* [19] work into mesh tension. This produced two screens with a final printing mesh tension of 15Ncm^{-1} in the warp and weft direction.

3.2.5 Substrate

The substrate used throughout the series of experiments was *Hello Silk* paper, supplied by the Robert Horne Group. This paper has a specific weight of 170gm^{-2} and is of exceptionally high quality producing minimal tone gain due to its calandered and relatively non-permeable nature. In addition, it is also one of the most widely used screen-printing papers of its kind.

3.2.6 Ink

For comparison, two solvent-based inks were used. The inks were a *Sericol Ultra-Tone*, used for printing halftones onto paper and board, and a *Sericol Trichromatic Mattplast*, which is used for printing paper, board, PVC and other plastics. These were chosen due to their proven performance in producing excellent graphical printability and print definition on a range of substrates. The maximum suggested mesh count for these solvent-based inks is 120 threads per cm. A further increase in mesh count would result in a reduced volume of ink within the screen. Due to the evaporation of the solvent in the ink, this would then lead to a quicker drying time, with the possibility of the ink drying in the mesh before it has been printed. Therefore, a *Sericol UV Speed* conventional UV ink was also investigated so that drying in would not occur when the mesh count was increased to 150 threads per cm. This ink is mainly used for printing graphics onto PVC and paper substrate. This was then dried with a Aktiprint T UV Drier. In addition, the design specification for the high-speed belt screen-printing press suggests the use of conventional UV inks. The inks used in the investigation were cyan and therefore all use the same type of phthalocyanine pigments to create the colour, thus minimising any variability due to the use of different colours.

3.3 Print Measurement

To produce prints of differing lightness, the thickness of the ink film needs to vary so that various amounts of light will be absorbed and reflected. However, this is almost impossible to achieve, but can be represented by breaking down the colour into a series of small dots to give the illusion of a variation in ink film thickness. These are referred to as halftone dots, the size of which will be in relation to the lightness of the original image, whilst maintaining the same hue and saturation. These range in

brightness from 0% area coverage (light), to 100% area coverage (dark). Therefore, the size and consistency of these printed dots will determine the quality of the image to be printed. The change in area of these printed dots, from the required area defined at the colour separation stage, is described as the tone gain, or dot gain, Figure 3.5, and will result in the reproduced image being too light or too dark. The tone gain includes both the mechanical gain (growth of the physical halftone dot) and optical gain (how the dot appears to the human eye) and is expressed as the percentage increase compared to its original area. Generally, tone gain is not a problem if it is consistent and can be predicted, as it can be compensated for at the pre-press stage with minor adjustments during printing.

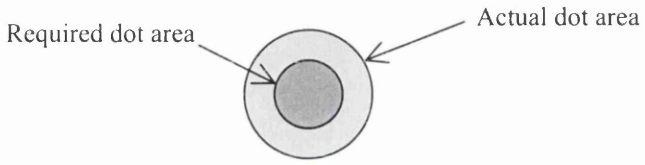

Figure 3.5 Illustration of Tone Gain

In order to establish the consistency of a printed image, its colour needs to be measured. There are two ways to achieve this. For solid areas, the film thickness can be measured, but this presents severe difficulties since some substrates absorb ink and the impracticability of measuring very thin ink films. However, it is possible to measure ink film thickness using white light interferometry [57], or reference the ink film thickness to a grey level using image analysis techniques [59]. There are several different types of instruments that are specifically designed for the measurement of colour. This is achieved by measuring the reflectance spectrum of the ink relative to the substrate with a spectrophotometer, a spectrocolormeters or a colorimeter [60]. For this work, a Gretag Macbeth Spectrolino reflectance spectrophotometer was used. The density of each of the tonal gradations is calculated from the reciprocal of the reflection of the printed sample, Equation 3.1. [61]

$$Density = \log_{10} \frac{1}{Reflectance} \qquad \text{Equation 3.1}$$

a = *Optical dot area*

D_h = *Halftone density*

D_s = *Solid density*

Then;

$$D_h = -log\left[1 - a\left(1 - 10^{-D_s}\right)\right] \qquad \text{Equation 3.2}$$

The density of each of the tonal gradations can then be related to the density of the solid printed area, expressed via the Murray Davies Equation [60];

$$a = \frac{1 - 10^{-D_h}}{1 - 10^{-D_s}} \qquad \text{Equation 3.3}$$

The tone gain can then be calculated by subtracting the required dot area, Equation 3.4.

$$\textit{Tone gain} = \textit{Optical dot area} - \textit{Original dot area} \qquad \text{Equation 3.4}$$

Once the tone gain has been calculated and the press settings characterised, it can then be quantified and compensated for at the pre-press and production stage to reproduce the required area coverage.

3.4 Traditional Blade Squeegee Screen-Printing Characteristics

To establish some guiding principles and to obtain a benchmark image for the roller squeegee experiments, the press was fitted with the medium hardness squeegee blade, printing through the 120-34 screen. The ink used was the *Ultra tone* solvent-based ink containing a combination of 15% thinners and 15% retarder. Thinners were added to the ink to reduce the viscosity and the retarder was used to delay the drying time of the ink on the screen. From this point, *thinning retarder* will be used to describe the combination of 50% thinners and 50% retarder. The squeegee speed and flowcoat speed were both set to $0.4ms^{-1}$, with a squeegee pressure of 4.5b and a snap-off gap of 4.5mm. A scan of the printed image can be seen in Figure 3.6, showing a clear crisp image, with no obvious excessive tone gain. This highlights that the chosen press settings, summarised in Table 3.1, to be appropriate for successful screen-printing

with a blade squeegee. Thus, preliminary press settings have been established that produce successful prints.

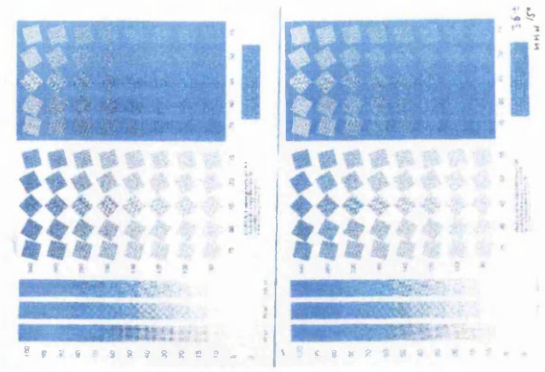

Figure 3.6 Squeegee Blade Printed Image

Ink	Solvent-based
Thinners	15%
Retarder	15%
Squeegee pressure	4.5b
Squeegee speed	0.4m/s
Squeegee Hardness	Medium
Squeegee angle	75° from horizontal
Snap-off gap	4.5mm
Mesh	120-34
Substrate	Hello Silk

Table 3.1 Initial Press Settings

3.5 Preliminary Roller Squeegee Print Trials

Using the press settings that were used in the blade squeegee trials, a series of experiments were undertaken to establish the feasibility of printing using a roller squeegee. However, as graphic printing with a roller squeegee has attracted minimal research, little is known about this variant of the process.

Initial runs were carried out using the 50mm diameter roller squeegee. After the squeegee had traversed the screen, a considerable amount of ink remained on the screen surface. The resultant prints were flooded out and rivulets of ink were created within image areas of more then 30% open area, Figure 3.7. Therefore, this prevented

the tone gain from being measured with the spectrophotometer. In addition, this excessive ink transfer resulted in the substrate adhering to the underside of the screen.

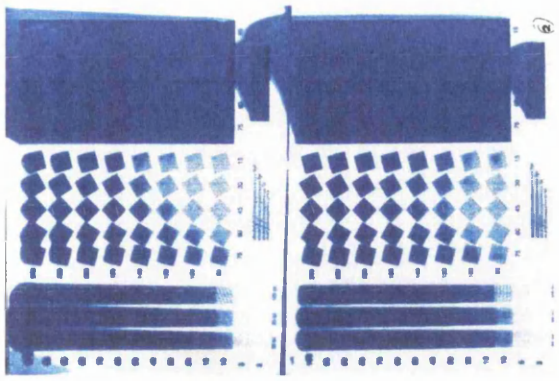

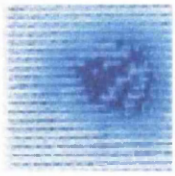

Magnified tonal area containing rivulets

Figure 3.7 Roller Squeegee Printed Image

In an attempt to reduce ink transfer, the squeegee pressure was then increased to 4.5b (to reduce the ink left on the screen surface after the printing stroke) and the squeegee speed increased to its maximum value. However, this produced no improvement in print quality, with the increase in pressure only removing slightly more ink from the screen surface.

To reduce the tack of the ink, which could help prevent the substrate sticking to the screen, quantities (by volume) of 30%, 50% and 75% *thinning retarder* were added to the ink. This prevented the substrate from sticking to the screen, but previous work by *Jewell and Claypole* [62] showed that the addition of thinners increases the tone gain. This proved to be the case, as the reduction in the viscosity of the ink created an increase in tone gain, with only the prints below 10% open area being successfully printed before flooding and rivulets were clearly evident, Figure 3.8.

Figure 3.8 Roller Squeegee Printed Image Flooded Above 10% Open Area

Each of these studies was then repeated using the 30mm diameter roller squeegee. However, excessively high ink transfer still occurred producing rivulets that prevented the samples from being measured.

This initial trial showed that the roller squeegee system produces a significant increase in ink transfer compared with that of a squeegee blade. This occurs to the extent that it makes it impractical to print, and in order to resolve this, further insight is required. A number of possible reasons for the excessive ink transfer were considered, which were explored in the next section. These reasons are the ink not being removed from the screen after the printing stroke, printing screen and contact effects, ink pumping prior to gasketting on the substrate and the increase in hydrodynamic pressure in the nip contact region.

3.5.1 Potential Causes for High Ink Coverage

3.5.1.1 Ink Removal From Printing Screen

As reported in the literature review, a well known factor for influencing the ink film deposit and the image definition is the squeegee failing to remove all of the ink from the screen surface [15], as seen with the roller squeegee. For thick film ink application, blunted or intentionally rounded squeegees can be used as they also fail to remove all of the ink from the screen [6]. The remaining ink on the screen surface is then drawn through the mesh open area, immediately after snap-off, and onto the substrate producing the thick ink deposit.

3.5.1.2 Screen and Contact Effects

Due to the radii of the roller squeegee, the contact width and the contact duration of the squeegee upon the screen will be significantly greater than if a blade squeegee were to be used. Therefore, an increase in the ink deposit would occur.

A further influencing factor for the volume of ink deposited on the substrate is the mesh count of the screen. The screen used in this experiment has 120 threads per cm. If the screen mesh count were to be increased, whilst keeping the same thread diameter, the effective ink volume within the mesh is reduced and the resistance of the ink flow through the screen will be increased. Therefore, less ink can be

transferred to the substrate, producing a thinner ink film and a reduction in tone gain. This model is supported by a screen-printing Ink Transfer Modeller (ITM), developed by *Abbott* [43]. The program calculates the ink film thickness based on a mathematical model with the assumption that free surface energy dominates the ink. The model embodies the *Landau Levich* equation, as mentioned in the literature review, and assumes that the ink is pulled out of the printing screen rather than flowing from it. This model allows the input of a number of screen-printing variables including mesh type, mesh tension, ink rheology and screen set-up. Using this model, the effect of the mesh type upon the ink deposit can be studied by setting the appropriate variables to the specific values used in the previous print trials, including the press settings and the ink type. The values of which can be seen in Figure 3.9.

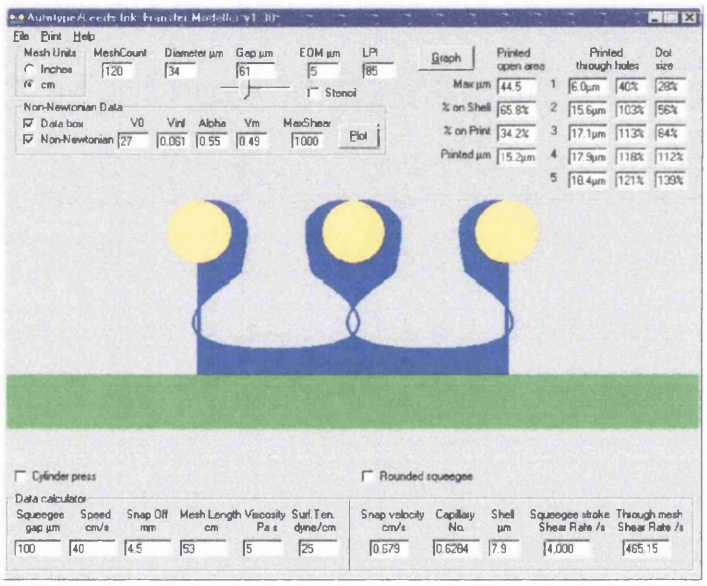

Figure 3.9 ITM Settings for Flatbed press and Ultra Tone Ink

Figure 3.10 illustrates the change in the solid density ink film thickness, resulting from an alteration in the mesh ruling, as calculated with the ITM, whilst maintaining a mesh diameter of 34µm. The figure shows that the ink film thickness reduces as the mesh ruling increases, due to the reduction in the ink volume within the screen. Additionally, increasing the mesh count increases the shear rate, which decreases the viscosity of the ink. This then has the effect of increasing the relative amount of liquid that can transfer from the mesh to the substrate [43].

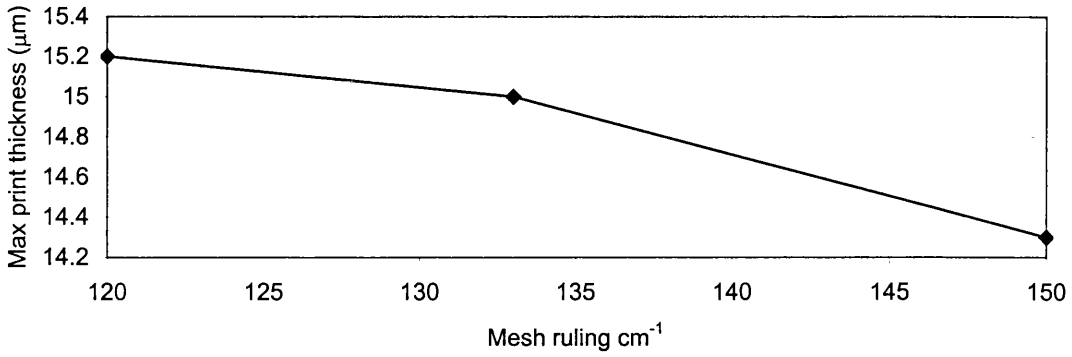

Figure 3.10 Effect of Mesh Ruling Upon Ink Film Thickness

The snap-off gap also effects the ink film thickness, where an increase in snap-off gap increases the snap-off speed and will decrease the ink deposit, as calculated by ITM, Figure 3.11. The snap-off gap also has a strong interaction with the mesh tension, where an increase in the snap-off gap has the effect of increasing the mesh tension. Additionally, a low snap-off gap and low mesh tension can result in the substrate adhering to the screen [63].

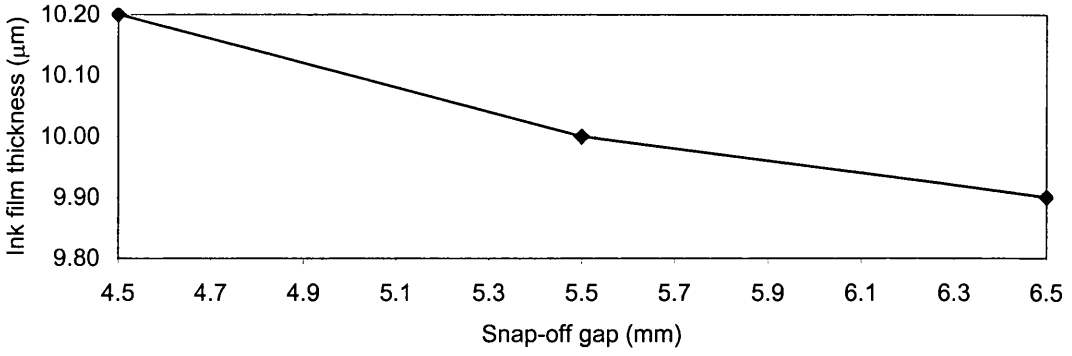

Figure 3.11 Effect of Snap-off Gap and Speed Upon Ink Film Thickness

3.5.1.3 Ink Pumping Prior to Gasketting

The rotational effect of the squeegee could also be inducing hydrodynamic pressure within the ink bow wave that is created by the linear movement of the squeegee. This pressure build up could be forcing the ink through the screen, effectively pre-printing in the bow wave, Figure 3.12. This will result in ink on the under side of the screen being transferred to the substrate in the printing junction. The pressure required to force ink through the screen is further investigated in Appendix A.

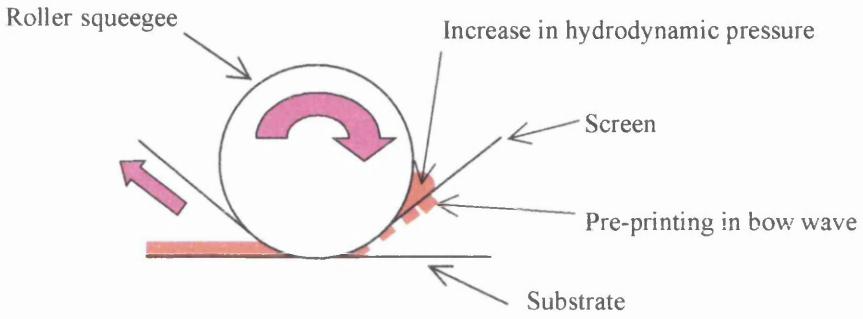

Figure 3.12 Pre-printing in Bow Wave

As stated in the literature review, the pressure generated within the bow wave created by a blade squeegee has previously been investigated [33] [35]. The work by *Jewell et al* used the Computational Fluid Dynamics (CFD) package, FLUENT. By reducing the squeegee angle, this will have a similar effect as if a roller squeegee were to be used. However, without complex modelling, the rotation of the squeegee is not possible as this would necessitate the two moving surfaces pumping the ink in-between the squeegee and the screen. Therefore, at this stage it was deemed appropriate to further discuss *Jewell's* [35] work into reducing the squeegee angle. Using Newtonian ink, the squeegee angle was reduced from 85° to 25° from the horizontal, with the boundary conditions set as in Figure 3.13.

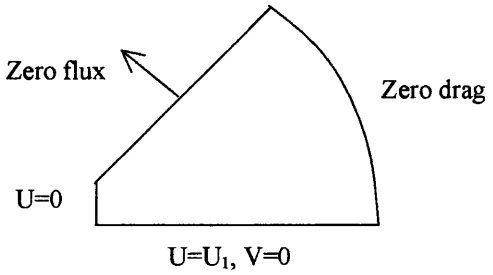

Figure 3.13 Bow Wave Model Boundary Conditions

This was modelled at $0.4ms^{-1}$ and $0.8ms^{-1}$, the results of which can be seen in Figure 3.14. These results show a minimal change in the maximum pressure within the bow wave, indicating that the reduction in the squeegee angle has a minimal effect. These results are further emphasised by Figure 3.15, which show minimal variation in the pressure generated within the ink roll. It can also be noted that the pressure within the bow wave is effectively zero, with the pressure near to the squeegee tip being several orders of magnitude greater than in the ink roll.

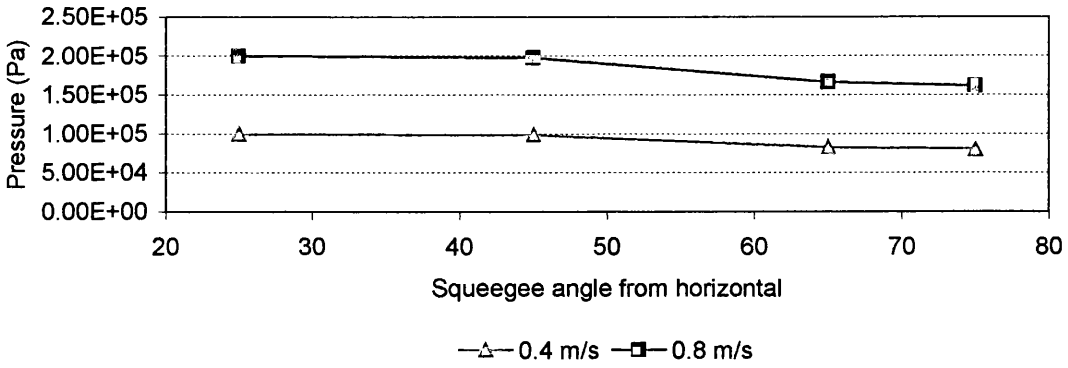

Figure 3.14 Pressure Near to Squeegee Tip, With Alteration in Squeegee Angle

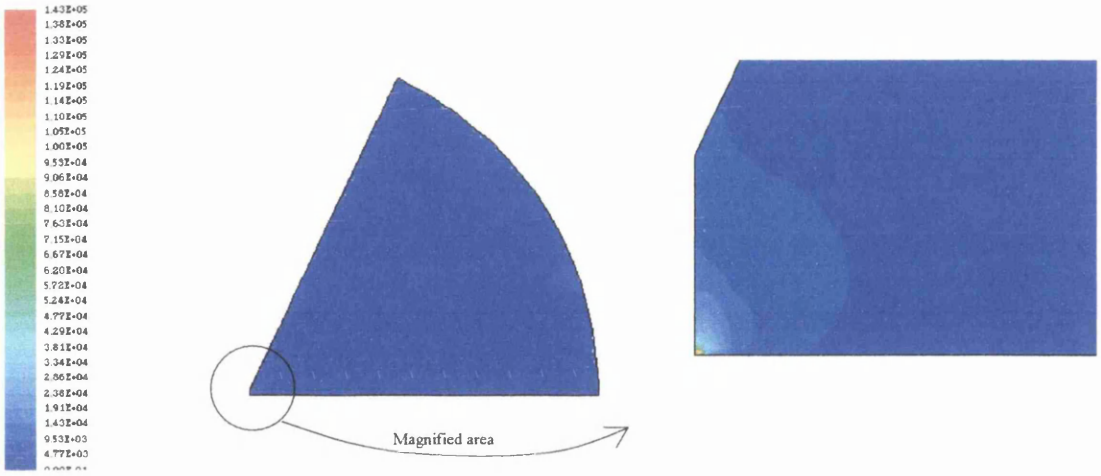

Figure 3.15 Pressure Build Up Within Ink Roll and Close Up of Pressure at Squeegee Tip.

3.5.1.4 High Pressure Generation

A further cause of increased tone gain could be the rotating action of the squeegee. This action effectively produces two moving surfaces, the rotating squeegee and the screen, as opposed to one moving surface when a fixed blade squeegee is drawn over the screen. Therefore, when a roller squeegee is used, theoretically the hydrodynamic pressure within the ink film will be doubled. Clearly, this will lead to a significant increase in ink flow through the screen and onto the substrate, Figure 3.16. This is a well know phenomenon in fluid dynamics and was highlighted by *Hawkyards* [55] paper describing rotary screen-printing.

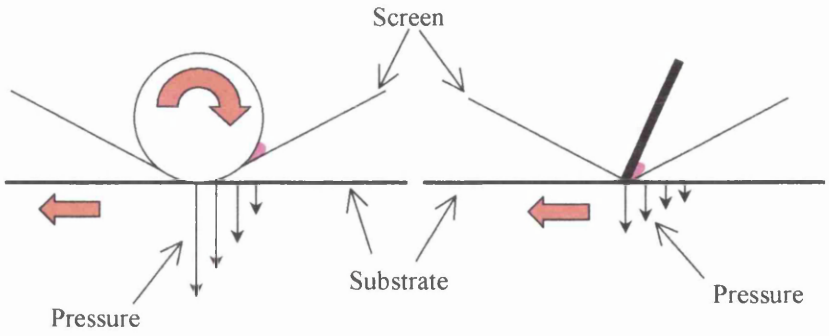

Figure 3.16 Schematic of Pressure Distribution With Roller and Blade Squeegee

3.6 Closure

This chapter has described in detail the set-up of the screen-printing press on which trials were performed. To establish the feasibility, runs using conventional squeegees and the new roller squeegee were performed.

The initial trials with the *Ultra tone* using a blade squeegee produced clear and sharp images under similar press settings. However, when the conditions were replicated using roller squeegees, excessive ink transfer occurred. A number of reasons were postulated that could explain the high ink coverage. This pointed to a need to increase the flow resistance through the screen and to reduce the volume of ink within the screen open area. The next chapter will focus on further investigations to explore means of achieving this.

Chapter 4

Secondary Experimental Study

4 Secondary Experimental Study

4.1 Introduction

The initial print trials discussed in the previous chapter, using the 120-34 screen and the *Ultra-Tone* ink, showed excess ink coverage leading to the image being flooded and containing rivulets. Following the arguments in the preceding chapter, this led to the 120-34 screen being replaced with a 150-34 screen to reduce the ink deposit by increasing flow resistance and reducing screen volume. Also, a conventional UV system *(UVspeed)* and a solvent-based system containing 20% thinning retarder *(Mattplast)* was used to provide a comparison between different ink types that have different viscosity levels. In this case, the resultant prints were clear and sharp and absent from excessive tone gain and rivulets, Figure 4.1.

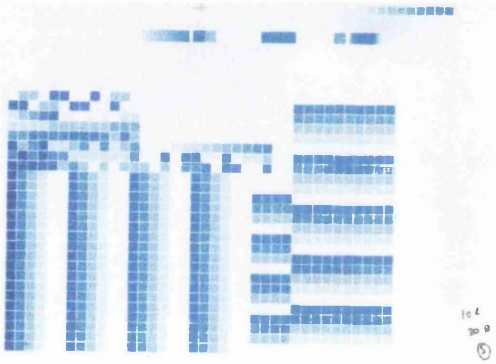

Figure 4.1 Roller Squeegee Printed Sample Using 150-34 Screen

On achieving a good print, the aim of this chapter is to fully explore the process parameters to developing a clear understanding of the application of roller squeegees in screen-printing. The experiments are divided into three separate sections, with the initial section exploring a broad range of process parameters to identify the most suitable conditions for successful screen-printing using the roller squeegee. The second series of experiments focuses on a test schedule to establish the importance and the effect of the previously investigated parameters, using an orthogonal array approach. The final section is a confirmation study into roller squeegee screen-printing used to explore and develop a more detail understanding derived from the previous experiments.

In planning the experimental strategy, consideration was given to isolate individual mechanisms. However, the interaction between process variables prevented clear isolation of effects, but as the results are presented, explanations are suggested and the numerical models in Chapter 5 will be used to gain further insight.

4.2 Roller Squeegee Feasibility Study

This section is a further investigation into roller squeegee screen-printing, with the aim of obtaining the correct press and parameter settings needed to print successfully with a roller squeegee. Once this study has been completed, the knowledge gained will be used to further develop the characteristics and understandings of roller squeegee screen-printing.

4.2.1 Introduction

An experimental programme was devised to explore process parameters with attention focused on the interface between the squeegee and screen subsystem. In this instance the parameters of screen tension, snap-off gap, flow-coat speed and flood-coat gap were maintained constant as itemised in Table 4.1. At this stage in the studies, it was decided that the investigation of these particular parameters was not warranted until the direct effect of the squeegee and the other more relevant press parameters were investigated.

Parameter	Mesh tension	Snap-off gap	Flow-coat speed	Flow-coat gap
Setting	$15Ncm^{-1}$	4.5mm	$0.4ms^{-1}$	0.5mm

Table 4.1 Fixed Press Settings

Also, to remove as much ink as possible from the printing screen after the printing stroke, the squeegee pressure was set to the maximum pressure of 4.5bar. The two roller squeegees were then used to print with the conventional UV and the solvent-based ink at speeds of $0.2ms^{-1}$, $0.4ms^{-1}$ and $0.8ms^{-1}$, with the roller squeegee rotating and locked. A comparison could then be made between prints produced with the squeegee rotating and not rotating. In a full factorial analysis, this leads to 24 individual experimental conditions as summarised in Table 4.2.

Speed (status)	Ink type		Squeegee diameter	
0.2 ms^{-1} (Rotate)	Solvent-based	Conventional UV	30mm	50mm
0.4ms^{-1} (Rotate)	Solvent-based	Conventional UV	30mm	50mm
0.8ms^{-1} (Rotate)	Solvent-based	Conventional UV	30mm	50mm
0.2ms^{-1} (Locked)	Solvent-based	Conventional UV	30mm	50mm
0.4ms^{-1} (Locked)	Solvent-based	Conventional UV	30mm	50mm
0.8ms^{-1} (Locked)	Solvent-based	Conventional UV	30mm	50mm

Table 4.2 Feasibility Study Experimental Programme

For completeness and for a comparative evaluation, a number of printed samples were produced with a blade squeegee. These were then analysed against the characteristics of the samples produced by the roller squeegee. A medium hardness squeegee (of approximately 70 Shore A hardness), was set at 15° from the vertical, with a squeegee pressure of 4.5bar. The remaining parameters were set to those in Table 4.1

To minimise experimental error, five prints were prepared at each test condition and the measurement results averaged. The print quality was measured using a spectrophotometer configured to measure density from which tone gain characteristics can be recovered via the Murray-Davies equation [60] (refer to Section 3.3). This would then allow a comparison to be made of the change in density of each individual print and also an assessment of the printed area coverage compared to the required area coverage, resulting from the alteration of the press parameters.

4.2.2 Density Evaluation

The density measured on the half tone patches, for the conventional UV ink, printed with the blade squeegee and the 30mm and 50mm diameter roller squeegees, are depicted in Figure 4.2 to Figure 4.7. Here, open areas below 15% have failed to print due to the tone loss encountered.

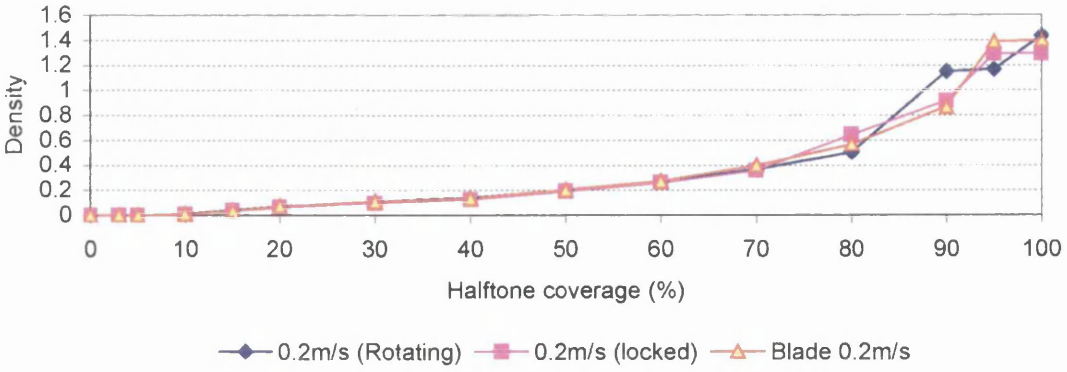

Figure 4.2 Density For 30mm Squeegee at 0.2ms^{-1}, Conventional UV Ink

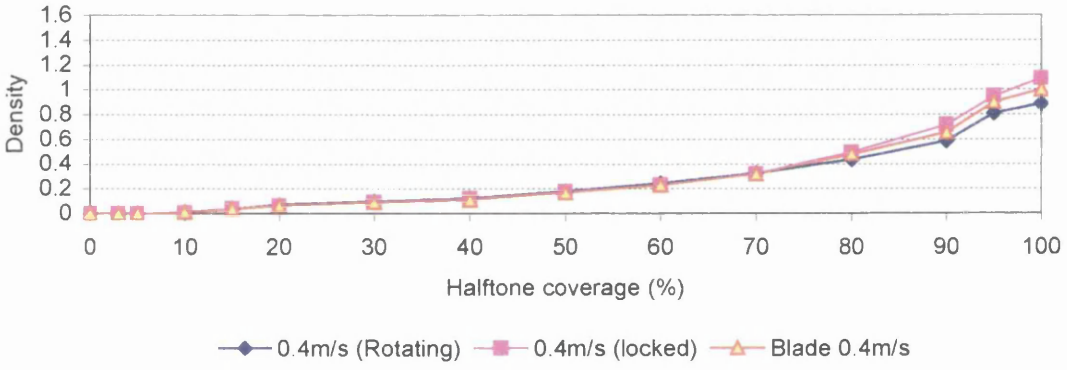

Figure 4.3 Density For 30mm Squeegee at 0.4ms^{-1}, Conventional UV Ink

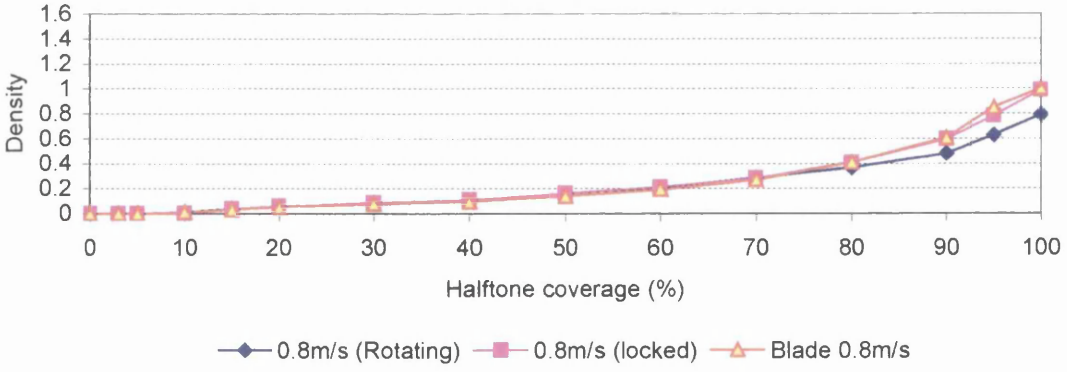

Figure 4.4 Density For 30mm Roller at 0.8ms^{-1}, Conventional UV Ink

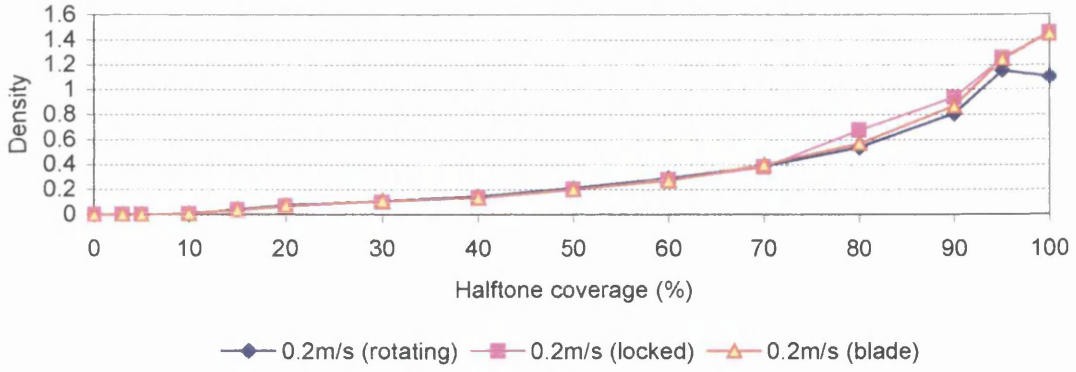

Figure 4.5 Density For 50mm Squeegee at $0.2ms^{-1}$, Conventional UV Ink

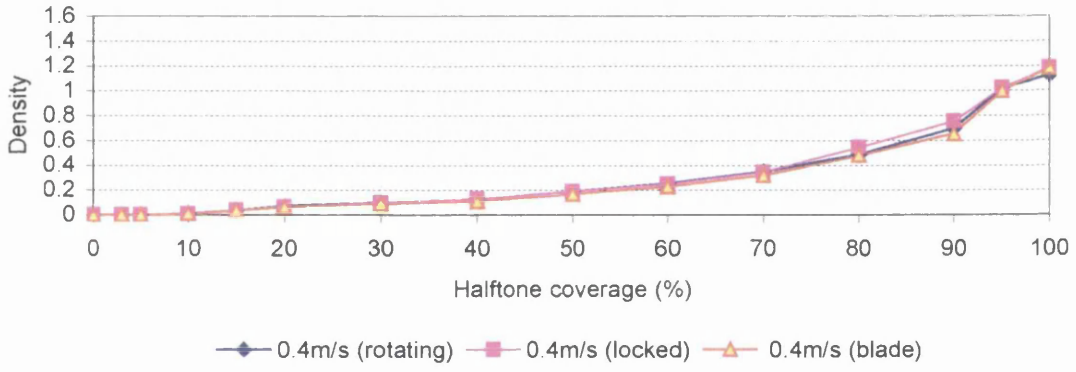

Figure 4.6 Density For 50mm Squeegee at $0.4ms^{-1}$, Conventional UV Ink

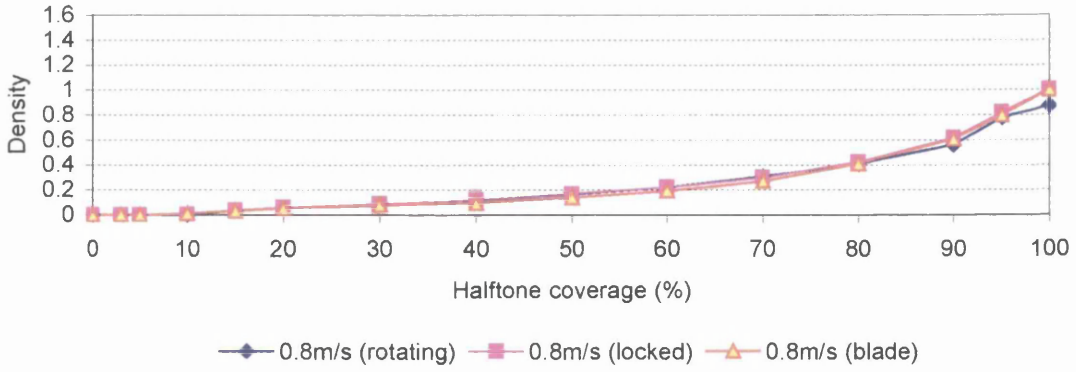

Figure 4.7 Density For 50mm Squeegee at $0.8ms^{-1}$, Conventional UV Ink

The general trend for the roller squeegees is for less ink to be deposited as the printing speed is increased. This may be attribute to either a reduced contact duration or snap-off speed, but there are conflicting results. A numerical evaluation has shown that as the speed increases, the snap-off speed also increases, which has the effect of reducing the ink deposit [43]. This was highlighted using experimental studies with a cylinder screen-printing press, which resulted in an increase in printing speed, reducing the ink deposit [64] [65]. However, contrary to this, experimental studies on a flat-bed screen-printing press have shown that an increase in printing speed will increase the ink deposit, although no valid explanation was given for this phenomenon [66]. Additionally, a recent extensive experimental study has shown that an increase in snap-off speed increases the ink deposit [67].

These conflicting results can probably be attributed to the different process mechanics and the difference in printing speeds that are exhibited within the different styles of screen-printing. However, more importantly, the results also highlight that very little is known about the physics within the screen-printing process, leaving a substantial area of further work to be carried out.

The results from the roller squeegee experiments show a minimal change in print density in the mid-tone and highlight regions, with the variation of speed and squeegee rotation having a significant effect on the print density when printing above an open area of 70%. The tendency for the blade squeegee is to produce slightly lower ink deposits than the locked squeegee, but unexpectedly, a higher ink deposit than the rotating squeegee at the corresponding speeds. It would be expected that the locked roller squeegee would deposit a higher amount of ink than the blade squeegee, as previous work has shown that the smaller the effective squeegee angle and the rounder the squeegee tip, the more ink is deposited onto the screen surface [15] [68]. This has been attributed to the rounder squeegee tip allowing a greater amount of ink to pass under the squeegee blade, increasing the amount of ink that can pass through the mesh openings. Additionally, the round squeegee leads to a larger contact area, an extended contact duration and a reduction in snap off speed. The rotating squeegee would be expected to produce a higher ink deposit than the locked squeegee and the blade squeegee, due to the increase in hydrodynamic pressure within the nip contact region. An increase in ink deposit would then be anticipated due to an enhanced flow

through the screen, but as shown from Figure 4.2 to Figure 4.7 the ink deposit reduces for the rotating squeegee.

There are a number of possible reasons why the rotating squeegee produces a lower print density than the locked squeegee. Under conditions created by the locked squeegee, significantly higher shearing action occurs within the ink, leading to a reduction in viscosity as the ink shear thins due to the high shearing action near the screen suirface. Through modelling, this has been shown to increase the relative amount of ink that can be transferred through a printing-screen [43] and this has also been supported by experimental investigations [62]. Therefore, a reduction in the ink viscosity adjacent to the screen surface will increase the ink flow through the screen, increasing the ink deposit. This suggests the dominant effect of the shear mechanism over the pressure mechanism in ink transfer for this squeegee system.

Upon close visual inspection of the printing process in which the squeegee was locked, it was apparent that the screen was adhering to the substrate immediately after the point of contact with the screen, Figure 4.8. As the speed was increased, the extent of adhesion was reduced. This occurred until a speed of $0.8ms^{-1}$ was reached where the screen appeared to no longer adhere to the substrate, possibly due to either the reduction in contact time with the increased speed or the increase in snap-off speed.

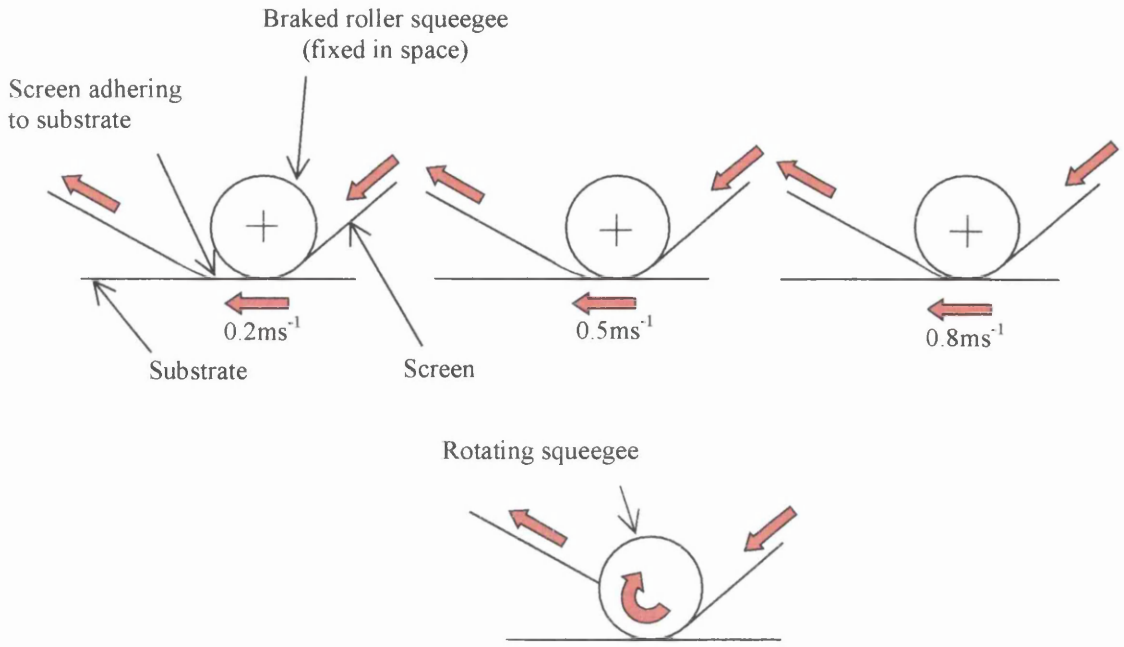

Figure 4.8 Screen Adhering to Substrate at Respective Speeds

For the rotating squeegee, the rotating action of the squeegee effectively peels the screen from substrate surface, preventing adhesion between these components and this is also contrasted schematically in Figure 4.8. This has the effect of increasing the snap-off speed and reduces the contact time with the screen and according to previous work, this will reduce the ink deposit [68]. This also supports the trends that were observed in Figure 4.2 to Figure 4.7.

To prevent the screen from adhering to the substrate, the mesh tension can be increased and this will affect the snap off speed indirectly. Also, by increasing the snap-off gap, the snap-off speed is increased and this may further reduce the ink deposit. An additional experimental study into the snap-off gap was carried out to investigate this. Details of this will be discussed more fully later in the chapter.

4.2.3 Tone-gain Evaluation

During the printing process, many factors affect the size and consistency of the dots that make up the halftone areas. The variation in the size of these dots is referred to as the *tone gain* and this reflects the increase in the halftone coverage from the actual halftone coverage that is required as defined by the original image. Therefore, a perfectly reproduced print will have a tone gain of zero throughout the halftone coverage. For this reason, it is important to establish what effect the roller squeegee

will have upon the reproduction of the halftone areas. However, it must also be noted that the tone gain is calculated using the individual area coverages and the density of the solid area. Therefore, an absolute comparison between two tone gain curves must account for possible differences in the solid densities. The current comparisons are normalised with respect to solid density and may be considered as relative tone gain. This is suitable for comparing process effects.

The tone gain characteristics, that correspond to the previous density plots, are shown in Figure 4.9 to Figure 4.14. In each case, the tonal plots show a considerable amount of tone loss for the 30mm and the 50mm diameter squeegees, with no tone gain occurring until printing above an open area of 80%. The curves show that the decrease in tone gain for the roller squeegee at the higher speed is consistent with the results from the blade squeegee. Indeed, the blade squeegee results show a lower value of tone gain than the roller squeegees. Following the preceding conflicting information, the reasons are not precisely clear. However, this may be attributed to the smaller contact point of the blade squeegee. This will limit the amount of ink that is likely to produce the tone gain. This can also explain the slightly lower tone gain observed for the 30mm diameter squeegee when compared with the 50mm diameter squeegee, where the smaller squeegee is in contact with the substrate for less time and the snap-off speed is slightly higher. The tone gain produced by the rotating squeegee is generally greater than that produced with the locked squeegee at a similar printing speed for both squeegees. Again, this may be attributed to the mechanisms highlighted previously concerning the relative importance of pressure and shearing mechanisms at the screen surface. The gain characteristics appear to be influenced by the higher pressure associated with the rotational squeegee.

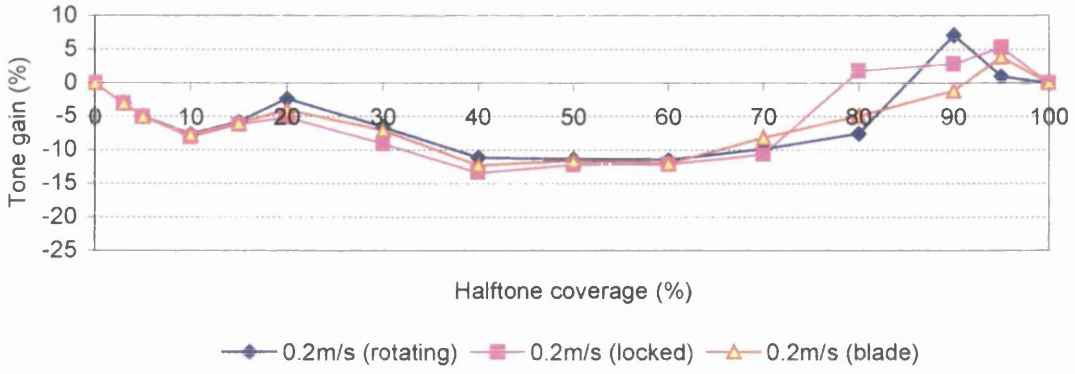

Figure 4.9 Tone Gain For 30mm Squeegee at $0.2ms^{-1}$, Conventional UV Ink

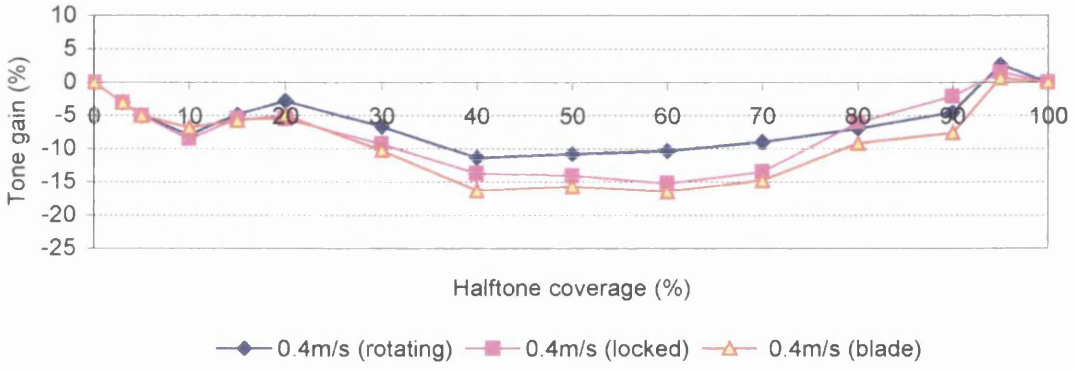

Figure 4.10 Tone Gain For 30mm Squeegee at $0.4ms^{-1}$, Conventional UV Ink

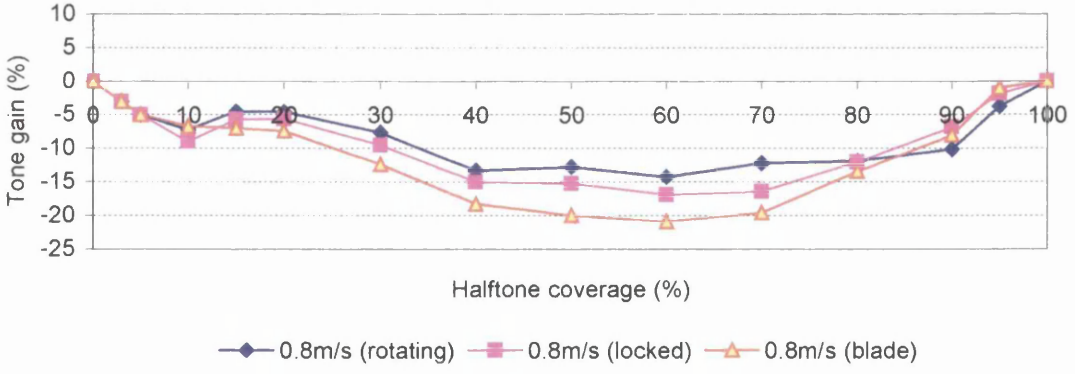

Figure 4.11 Tone Gain For 30mm Squeegee at $0.8ms^{-1}$, Conventional UV Ink

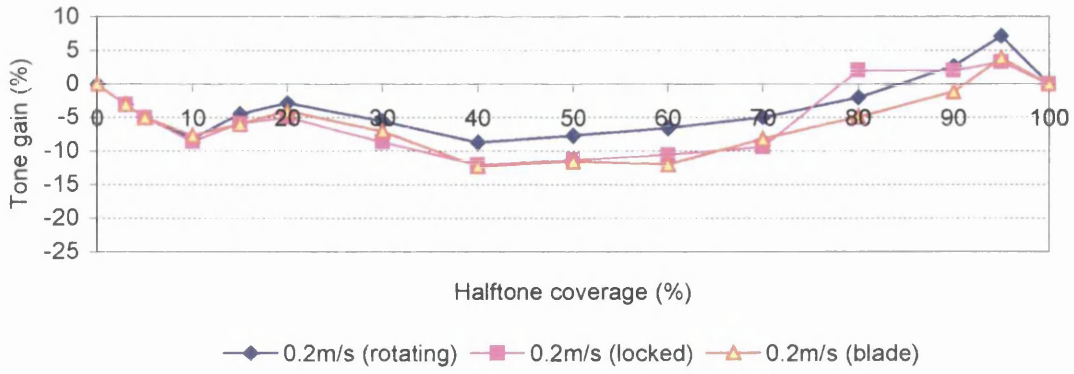

Figure 4.12 Tone Gain For 50mm Squeegee at $0.2ms^{-1}$, Conventional UV Ink

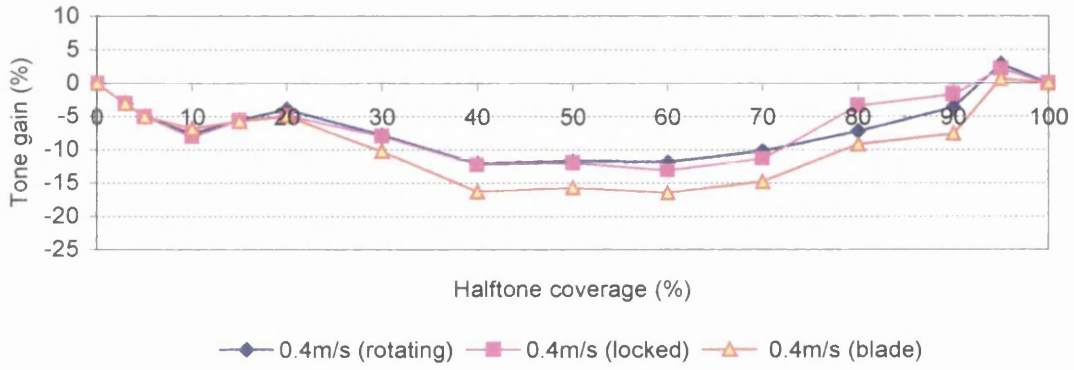

Figure 4.13 Tone Gain For 50mm Squeegee at $0.4ms^{-1}$, Conventional UV Ink

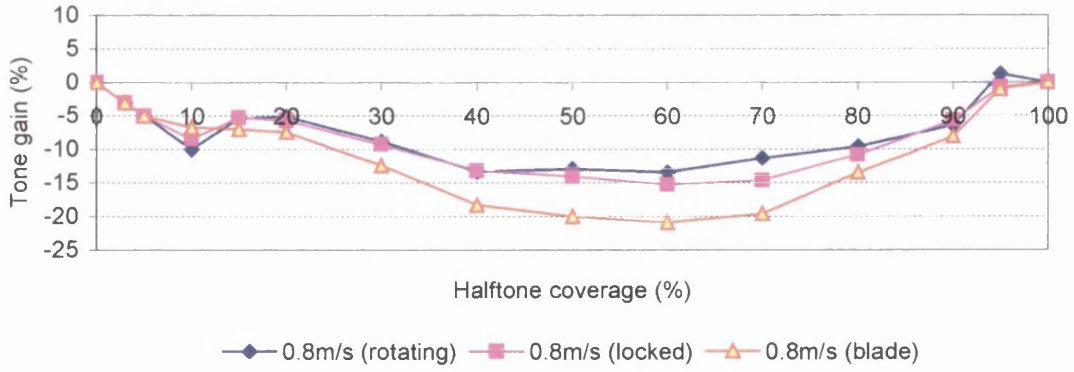

Figure 4.14 Tone Gain For 50mm Squeegee at $0.8ms^{-1}$, Conventional UV Ink

4.3 Comparison of Ink Types

The previous trials were carried out with *UVspeed* ink, which is a conventional UV ink. To further develop the understanding of roller squeegee screen-printing, an additional series of experiments were carried out using a different ink whilst printing at the same press settings as the previous experiments. This ink type was a solvent-based ink, known as *Mattplast*. The manufacturers of this ink do not recommend that this ink is used in conjunction with a 150-34 screen as the volume of ink within the mesh openings is sufficiently small enough for the ink to dry in the screen before it is printed. However, the previous experimental trials showed that, when using a roller squeegee, a quantity of ink remained on the screen surface after the printing stroke. Thus, the ink is less likely to dry in the screen. Therefore, it was deemed appropriate to use this ink with the specified screen resolution. The viscosity profiles of the ink types can be found in Appendix B. The viscosity of the conventional UV ink can be seen to be significantly higher than the solvent-based ink because the latter includes the addition of the thinners and retarder.

4.3.1 Density Evaluation

When the blade squeegee was used to print the solvent-based ink, all the ink from the screen surface was removed and the ink within the open areas of the mesh dried in. This prevented the solvent-based ink from being printed with a blade squeegee. However, this did not occur when the roller squeegee was used, thus, the volume of ink was sufficient to prevent it from drying in the mesh.

The density plots for the prints produced using the solvent-based ink, for the 30mm and 50mm diameter squeegees are shown in Figure 4.15 to Figure 4.20. These show a higher maximum ink density for the larger diameter squeegee when compared with the smaller squeegee. However, in each case, the density of the 100% open area maintains a level of 1.2 for both squeegee diameters, but falls from a different maximum for each roller size as 100% coverage is achieved. In screen-printing, a higher ink density is often produced in the shadow regions [62] [69]. This occurs since sufficient ink is transferred in the shadow region to produce a solid printed area. The larger deposit in the shadow region is a result of ink being deposited from within the volume of the mesh together with the volume of ink contained within the stencil.

Under some circumstances, the rotating squeegee gives a higher print density than the locked squeegee. This is affected by speed and open area. Generally, the density is lower for the smaller squeegee when subject to rotation and conversely for the larger squeegee. In this instance, the lower density for the smaller diameter roller may be caused by reduced contact duration, whereas pressure may be more important for the larger diameter squeegee. However, further work into this phenomenon is required and will be investigated later in the thesis.

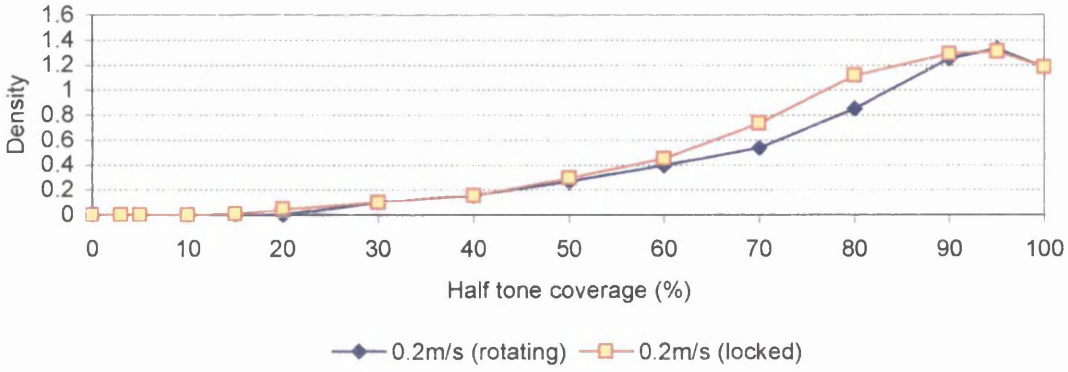

Figure 4.15 Density For 30mm Squeegee at $0.2ms^{-1}$, Solvent-based Ink

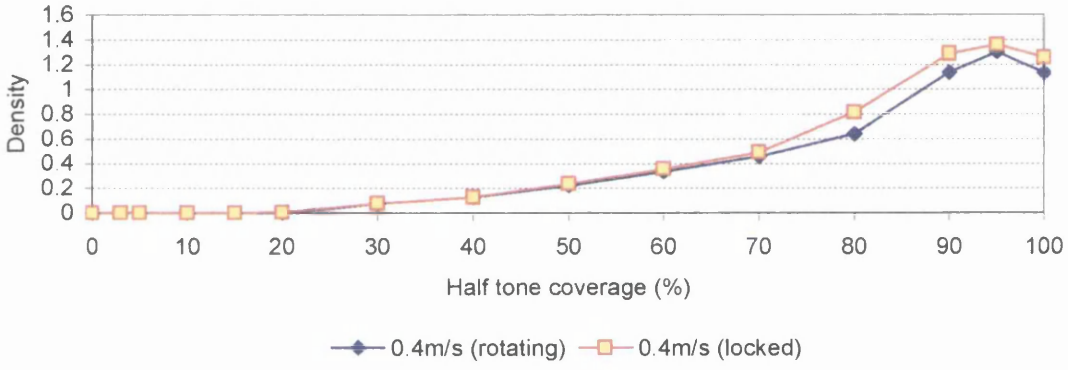

Figure 4.16 Density For 30mm Squeegee at $0.4ms^{-1}$, Solvent-based Ink

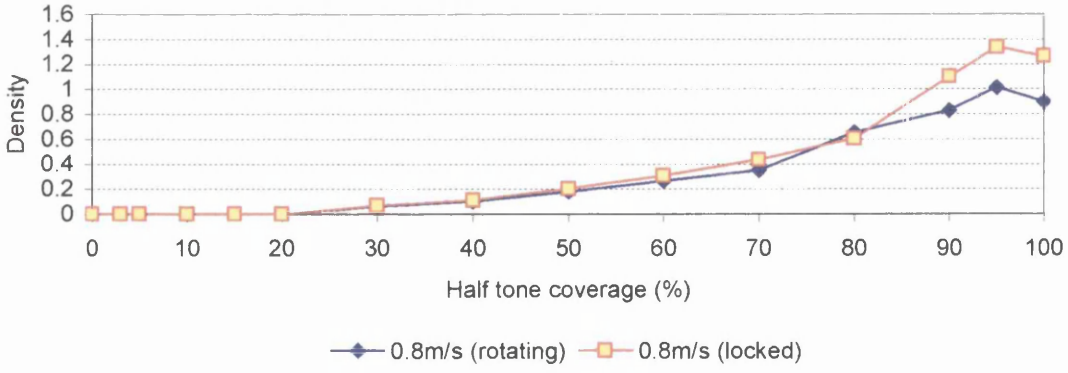

Figure 4.17 Density For 30mm Squeegee at $0.8ms^{-1}$, Solvent-based Ink

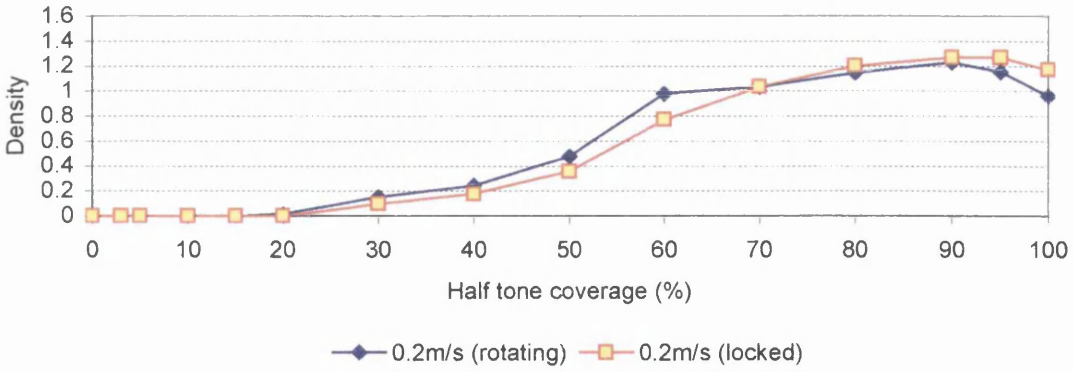

Figure 4.18 Density For 50mm Squeegee at $0.2ms^{-1}$, Solvent-based Ink

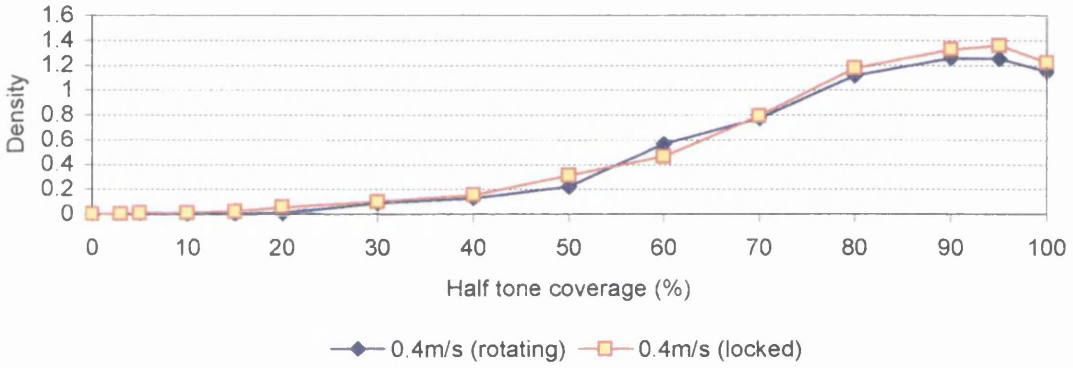

Figure 4.19 Density For 50mm Squeegee at $0.4ms^{-1}$, Solvent-based Ink

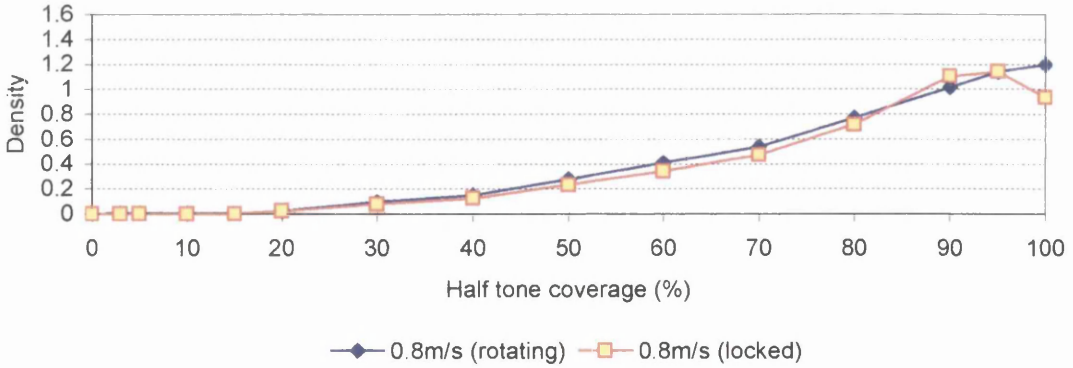

Figure 4.20 Density For 50mm Squeegee at $0.8ms^{-1}$, Solvent-based Ink

4.3.2 Tone-gain Evaluation

The tone gain plots for the solvent-based ink, printed with the 30mm and 50mm roller squeegees, both indicate tone loss in the highlight region and tone gain in the shadow regions, Figure 4.21 to Figure 4.26. As the diameter is increased, the tone gain increases due to the mechanisms that were described previously. However, the difference in the tone gain between the two roller squeegees is considerably greater than that observed with the previously investigated ink.

For the 30mm diameter squeegee, the tone loss was sufficient to prevent the majority of press settings from printing below the 20% open area. Conversely, when printing at the slower print speeds, there was sufficient tone gain to produce a solid area when printing above 90% area coverage. Generally, the prints produced with the braked squeegee have a greater tone gain than those prints produced with the rotating squeegee. As the print speed is increased, this difference in tone gain resulting from the squeegee rotating and not rotating reduces. This occurs until a speed of $0.8ms^{-1}$ is achieved, where at this speed, the difference is insignificant when printing below 70% open area.

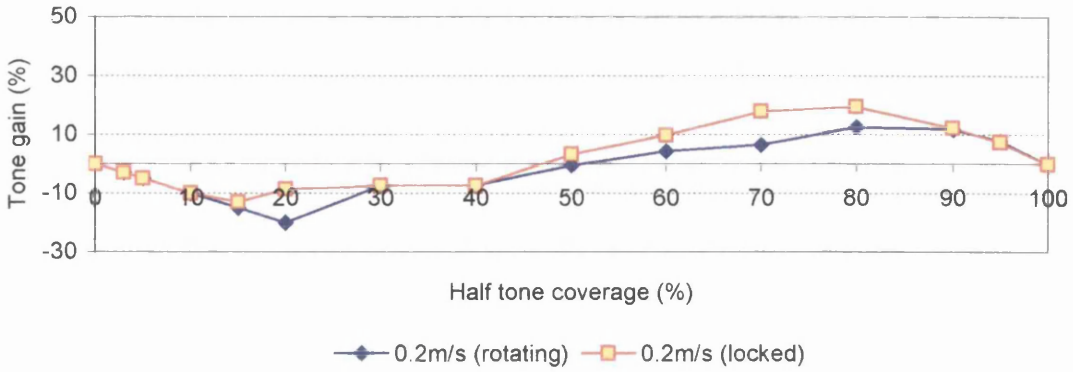

Figure 4.21 Tone Gain For 30mm Squeegee at 0.2ms^{-1}, Solvent-based Ink

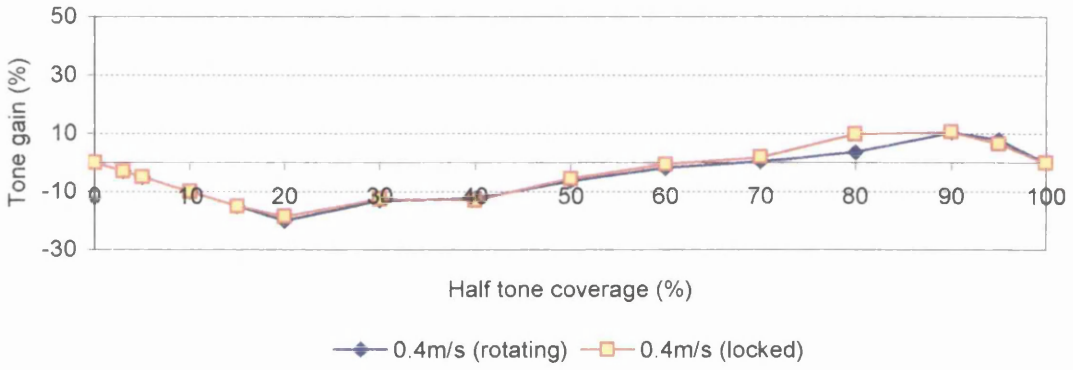

Figure 4.22 Tone Gain For 30mm Squeegee at 0.4ms^{-1}, Solvent-based Ink

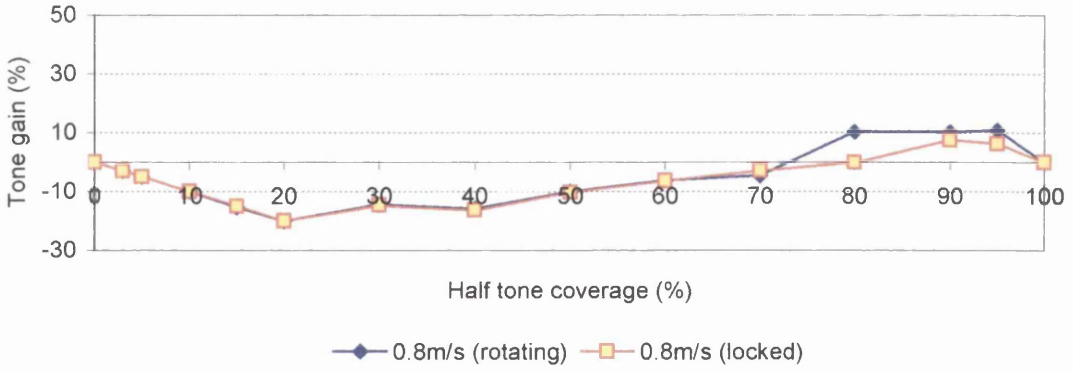

Figure 4.23 Tone Gain For 30mm Squeegee at 0.8ms^{-1}, Solvent-based Ink

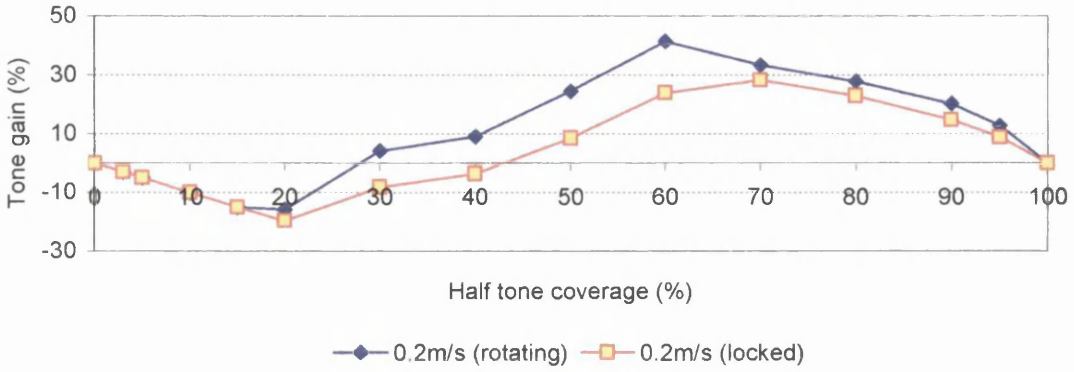

Figure 4.24 Tone Gain For 50mm Squeegee at 0.2ms^{-1}, Solvent-based Ink

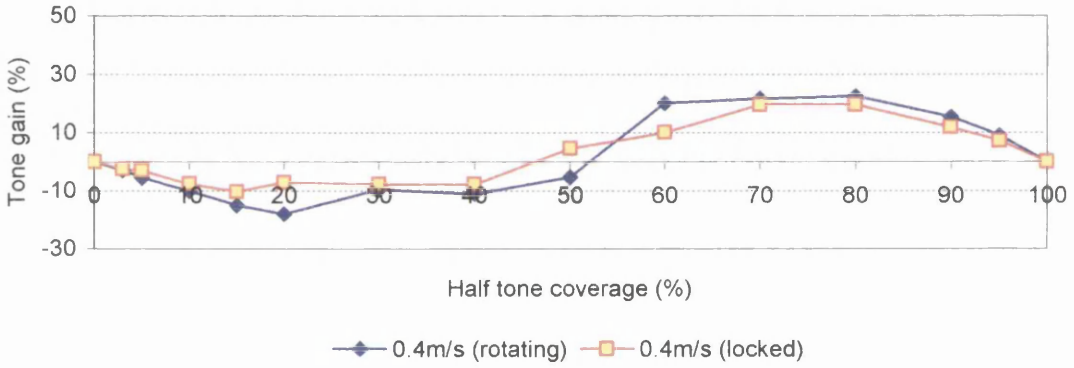

Figure 4.25 Tone Gain For 50mm Squeegee at 0.4ms^{-1}, Solvent-based Ink

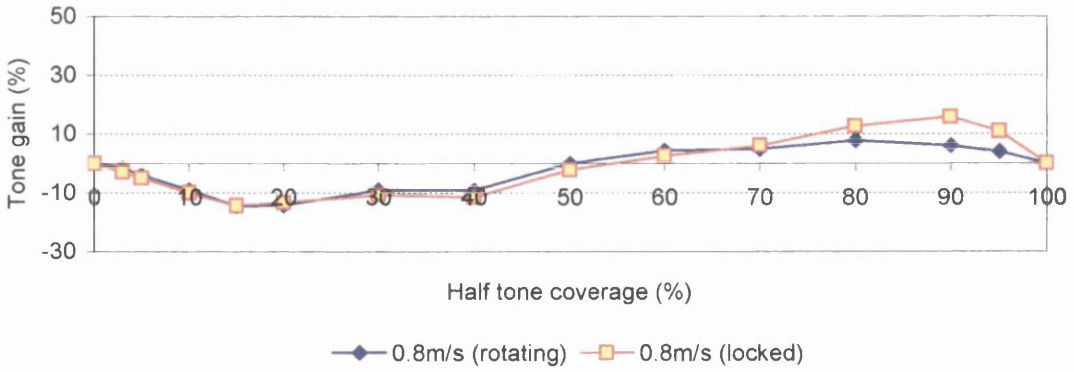

Figure 4.26 Tone Gain For 50mm Squeegee at 0.8ms^{-1}, Solvent-based Ink

4.4 Summary Comments

From this initial successful investigation of printing using the roller squeegee, the common trend for each squeegee scenario is for the ink deposit to reduce as the print speed increases. This sometimes occurs with traditional blade squeegees, but the extent to which this occurs is dependent upon the press configuration and the squeegee type. Possible reasons for this reduction in ink deposit with an increase in speed is likely to be because of a reduced contact duration of the squeegee upon the screen or the alteration in snap-off speed. This reduction in contact duration will have the effect of limiting the ink flow though the screen. This could also explain the difference in the ink deposits created by the different squeegee diameters.

The locked squeegee repeatedly produced a higher ink deposit than the rotating squeegee, despite there theoretically being more hydrodynamic pressure distribution within nip junction present when the squeegee is rotating. Two possible theories have been postulated for this occurrence. One theory is the shearing action of the locked squeegee, which will reduce the viscosity of the ink and aid the flow through the print screen increasing the ink deposit. The second theory was the adhesion of the screen to the substrate when the squeegee was locked, reducing the snap-off speed of the screen, creating an increase in ink coverage. A further investigation into the effect of increasing the snap-off gap when using the roller squeegee for screen-printing will be set out later in the chapter.

4.5 Process Parameter Investigation

Having completed the preliminary study and establishing feasible printing conditions, an orthogonal array experiment was carried out to evaluate the effect of screen-printing parameters when printing with a roller squeegee. This will enable the identification of the parameters that need to be closely controlled and the parameters that may be relaxed. The conventional UV ink was used in preference to the solvent-based ink, since it is likely to be a more appropriate system in application as stipulated in the specification for the high-speed belt press design.

4.5.1 Strategic Approach

An orthogonal array technique was chosen since it enables the parameters associated with the roller squeegee to be studied fully while reducing the number of experiments that need to be carried out. It also allows the interactions between the parameters to be studied. An L_8 orthogonal array was used to investigate the effect of the two different squeegee diameters, squeegee pressure and squeegee rotation. The array chosen only investigates two levels for each parameter, and therefore assigns a linear dependence. However, this array was chosen due to two squeegees being available that could be either locked or free to rotate. Additionally, a high squeegee pressure is required to remove the ink from the screen and the alteration of the squeegee pressure is unlikely to have a large effect on the print due to the rigid nature of the squeegee and the lack of local tip deformation that is associated with a blade squeegee [19]. Therefore, the pressures were set to 3.5b and 4.5b. The experiment settings are itemised in Table 4.3, where the structure dictates the experimental procedure and the analysis strategy. The structure of the orthogonal array allows the effect of the variance of a single parameter to be studied, where the effect of the remaining parameters average each other out through the design of the array. If the reader is unfamiliar with orthogonal array techniques, a further explanation can be found in *Phadke* [70]. The array also allows interactions to be studied, i.e.; when the effect of varying both parameters together is greater than the effect of varying any one of them. The interactions studied were between the squeegee diameter/squeegee pressure, squeegee diameter/squeegee rotation and the squeegee pressure/squeegee rotation, and these are summarised graphically in Figure 4.27. To investigate the effect of speed, the experimental procedure defined in the matrix was carried out three times, once for each print speed. These speeds were now set to $0.4ms^{-1}$, $0.6ms^{-1}$ and $0.8ms^{-1}$. These speeds were chosen to investigate high-speed applications, whilst studying the effect of the individual parameters throughout a broad range of press speeds, as the previous trials exhibited a strong speed dependency. In addition, testing more than two print speeds will indicate whether the speed has a linear effect on the print characteristics of density and tone gain.

Exp.	Squeegee diameter (1)	Squeegee pressure (2)	Interact (3)	Squeegee lock (4)	Interact (5)	Interact (6)	Noise (7)
1	30mm	3.5b	1	On	1	1	1
2	30mm	3.5b	1	Off	2	2	2
3	30mm	4.5b	2	On	2	2	2
4	30mm	4.5b	2	Off	1	1	1
5	50mm	3.5b	2	On	1	1	2
6	50mm	3.5b	2	Off	2	2	1
7	50mm	4.5b	1	On	2	2	1
8	50mm	4.5b	1	Off	1	1	2

Table 4.3 L_8 orthogonal array [71]

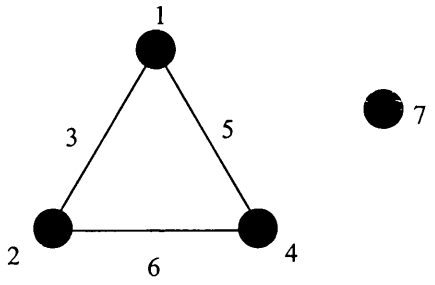

Figure 4.27 Corresponding Linear Graph For L_8 Orthogonal Array [71]

The test was carried out through a continuous run and so to ensure the effect of altering the parameters had taken place, three samples were printed and discarded. A further ten samples were then printed and measured at these experimental settings. This allows the process to settle following any change and furthermore enables the variation in print consistency to be studied, whilst minimising any experimental error that may be present by averaging the results. In addition, printing ten samples also allows the standard deviation to be assessed. As with the previous studies, the results are presented with the density plots preceding the tone gain curves.

4.5.2 Density Evaluation

The standard deviation for each experiment showed that minimal variation occurs throughout each experiment, with Table 4.4 indicating the typical standard deviation for print density that was achieved, verifying a consistent and reproducible printing process.

Halftone coverage	Average density	Standard deviation
100	1.13	0.031
95	0.604	0.022
90	0.474	0.015
80	0.34	0.008
70	0.247	0
60	0.183	0
50	0.132	0.004
40	0.09	0
30	0.07	0
20	0.05	0
15	0.02	0
10	0	0
5	0	0
3	0	0
0	0	0

Table 4.4 Standard Deviation Associated with Measurements

The change in print density, created by the variation of the press parameters can be seen in Figure 4.28 to Figure 4.38, where any variation in the solid print density of above 0.08 will be visible to the unaided eye [72].

The effect of the squeegee diameter upon print density for the three print speeds is shown in Figure 4.28 to Figure 4.30. For clarity, the alteration in density resulting from the change in speed for the 30mm diameter squeegee is shown in Figure 4.31 and a similar trend was seen for the 50mm diameter squeegee. As the print speed increases, the density reduces in a similar trend to that calculated with the ITM. To highlight this, Figure 4.32 [43] shows the predicted trend in ink deposit using the ITM software, as mentioned in the previous chapter. These results use the screen and conventional UV ink properties together with the corresponding process settings. The

decay in ink film thickness is approximately linear, in a similar trend to the decrease in density, therefore, lending support to the explanation. Here, the ink deposit reaches its lowest value as the speed achieves its maximum. However, it must also be noted that as the speed increases, so the contact duration of the squeegee upon the screen reduces, which will reduce the quantity of ink flow onto the substrate.

As the squeegee diameter increases, the ink density also increases, with a minimal effect on open areas below 80%. This increase in diameter decreases the included angle between the squeegee and the mesh. Past studies have shown this to be a dominant factor for the ink deposit, which increases as the squeegee angle is reduced [16] [73]. Additionally, the 50mm diameter squeegee has a greater contact area and duration on the screen, which will also lead to an increase in the ink deposit [68].

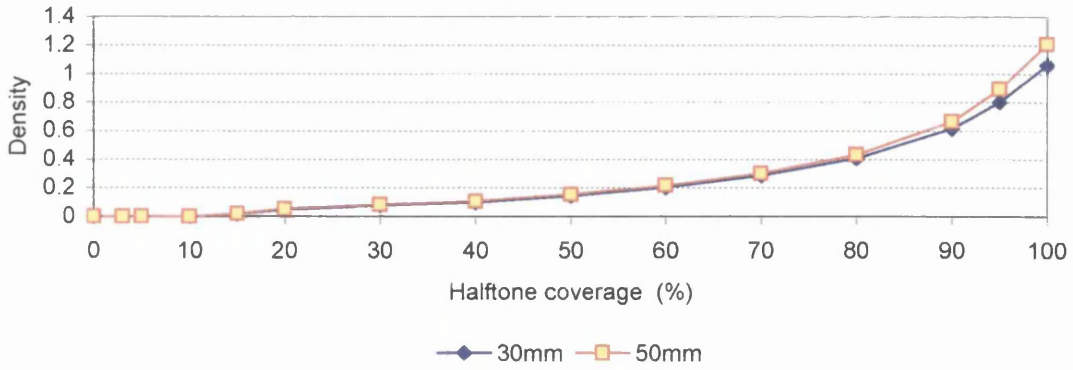

Figure 4.28 Print Density For 30mm and 50mm Squeegee Diameter at $0.4ms^{-1}$

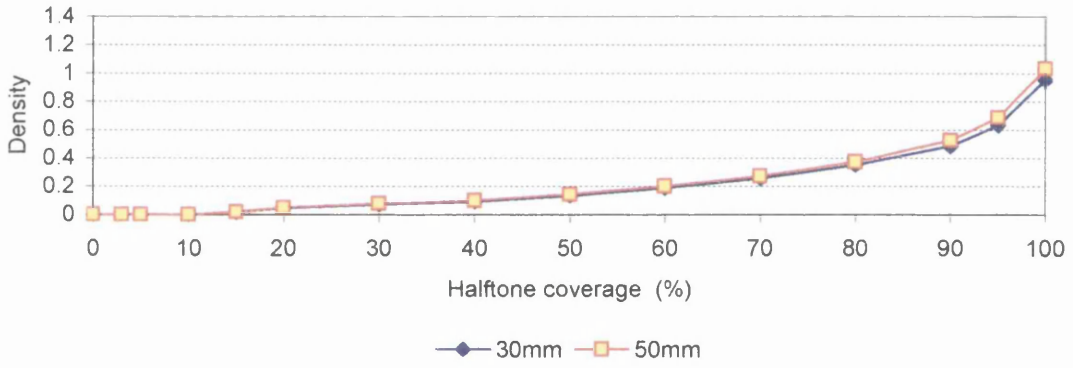

Figure 4.29 Print Density For 30mm and 50mm Squeegee Diameter at $0.6ms^{-1}$

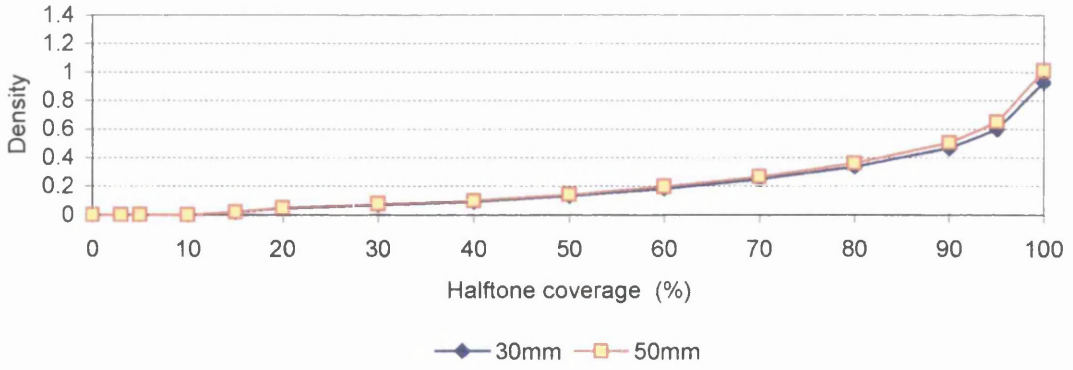

Figure 4.30 Print Density For 30mm and 50mm Squeegee Diameter at $0.8ms^{-1}$

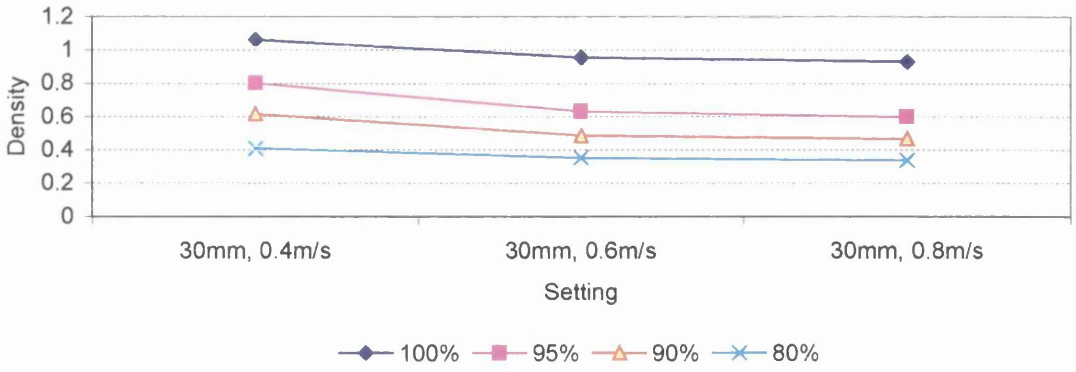

Figure 4.31 Density Change With Respect to Speed For 30mm Squeegee

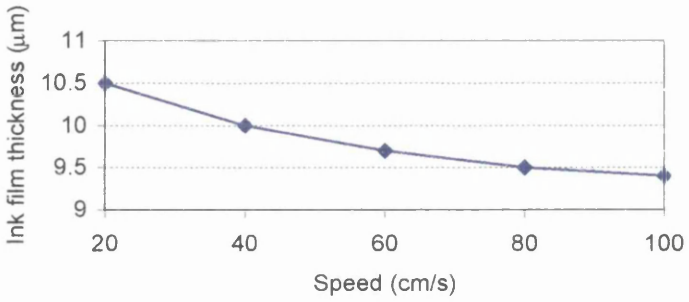

Figure 4.32 Predicted Blade Squeegee Ink Film Thickness From ITM

Figure 4.33 to Figure 4.35 show the effect of rotating and locking the roller squeegee at speeds of $0.4ms^{-1}$, $0.6ms^{-1}$ and $0.8ms^{-1}$. For the slowest print speed, there is a negligible effect on print densities below 80% coverage, but for areas greater than this there is a significant increase in density created by locking the squeegee. As the print speed is increased, the overall print density decreases in a non-linear manner, in a similar trend to Figure 4.31, and this is attributed to the dominating impact of film shearing. However, the solid density is greater for the locked squeegee compared with the rotating squeegee and this was observed for the initial study. Of the parameters investigated in this part of the study, the rotation of the squeegee has proven to be the most dominant factor, affecting the solid density by almost 0.4, which will in turn have a significant influence on the tone gain. Therefore, any slip

that is present with the roller squeegee will have an impact on the reproduction of solid areas, but almost no impact on halftones below 90%.

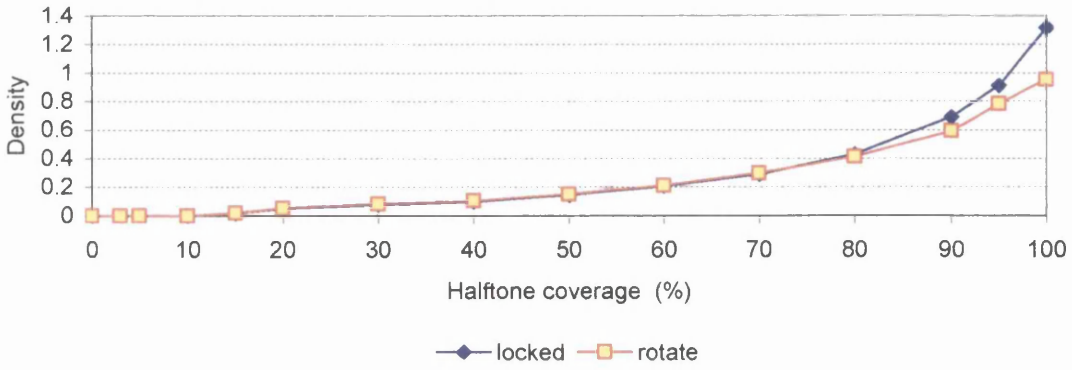

Figure 4.33 Print Density For Locked and Rotating Squeegee at 0.4ms^{-1}

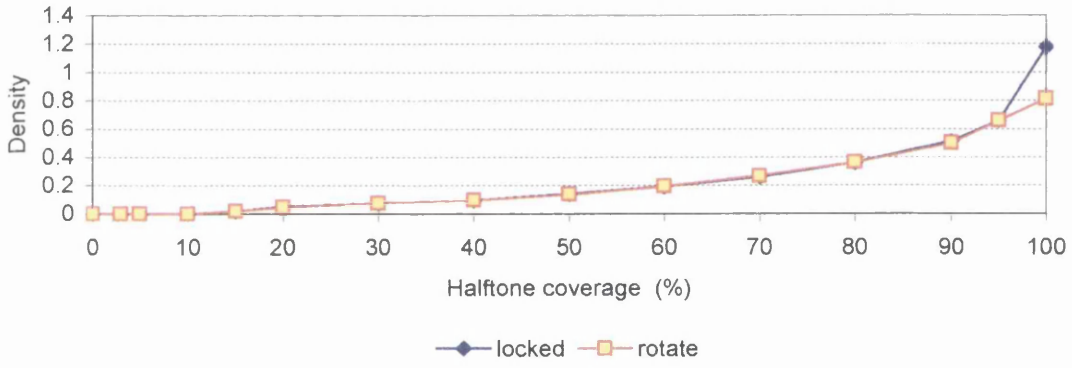

Figure 4.34 Print Density For Locked and Rotating Squeegee at 0.6ms^{-1}

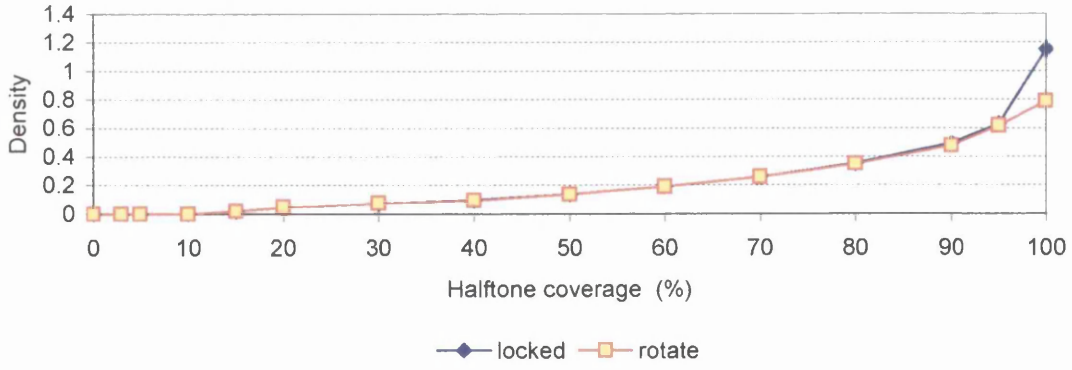

Figure 4.35 Print Density For Locked and Rotating Squeegee at 0.8ms^{-}

The variation in ink density, as a result of an increase in squeegee pressure, for print speeds of $0.4ms^{-1}$, $0.6ms^{-1}$ and $0.8ms^{-1}$, can be seen in Figure 4.36 to Figure 4.38. At a print speed of $0.4ms^{-1}$, there is a negligible difference in the ink deposit as the squeegee pressure is adjusted, where an increase in pressure when using blade squeegees has been proven to increase the ink deposit [16]. However, an increase in pressure increases the ink deposit at the higher print speeds. This can be attributed to an increase in speed increasing the hydrodynamic pressure within the contact point, emphasising any change in squeegee pressure that is applied. From the parameters investigated, the squeegee pressure range explored affects the ink density the least. This is to be expected because when the roller squeegee is used, an alteration in pressure of 1bar will have a minimal effect upon the contact profile. As the print speed is increased, the ink deposit decreases non-linearly, in accordance with some of the previous blade squeegee printing trials [64] [65].

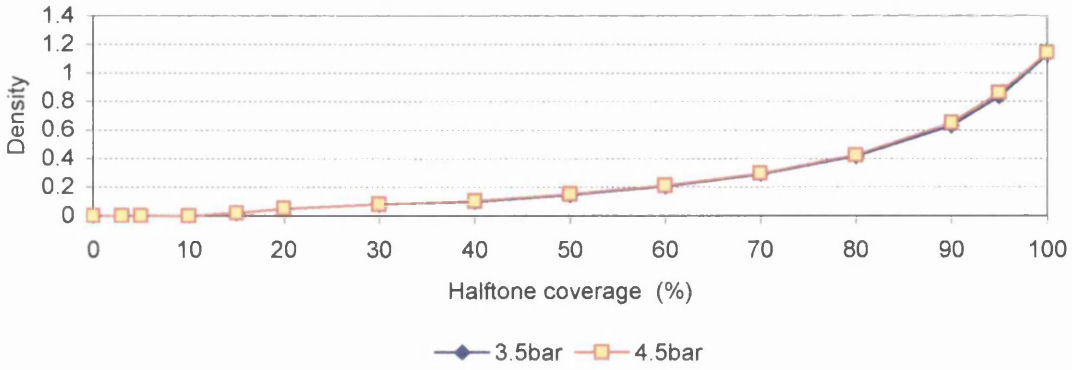

Figure 4.36 Print Density For 3.5bar and 4.5bar Squeegee Pressure at 0.4ms^{-1}

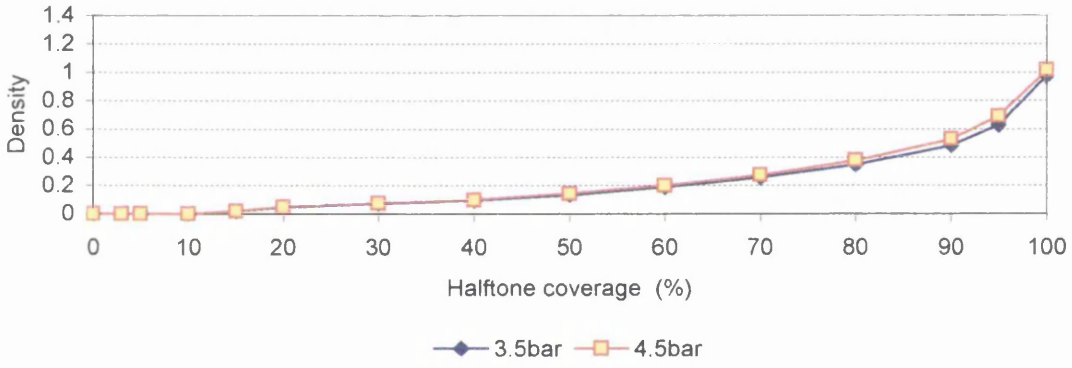

Figure 4.37 Print Density For 3.5bar and 4.5bar Squeegee Pressure at 0.6ms^{-1}

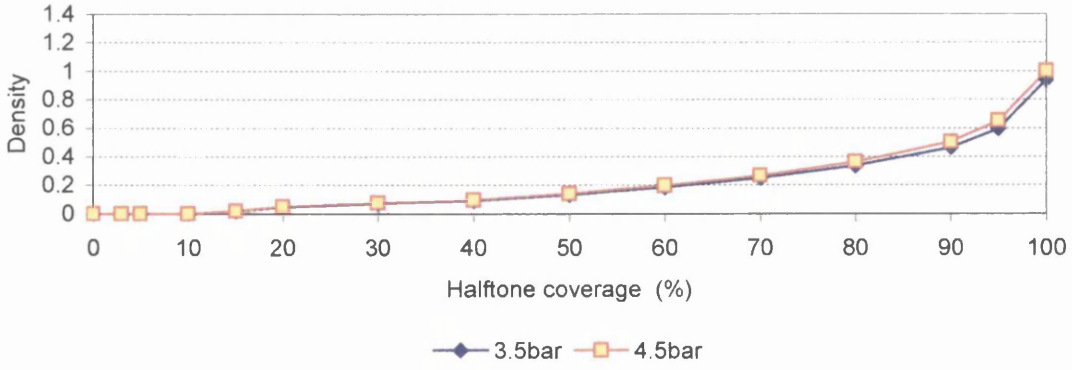

Figure 4.38 Print Density For 3.5bar and 4.5bar Squeegee Pressure at 0.8ms^{-1}

Figure 4.39 to Figure 4.41 summarise the interactions for the roller squeegee experiment for the 80%, 90% and 100% halftone coverage for print speeds of $0.4ms^{-1}$, $0.6ms^{-1}$ and $0.8ms^{-1}$ respectively. Only these are displayed since the previous experiments have verified that process parameters have little impact below this coverage. The bar chart shows the change in density between the individual settings, depicted as (1) and (2) respectively. As can be seen from this figure, there is no noticeable difference between the two settings for each of the print speeds. Therefore, it can be assumed that the process parameters are independent. As no interactions were noted for the print densities, the interactions were omitted from the tone gain study.

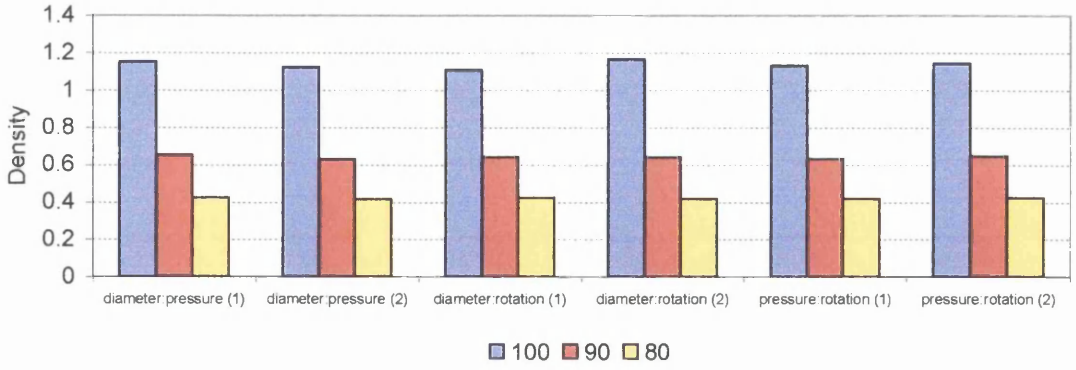

Figure 4.39 Roller Squeegee Interactions at a Speed of $0.4ms^{-1}$

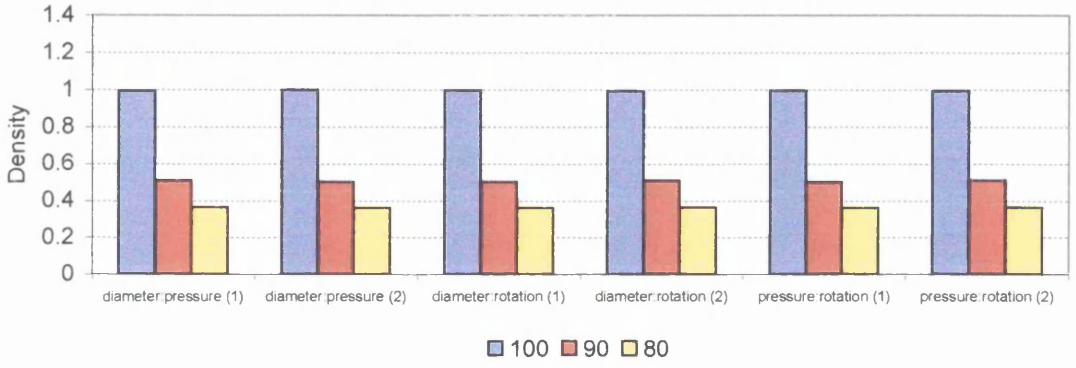

Figure 4.40 Roller Squeegee Interactions at a Speed of $0.6ms^{-1}$

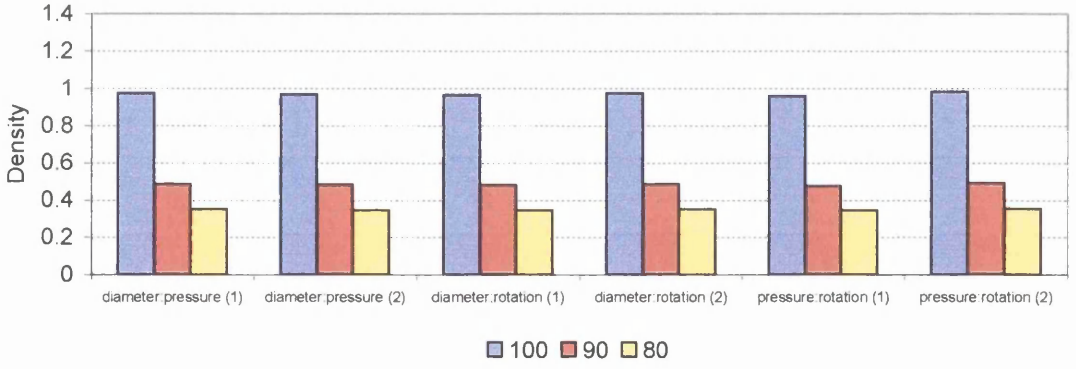

Figure 4.41 Roller Squeegee Interactions at a Speed of $0.8ms^{-1}$

4.5.3 Tone-gain Evaluation

Figure 4.42 to Figure 4.44 show the change in tone gain resulting from an increase in roller squeegee diameter, printing at a press speed of $0.4ms^{-1}$, $0.6ms^{-1}$ and $0.8ms^{-1}$ respectively. As seen previously, the larger squeegee diameter produced prints of higher print density than the smaller diameter squeegee. This was attributed to the larger squeegee having a greater contact duration and a reduced snap-off speed. This is also verified with the tone gain, where the 50mm diameter squeegee continuously produces higher tone gain than the 30mm diameter squeegee, signifying greater ink flow though the screen in relation to the solid density. The difference in tone gain increases as the print speed increases with the point of maximum difference occurring at an open area of 60% for each speed. An increase in roller diameter creates an increase in tone gain of slightly less than 1% for a 60% open area, at a print speed of $0.4ms^{-1}$. As the speed is increased to $0.8ms^{-1}$, this difference in tone gain increases to approximately 1.3%. The overall tone gain decreases as the print speed increases possibly due to an increase in snap-off speed and a reduction in the contact duration. Of the parameters investigated, the variation in roller diameter has the least effect on the tonal reproduction, where a minimal difference occurs throughout the open areas.

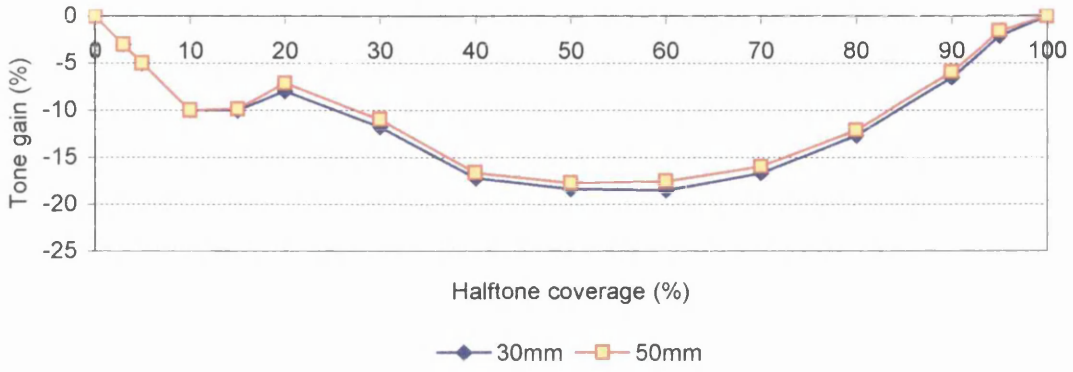

Figure 4.42 Tone Gain For 30mm to 50mm Squeegee at $0.4ms^{-1}$

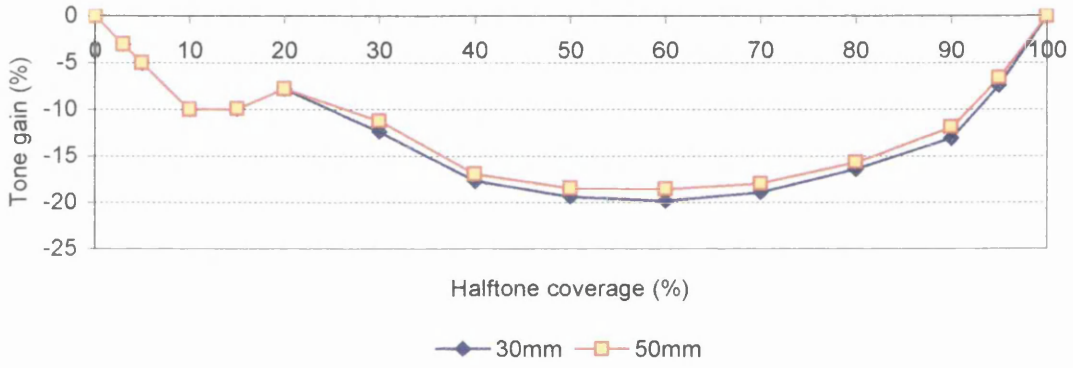

Figure 4.43 Tone Gain For 30mm to 50mm Squeegee at $0.6ms^{-1}$

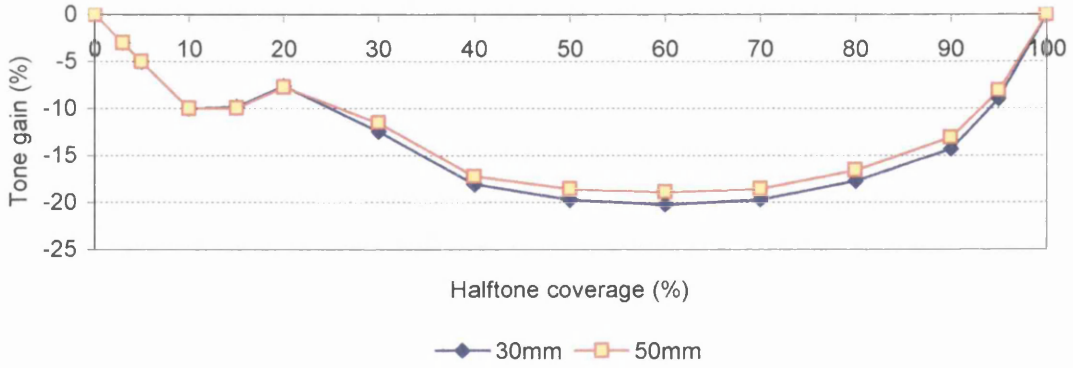

Figure 4.44 Tone Gain For 30mm to 50mm Squeegee at $0.8ms^{-1}$

The difference in tone gain resulting from the squeegee being locked and rotating is shown in Figure 4.45 to Figure 4.47. The overall tone gain can be seen to be reducing as the print speed increases, where tone gain for the locked squeegee reduces at a much greater rate than the rotating squeegee. This suggests that the tone is affected by a greater amount by a change in speed when the squeegee is locked than when it is free to rotate. This indicates that the shearing mechanism of the locked squeegee upon the ink is playing a vital role in the ink transfer characteristics.

Out of the parameters investigated, preventing the rotation of the squeegee has the greatest effect on ink deposit, producing up to 9% less ink coverage than the rotating squeegee. The solid print density was higher for the locked squeegee than the rotating squeegee in all cases.

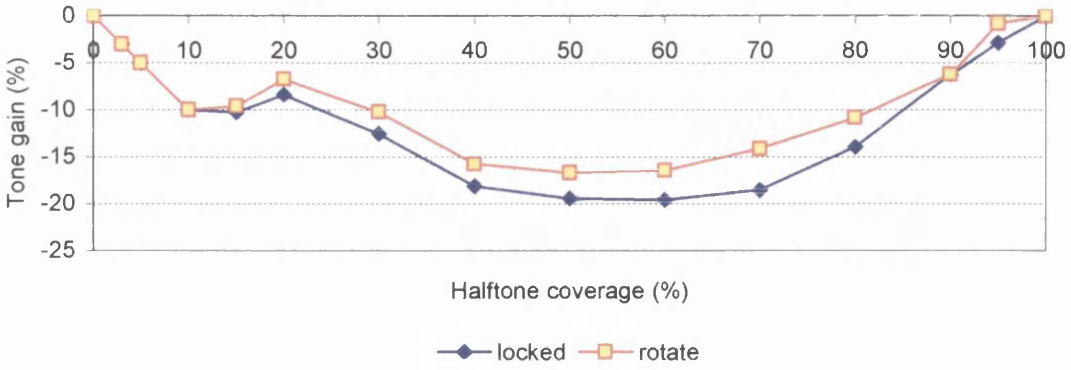

Figure 4.45 Tone Gain For Locked and Rotating Squeegee at 0.4ms^{-1}

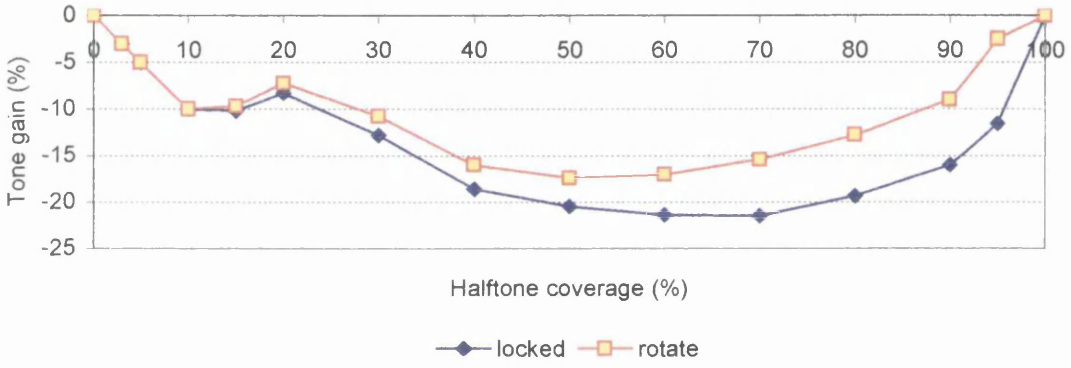

Figure 4.46 Tone Gain For Locked and Rotating Squeegee at 0.6ms^{-1}

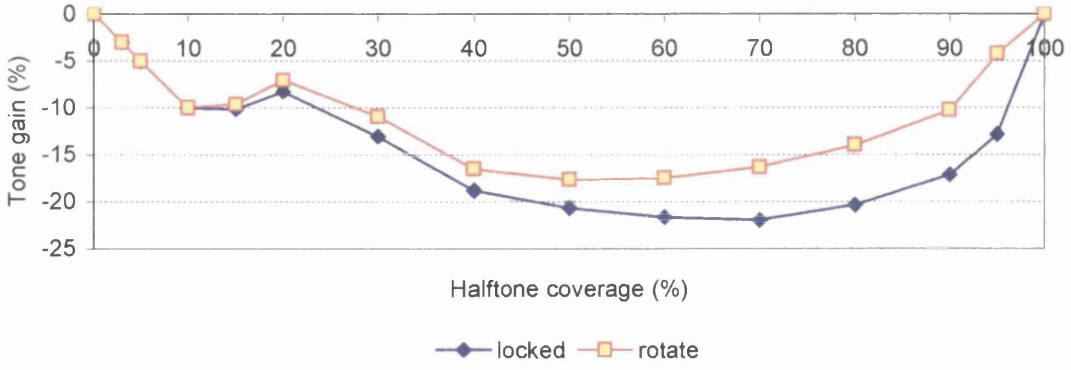

Figure 4.47 Tone Gain For Locked and Rotating Squeegee at 0.8ms^{-1}

Figure 4.48 to Figure 4.50 shows the effect of increasing the squeegee pressure from 3.5b to 4.5b, for print speeds of $0.4ms^{-1}$, $0.6ms^{-1}$ and $0.8ms^{-1}$ respectively. The figures show that with the squeegee pressure set to 4.5b, the tone gain is greater than at a squeegee setting of 3.5b, with the difference in tone gain increasing as the speed is increased. The 4.5b pressure will produce a higher tone gain than the 3.5b pressure, as the increase in pressure will increase the deformation of the point of contact of the squeegee. Therefore, this will result in a greater contact area and a slower snap-off speed, leading to an increase in ink coverage. However, from the parameters investigated, the alteration of the squeegee pressure has the least effect on tone gain due to the rigid nature of the roller squeegee, which will therefore have a minimal impact on the prints. Also, at higher pressure, more ink will be forced through the screen in the nip and this will also lead to a larger volume of ink through flow.

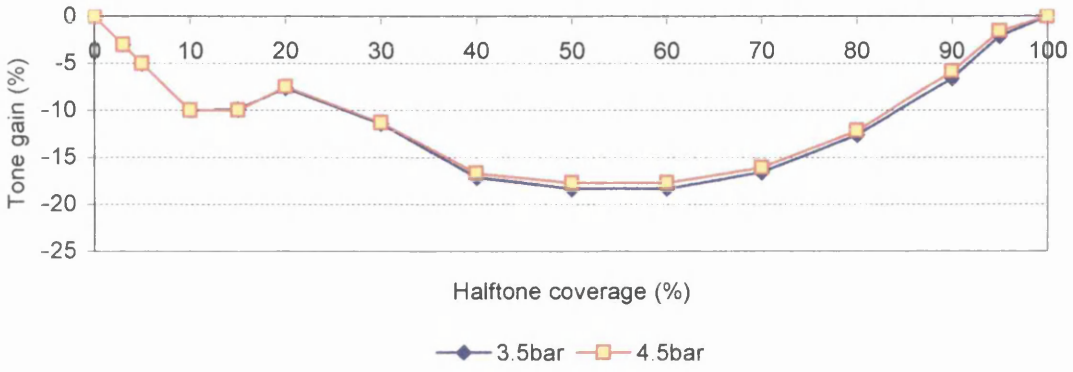

Figure 4.48 Tone Gain For 3.5bar and 4.5bar Squeegee Pressure at 0.4ms^{-1}

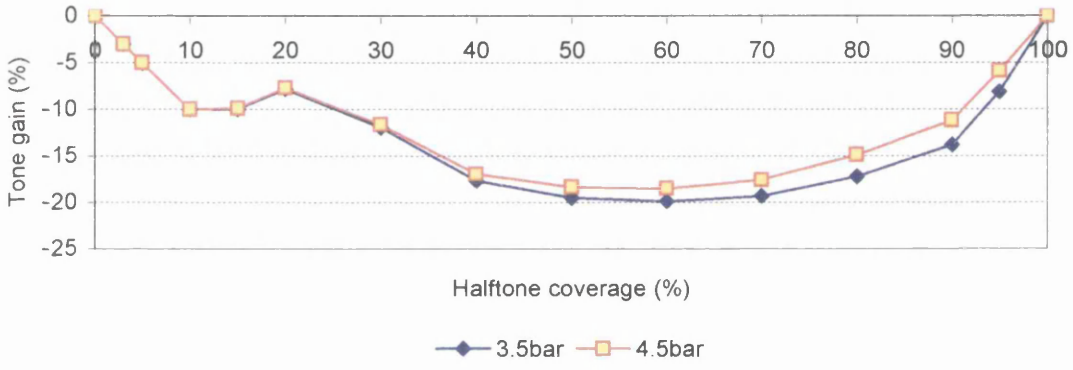

Figure 4.49 Tone Gain For 3.5bar and 4.5bar Squeegee Pressure at 0.6ms^{-1}

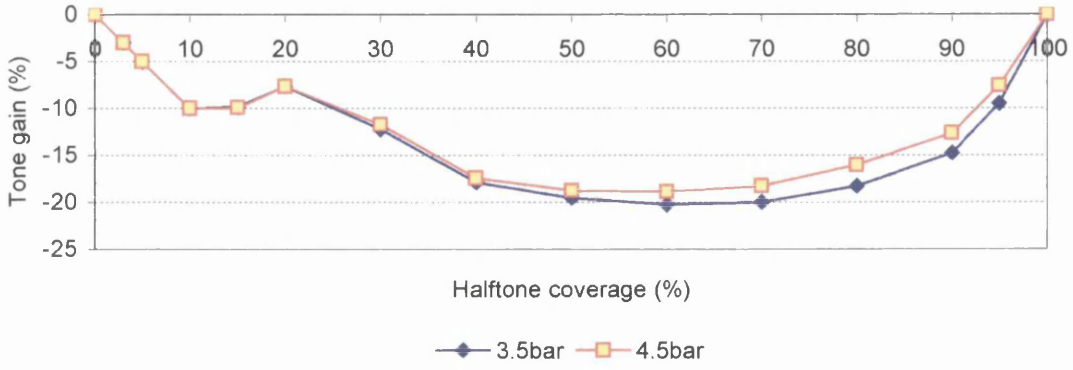

Figure 4.50 Tone Gain For 3.5bar and 4.5bar Squeegee Pressure at 0.8ms^{-1}

4.5.4 Summary Comments

An experimental programme to explore process parameters has been carried out using an orthogonal array technique. Here it was discovered that altering the squeegee pressure has a minimal effect on tonal reproduction, although printing at a higher printing speed caused the pressure to have a slightly greater effect. Similarly, the squeegee diameter had a small effect on the tonal reproduction. The rotation of the squeegee had the greatest effect on tonal reproduction where the tone gain created by the locked squeegee interacted strongly with the print speed due to the faster print speed increasing the shearing action within the ink film. This shearing mechanism has proved to be the dominating mechanism as the pressure generated by the rotating squeegee did not affect the tone gain as significantly over the same range of print speeds.

The study of the interactions highlighted that each parameter was independent. However, the parameters were seen to interact with the speed, as an increase in print speed influenced further the effect of the parameter being studied.

4.6 Confirmation Study

Two possible hypotheses have been proposed that could explain why the locked squeegee produces a higher ink deposit than the rotating squeegee. One of these theories is that the rotating action of the squeegee aids the snap-off speed of the screen therefore, increasing the ink deposit. Alternatively, with the locked squeegee, the screen adheres to the substrate, reducing the snap-off speed and increasing the ink deposit. Additionally, it is believed that the locked squeegee shear thins the ink, reducing its viscosity, allowing easier passage through the screen. This shearing mechanism is understood to be the dominating factor as it affects the ink deposit significantly compared to the rotating squeegee over a similar speed range.

The purpose of this section is to explore in more depth the impact of snap-off as this appears to hold information that will give a more clear insight to the mechanisms that are present.

4.6.1 Snap-off Study

As previously stated in Section 4.2, the screen adhering to the substrate is believed to reduce the snap-off speed and increase the contact duration, which will then lead to an increase in ink deposit when compared to when the screen fails to adhere to the substrate. In an attempt to verify this theory, a further set of trials was carried out where the snap-off gap is increased incrementally. This will increase the snap-off speed and will also increase the vertical force component associated with mesh tension, reducing the tendency for the mesh to adhere to the substrate. Using the 150-34 screen with the conventional UV ink, the snap-off gap was initially set to the press minimum of 4.5mm. The squeegee pressure remained fixed at a value of 4.5bar, as the pressure proved to have little effect on tonal reproduction in the orthogonal array experiments. Samples were printed at press speeds $0.2ms^{-1}$, $0.5ms^{-1}$ and $0.8ms^{-1}$, allowing a further study of the snap-off speed to be undertaken across the full range of print speeds. Also, to investigate the shear thinning effect of locking the squeegee, the experiments were carried out with the squeegee locked and rotating. This was carried out for both roller squeegees where three samples were printed at each press setting and the results averaged to minimise error. Only three samples were printed as the previous study in Section 4.5 highlighted minimal variation between prints. The snap-off distance was then increased to 5.5mm and 6.5mm, where this was the maximum snap-off gap allowable due to the geometry of the roller squeegee. This part of the study only focuses upon the densities of the prints and not the tonal plots, as the density of the prints dictate the tone gain. The orthogonal array experiments also highlighted the fact that altering the press parameters had little effect on the tonal densities below 60%. For this reason, only the density results for the 60%, 80% and 100% open areas were plotted from this series of experiments.

Figure 4.51 to Figure 4.53 represent the print densities produced by the 30mm diameter roller squeegee, rotating and locked, printing at speeds of $0.2ms^{-1}$, $0.5ms^{-1}$ and $0.8ms^{-1}$, with snap-off gaps of 4.5mm, 5.5mm and 6.5mm, for the 100%, 80% and 60% open areas. The general trend for the density in the 100% open area is for the ink deposit to decrease as the print speed increases. A similar trend is evident with an increase in snap-off height and hence snap-off speed. At the 4.5mm snap-off gap, the locked squeegee has produced prints of higher density than the rotating squeegee, as observed in the previous experiments. However, as the snap-off gap is increased,

which further increases the snap-off speed and reduces the likelihood of the screen adhering to the substrate, the difference in density between the rotating squeegee and the locked squeegee generally decreases. This occurs until the snap-off gap is set to 6.5mm. At this point, the increase in snap-off speed and the increase in the vertical component of the mesh tension resulted in the rotating squeegee producing higher print densities than the locked squeegee. Additionally, as the snap-off gap was increased, the screen no longer seemed to be adhering to the substrate, due to the effective increase in mesh tension.

The model that the locked squeegee causes the screen to adhere to the substrate is further verified from the results for the 80% and 60% open areas. These results show that, for similar press settings, the difference in density between the rotating and locked squeegee to be considerably less than occurred for the 100% open area. For the 60% open area, the rotating squeegee has produced a higher ink deposit than the locked squeegee for the 5.5mm snap-off gap, where this was achieved at 6.5mm for the 100% open area. The reason for this can be stated that less ink is transferred to the substrate at the lower open areas, therefore, the screen is less likely to adhere to the substrate when the squeegee is prevented from rotating.

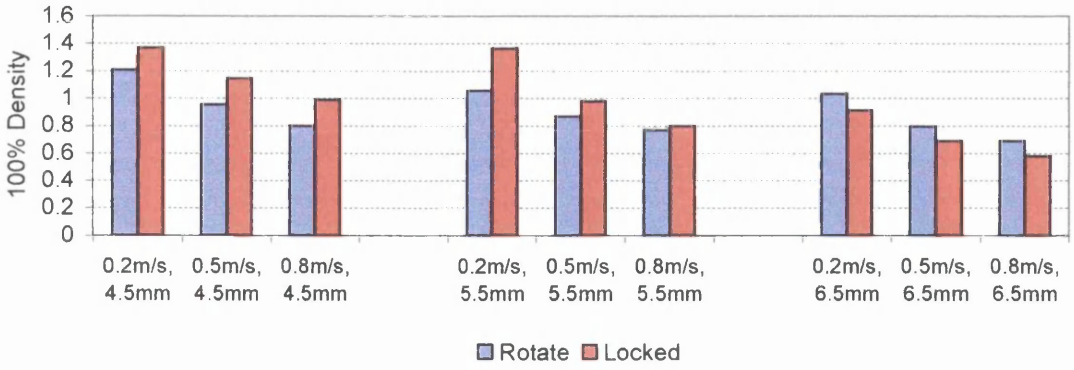

Figure 4.51 100% Open Area Print Density For 30mm Diameter Roller Squeegee

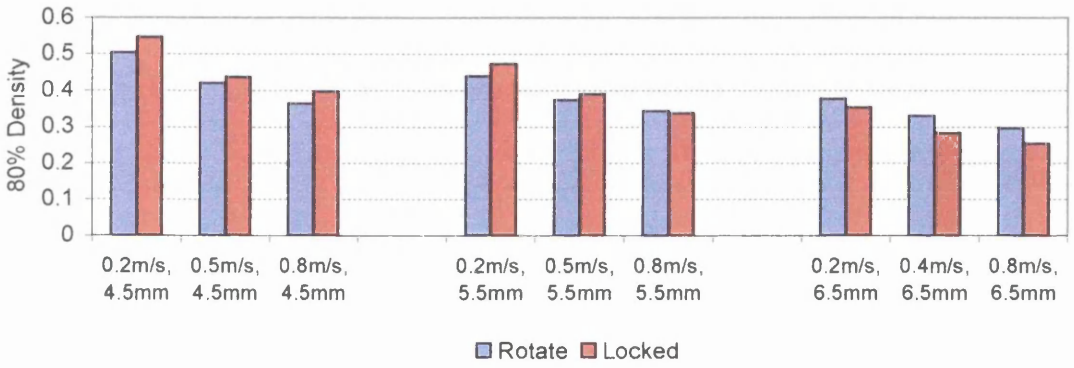

Figure 4.52 80% Open Area Print Density For 30mm Diameter Roller Squeegee

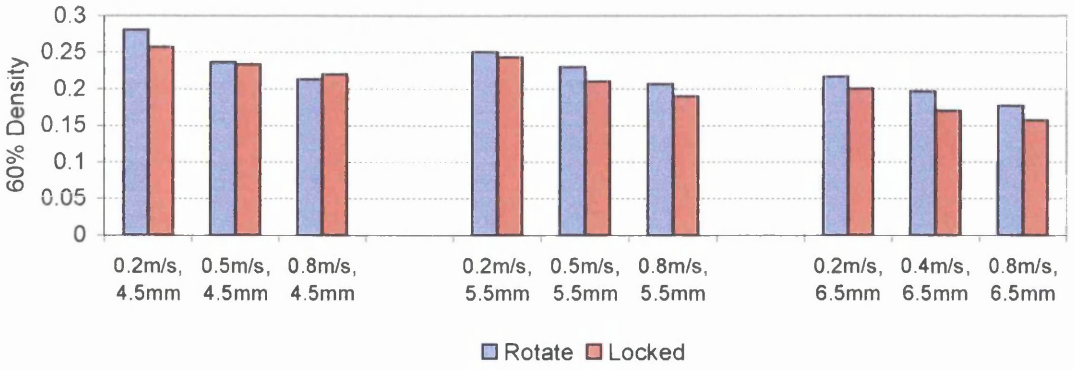

Figure 4.53 60% Open Area Print Density For 30mm Diameter Roller Squeegee

The results for the 50mm diameter squeegee are shown in Figure 4.54 to Figure 4.56. These predominantly show that the rotating squeegee generally produces prints of higher densities than the locked squeegee, with the exception of the 100% and 80% open areas at the 4.5mm snap-off gap. This has occurred at lower snap-off gaps and lower open areas than what was observed with the 30mm diameter squeegee. The reasons for this are that due to the larger diameter of the 50mm squeegee, the contact area of the screen and the squeegee is significantly greater than the 30mm diameter squeegee. Therefore, the screen has a higher probability of adhering to the 50mm diameter squeegee than adhering to the substrate. Ultimately, this will aid the snap-off of the screen from the substrate.

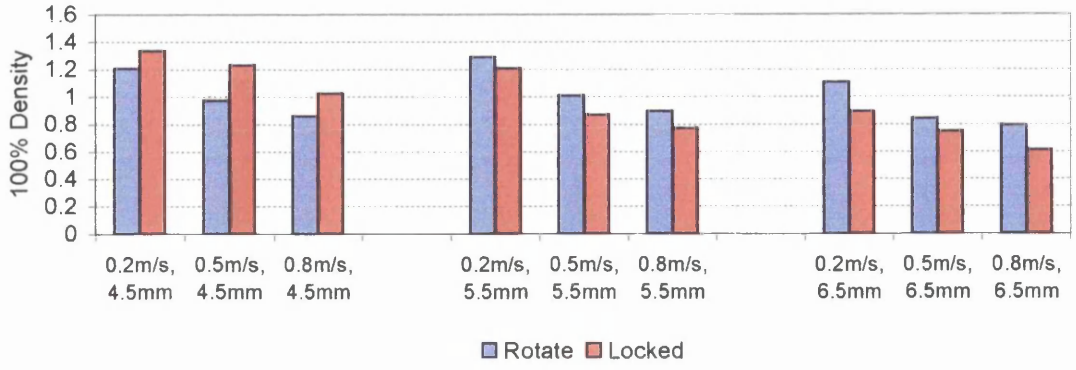

Figure 4.54 100% Open Area Print Density For 50mm Diameter Roller Squeegee

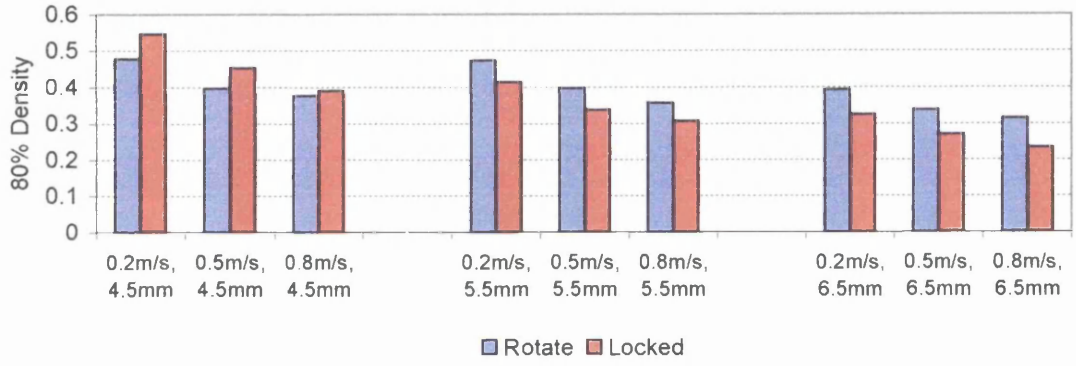

Figure 4.55 80% Open Area Print Density For 50mm Diameter Roller Squeegee

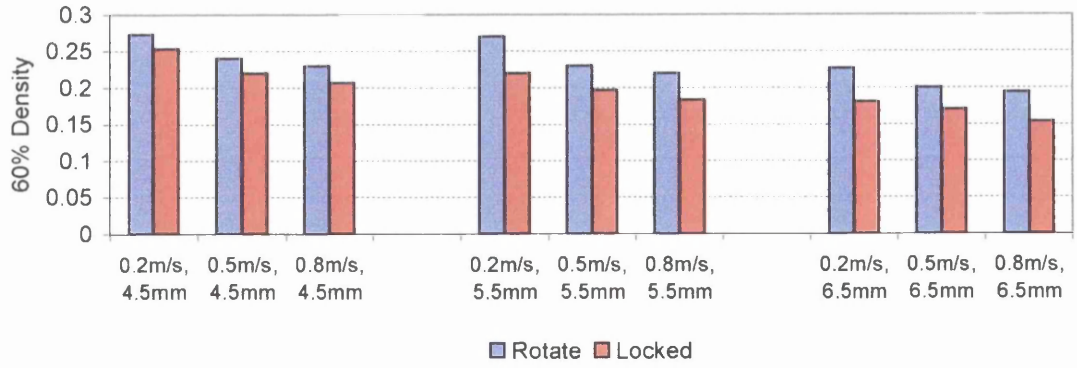

Figure 4.56 60% Open Area Print Density For 50mm Diameter Roller Squeegee

4.6.2 Summary Comments

A hypotheses has been developed and tested to establish the reasons why a rotating squeegee yields prints of a lower density than a locked squeegee, despite the rotating squeegee generating greater hydrodynamic pressure. This has been attributed to the screen adhering to the substrate when the squeegee is locked. Ultimately, this reduces the snap-off speed and results in an increase in ink deposit. However, when printing at lower coverage this does not occur due to insufficient ink for the screen to adhere to the substrate. The rotating effect of the squeegee reduces the ink deposit as the rotating action increases the snap-off speed.

4.7 Closure

A number of successful experiments into screen-printing with a roller squeegee have been described in this chapter. The initial trials proved that for this to be achieved, the screen needed to be 150-34, as a screen resolution lower than this produced excessive ink transfer. Additionally, it is possible to print solvent-based ink through a 150-34 screen using a roller squeegee, without the risk of the ink drying in the mesh. This is due to the roller squeegee failing to remove all of the ink from the screen surface, preventing the ink from drying in the mesh open areas.

The subsequent experiments were carried out to obtain an insight since parameter affects could not be isolated due to the complex interaction between process parameters. Contradicting expectations, when the roller squeegee was locked the prints contained a higher ink coverage than those produced with the roller squeegee rotating. Two potential reasons for this include increasing the snap-off speed and reducing the contact duration by effectively peeling the screen from the substrate. When the squeegee was locked, the screen adhered to the substrate, reducing the snap-off speed and therefore increasing the ink deposit. However, to prevent the screen from adhering to the substrate, the snap-off gap can be increased, which increases the vertical force component of the mesh tension. When the snap-off gap was increased sufficiently to prevent the screen from adhering to the substrate, the rotating squeegee produced considerably higher ink deposit than the locked squeegee. Presently, this is largely believed to be the increase in hydrodynamic pressure within the squeegee nip junction.

Locking the squeegee also had a considerable effect of shear thinning the ink, easing the flow of ink through the screen. This proved to be the dominant mechanism over the pressure distribution mechanism, as when the printing speed was increased, the ink deposit decreased considerably for the locked squeegee compared to that of the rotating squeegee. This was particularly evident for the solid density where the locking of the squeegee had a considerable influence, possibly due to the higher volume in ink transfer. Consequently, this affected the tone gain throughout the gradation. To further establish this shear thinning effect and to further study the pressure distribution model, a numerical evaluation will be carried out in the next chapter.

Chapter 5

Numerical Model Development and Investigation

5 Numerical Model Development and Investigation

5.1 Introduction

The literature review has shown that the modelling of the nip contact region within a roller train in coating applications is well developed. However, there has only been limited work on the study of the ink within the nip contact region of a squeegee in the screen printing process. The work that has been carried out in this area to date has focused upon modelling blade squeegees, where the deformation has been decoupled from the hydrodynamic pressure distribution beneath the squeegee nip [19]. Clearly, as the ink flows through the nip contact region, pressure is generated within the ink film. This pressure then deforms the squeegee, which then influences the ink film thickness in the nip contact region. The change in ink film thickness will then further affect the pressure distribution within the ink film. This type of problem is referred to as Soft Elasto Hydrodynamic Lubrication (SEHL) in a line contact and is likely to have a considerable effect on the ink transfer mechanism.

The aim of this chapter is to develop a numerical procedure that simulates the ink flow through the nip contact region of a deformable roller squeegee. For comparison purposes, this will be of similar dimensions and properties to those used in the previous print trials. Through calculation, this will enable process simulations to be carried out to provide further understanding of the ink flow in the screen-printing process. This will allow the ink film thickness and the hydrodynamic pressure distribution within the nip junction to be calculated. In addition, the ink flow through the screen can be calculated and then used to estimate the thickness of the ink that will be deposited onto the substrate. The numerical procedure is a development of previous work into the modelling of contact between lithographic printing press rollers using SEHL theory [74] [75]. The solution to the SEHL problem requires the calculation of the elastic deformation of the rubber-covered squeegee and that of the Reynolds equation, where the two solution procedures are then combined in an iterative strategy.

This chapter is divided into five main sections. The first two sections are an explanation of the solid mechanics and hydrodynamic governing equations used for the numerical analysis. A description is then given for the process used for solving

these equations. An investigation is then undertaken using an impermeable model, which investigates the general characteristics observed with the alteration of press parameters. A permeable model is then implemented, which assesses the impact of screen open area and calculates the expected ink deposits.

5.2 Rubber Coated Roller Squeegee Model

The rubber surface of the roller squeegee is assumed to be linearly elastic, where the governing equations are solved using the Boundary Element Method (BEM), as opposed to the Finite Element Method (FEM). This was chosen due to the reduction in computational output needed when compared with that when using the FEM. In addition, only the surface deformation dictates the ink film thickness and therefore it was not necessary to calculate the stress and strain within the elastomer.

Under conditions of large deformation, rubber is known to deform in a non-linear manner. Due to the nature of the application, and to reduce the model complexity, it can be assumed that the displacement of the rubber is small in comparison with its thickness, therefore assuming linear deformation with perfect elasticity. Additionally, the original form is maintained after the removal of the forces and it is assumed to be homogeneous and isotropic, where the material property is the same throughout and the elastic properties are the same in all directions [76]. This next section highlights the main features in the governing equations for the solid mechanics

5.2.1 Governing Equations of Solid Mechanics

Figure 5.1 shows a schematic of the internal stresses and body forces acting upon a finite volume of material, whilst neglecting any changes in orientation of the body due to displacements.

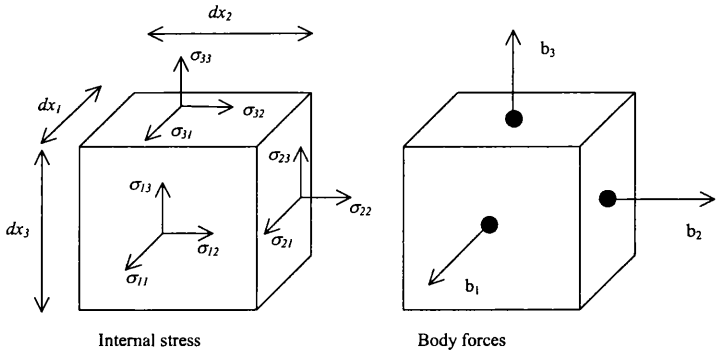

Figure 5.1 Internal Stress and Body Forces on Finite Volume

Through resolution of forces, the equilibrium of the volume can be expressed in terms of the stress field components, where under static equilibrium no inertia forces exist. The consequent governing equations for Figure 5.1 can be expressed as [77];

$$\frac{\partial \sigma_{11}}{\partial x_1}+\frac{\partial \sigma_{12}}{\partial x_2}+\frac{\partial \sigma_{13}}{\partial x_3}+b_1=0$$

$$\frac{\partial \sigma_{21}}{\partial x_1}+\frac{\partial \sigma_{22}}{\partial x_2}+\frac{\partial \sigma_{23}}{\partial x_3}+b_2=0 \qquad \text{Equation 5.1}$$

$$\frac{\partial \sigma_{31}}{\partial x_1}+\frac{\partial \sigma_{32}}{\partial x_2}+\frac{\partial \sigma_{33}}{\partial x_3}+b_3=0$$

This can be rewritten in indicial notation as;

$$\frac{\partial \sigma_{ij}}{\partial x_j}+b_i=0 \qquad i=1,2,3 \;\; j=1,2,3 \qquad \text{Equation 5.2}$$

Equilibrium on the boundary requires the satisfaction of the following boundary conditions;

$$p_i = \sigma_{ij} n_j = \overline{p_i} \qquad i = 1,2,3 \;\; j = 1,2,3 \qquad \text{Equation 5.3}$$

With the displacement constraints being;

$$u_1 = \overline{u_1},\; u_2 = \overline{u_2},\; u_3 = \overline{u_3},\; u_i = \overline{u_i} \qquad \text{Equation 5.4}$$

Where $\overline{u_i}$ are prescribed values.

The direct strain at any point can be defined by the ε_{ij} components of the strain vector, which in their indicial form can be written as;

$$\varepsilon_{ij} = \frac{1}{2}\left(\frac{\partial u_i}{\partial x_j} + \frac{\partial u_j}{\partial x_i}\right) \qquad i = 1,2,3 \;\; j = 1,2,3 \qquad \text{Equation 5.5}$$

For an isotropic body, the strains and stresses can then be related;

$$\sigma_{ij} = \lambda \tilde{\delta}_{ij} \frac{\partial u_k}{\partial x_k} + \hat{\lambda}\left(\frac{\partial u_i}{\partial x_j} + \frac{\partial u_j}{\partial x_i}\right) \qquad \text{Equation 5.6}$$

Where λ and $\hat{\lambda}$ are the Lame's constants, expressed in terms of the modulus of elasticity and Poisson's ratio;

$$\lambda = \frac{E}{(1+\upsilon)(1-2\upsilon)} \qquad \hat{\lambda} = \frac{E}{2(1+\upsilon)} \qquad \text{Equation 5.7}$$

Using the boundary conditions, Equation 5.3 and Equation 5.4, the governing equation, Equation 5.2, can be reduced by using an extended weighted residual method. This is achieved by subdividing the structure into a number of elements, whilst assuming a known variation of the approximating and weighting functions. This then provides an approximate numerical solution, Equation 5.8.

$$\int_{\Omega}\left(\frac{\partial \sigma_{jk}}{\partial x_j}+b_k\right)u_k^* d\Omega = \int_{\Gamma_2}\left(p_k-\overline{p_k}\right)u_k^* d\Gamma + \int_{\Gamma_1}\left(\overline{u_k}-u_k\right)p_k^* d\Gamma \qquad \text{Equation 5.8}$$

Note; $\Gamma_1 + \Gamma_2 = \Gamma\,(Total\ Surface)$

The general boundary integral formulation for solving three-dimensional small deformation problems can then be developed, Equation 5.9, details of which are provided in *Brebbia and Walker* [77]. This strategy can be applied to two-dimensions where the boundary integrals are line integrals and the body force terms are obtained by integrating over the area instead of the volume of internal elements.

$$c_{lk}^i u_k^i + \int_\Gamma p_{lk}^* u_k d\Gamma = \int_\Gamma u_{lk}^* p_k d\Gamma + \int_\Omega u_{lk}^* b_k d\Omega \qquad \text{Equation 5.9}$$

For the required solution of the boundary element integral equation, there are no thermal or gravitational effects and the body forces are zero. Therefore, the integral equation simplifies to;

$$c_{lk}^i u_k^i + \int_\Gamma p_{lk}^* u_k d\Gamma = \int_\Gamma u_{lk}^* p_k d\Gamma \qquad \text{Equation 5.10}$$

For the fundamental solution for the three-dimensional isotropic body, the Kelvin solution is used and corresponds to a concentrated force acting at a point in the infinite elastic space. For the displacement and the traction components, it can be written as Equation 5.11 and Equation 5.12 respectively.

$$u_{lk}^* = \frac{1}{16\pi G(1-\upsilon)}\left(\frac{(3-4\upsilon)\tilde{\delta}_{lk}}{r_i}+\frac{\partial r_i}{\partial x_l}\frac{\partial r_i}{\partial x_k}\right) \qquad \text{Equation 5.11}$$

$$p_{lk}^* = -\frac{1}{8\pi(1-\upsilon^2)r_i^{\,2}}\left[\frac{\partial r_i}{\partial n}\left((1-2\upsilon)\tilde{\delta}_{lk}+3\frac{\partial r_i}{\partial x_l}\frac{\partial r_i}{\partial x_k}\right)+(1-2\upsilon)\left(\frac{\partial r_i}{\partial x_l}n_k-\frac{\partial r_i}{\partial x_k}n_l\right)\right]$$

Equation 5.12

Where;

$$\frac{\partial r_i}{\partial x_k} = \frac{r_k}{r_i} \qquad \text{Equation 5.13}$$

and the Kronecker delta is defined by;

$$\tilde{\delta}_{lk} = \begin{cases} 0 \; if \; l \neq n \\ 1 \; if \; l = n \end{cases} \qquad \text{Equation 5.14}$$

For analysis purposes, the elastomer surface can be assumed to be a flat surface within the contact region of the model. Previous work into modelling the surface as a flat surface as oppose to a curved surface has shown a negligible difference between the two solutions [78]. To obtain the integrals of the elasticity equation, the boundary of the elastomer is divided into a number of linear elements, which has proven to be successful in previous studies [79]. Linear elements were used in preference to quadratic elements, as the latter requires numerical integration whereas the linear counterpart in a plane model allows the element integrals to be solved analytically, requiring less computing time. This also allows a Poisson's ratio of 0.5 to be used whilst avoiding the numerical singularity that is normally associated with this value [80] [81]. The circumference of the roller is then represented as a flat elastomer surface, with the pressure load (on the right hand side of Equation 5.10) being applied from points X_a to X_b, Figure 5.2.

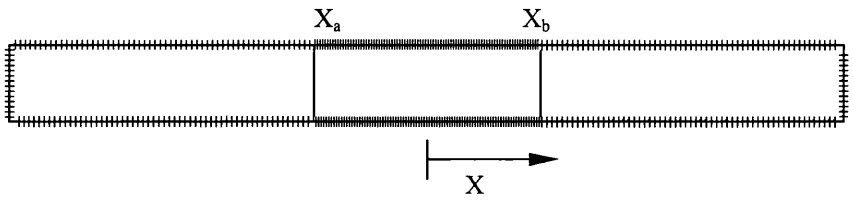

Figure 5.2 Elastomer Layer Linear Elements

5.3 Hydrodynamic Model

It is thought that the pressure that is generated within the nip contact region is a vital component in the ink transfer mechanism in the screen-printing process. As well as governing the ink flow into the screen, it will also affect the deformation of the roller squeegee, which will then have a further impact upon the ink pressure.

This section will focus upon the development of the hydrodynamic equation to model the non-Newtonian ink behaviour within the nip contact region of the roller squeegee. The hydrodynamic equations were then solved using the Finite Difference Method (FDM). The model is constructed to allow exploration of the parameters that are likely to affect the behaviour in the screen-printing nip. Additionally, the model will allow full analysis of the ink flow though the screen.

5.3.1 Governing Equations for Thin Film Flow

A typical thin film fluid section is shown in Figure 5.3. As the film thickness is small in comparison with the other geometry, fluid acceleration is neglected and the equation reduces to a balance between pressure gradient and shear stress terms. Thus, the flow around any small section can be represented by the Stokes equation, expressing the conservation of momentum. Also, continuity expresses the mass balance within the domain. In the analysis, the ink film is transformed from the nip contact region and mapped using a cartesian framework.

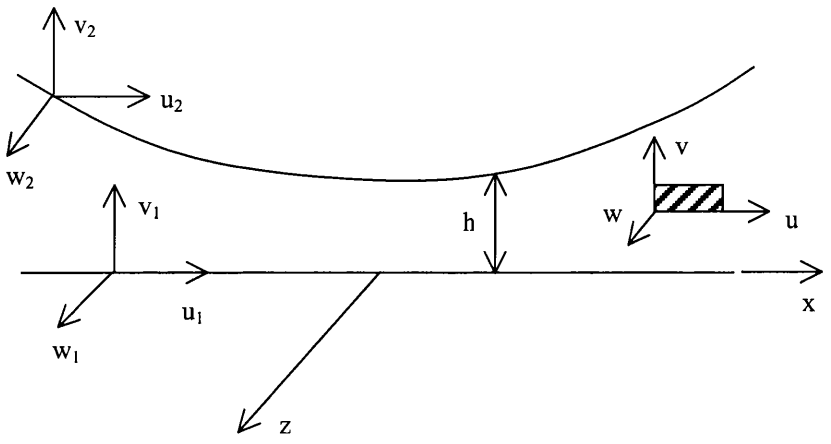

Figure 5.3 Thin Film Section

Using the Stokes equation and continuity, *Dowson* [42] derived the Reynolds equation for the behaviour of a Newtonian fluid. It was assumed that;

- The radius of the roller is large in comparison with the ink film thickness.
- Body forces and inertia are small compared with the viscous and pressure terms.
- There is no slip between the ink and boundaries.
- The pressure through the thickness of the film is constant. This can be assumed to be applicable to the permeable model as the fluid velocity through the screen is relatively small.
- Flow is laminar.
- Viscosity is constant through the film thickness.
- The fluid is Newtonian.

The force balance on the fluid in the film can be written in orthogonal directions in a cartesian framework. These equations express a balance between the pressure and viscous forces within the film and assuming no pressure difference across the ink film exists, the force balance may be neglected.

$$\frac{\partial p}{\partial x} = \frac{2\partial}{3\partial x}\mu\left[\frac{\partial u}{\partial x} - \frac{\partial w}{\partial z}\right] + \frac{2\partial}{3\partial x}\mu\left[\frac{\partial u}{\partial x} - \frac{\partial v}{\partial y}\right] + \frac{\partial}{\partial y}\mu\left[\frac{\partial u}{\partial y} + \frac{\partial v}{\partial x}\right] + \frac{\partial}{\partial z}\mu\left[\frac{\partial w}{\partial x} + \frac{\partial u}{\partial z}\right]$$

$$\frac{\partial p}{\partial z} = \frac{2\partial}{3\partial z}\mu\left[\frac{\partial w}{\partial z} - \frac{\partial u}{\partial x}\right] + \frac{2\partial}{3\partial z}\mu\left[\frac{\partial w}{\partial z} - \frac{\partial v}{\partial y}\right] + \frac{\partial}{\partial x}\mu\left[\frac{\partial w}{\partial x} + \frac{\partial u}{\partial z}\right] + \frac{\partial}{\partial y}\mu\left[\frac{\partial w}{\partial y} + \frac{\partial v}{\partial z}\right]$$

Equation 5.15

Assuming the velocity gradients over the film thickness are the most dominant, Equation 5.15 reduces to;

$$\frac{\partial p}{\partial x} = \frac{\partial}{\partial y}\mu\left[\frac{\partial u}{\partial y}\right]$$

$$\frac{\partial p}{\partial z} = \frac{\partial}{\partial y}\mu\left[\frac{\partial w}{\partial y}\right]$$

Equation 5.16

By continuity, the mass balance is represented by;

$$\frac{\partial}{\partial x}(\rho u)+\frac{\partial}{\partial y}(\rho v)\frac{\partial}{\partial z}(\rho w)=0 \qquad \text{Equation 5.17}$$

Over the range of pressure excursions in the nip contact, the density does not change, therefore;

$$\frac{\partial u}{\partial x}+\frac{\partial v}{\partial y}+\frac{\partial w}{\partial z}=0 \qquad \text{Equation 5.18}$$

The generalised pressure equation, for a one-dimensional Newtonian fluid was derived as being;

$$\frac{\partial}{\partial x}\left[h^3\frac{\partial p}{\partial x}\right]=12\mu U_2\frac{\partial h}{\partial x}-6\mu\frac{\partial}{\partial x}\left[h(U_2-U_1)\right] \qquad \text{Equation 5.19}$$

For a non-Newtonian fluid, a more complex derivation is required that will account for the variation in fluid viscosity over the ink film thickness. Using the same assumptions, a generalised pressure equation for a non-Newtonian fluid can be developed [42]. Assuming that the flow is unidirectional, $V_1=V_2=0$, with no squeezing action, $W_1=0$, $W_2=U\frac{\partial h}{\partial x}$ for two moving surfaces the equation can be written as;

$$\frac{d}{dx}\left[G\frac{dp}{dx}\right]=U_2\left[\frac{dh}{dx}\right]+(U_1-U_2)\left[\frac{dF}{dx}\right] \qquad \text{Equation 5.20}$$

Where;

$$G=\int_0^h\frac{y}{\mu}(y-F)dy \qquad \text{Equation 5.21}$$

$$F_1=\int_0^h\frac{y}{\mu}dy \qquad \text{Equation 5.22}$$

$$F_0 = \int_0^h \frac{1}{\eta} dy$$ Equation 5.23

$$F = \frac{F_1}{F_0}$$ Equation 5.24

The film thickness can be calculated via Equation 5.25, where h_0 represents the surface separation, where a negative value represents roller engagement.

$$h(x) = h_0 + \frac{x^2}{2R} + u(x)$$ Equation 5.25

It is well known that the variation in the press parameters influences the amount of ink that is transferred through the printing screen and onto the substrate. This ink flow through the screen is believed to be due to the pressure distribution within the nip region, which will therefore decrease as ink is forced through the screen. Therefore, to accurately model the ink behaviour in the nip junction, it is necessary to take into account this pressure loss. This will also allow the ink flow through the screen to be calculated along with an estimation of the thickness of the ink deposit. To model the ink flow through the screen, the individual open areas can be assumed to be constructed from a series of small vertical pipes, which are perfectly round. Using these assumptions, the flow though the screen has been calculated as being fully developed, laminar and creeping flow (see Appendix A). Therefore, the model for the ink flow through the screen can be derived from Darcy's law, whilst assuming a linear pressure gradient through the screen. However, this can only be used as an approximate representation of the screen open area, as the mesh open area is constructed from woven mesh fibres, restricting the flow through the screen. Additionally, to model the variation in open area, the cylinder diameter will be a direct representation of the screen open area and the screen ruling, with the screen thickness representing the cylinder length.

Modifying the generalised pressure equation, to account for the screen permeability, Equation 5.20 becomes;

$$\frac{d}{dx}\left[G\frac{dp}{dx}\right] = U_2\left[\frac{dh}{dx}\right] + \left(U_1 - U_2\right)\left[\frac{dF}{dx}\right] - f(v) \qquad \text{Equation 5.26}$$

The term *f(v)* in Equation 5.20, is used to describe the flow velocity through the screen, where the negative sign indicates a positive velocity for a negative pressure gradient. Modifying Darcy's law, Equation 5.27 can be used to describe the ink flow through the screen. This equation is a function of the screen permeability and the percentage of open area, thus, allowing the ink flow through various screen openings to be modelled. Additionally, this equation takes into account the fluid viscosity, which in the case of a non-Newtonian fluid, varies across the film height. For this reason, and as suggested by the experimental evidence, the viscosity of the fluid is taken from the screen surface, directly above the mesh open area. The format of this equation assumes that the roller and the screen produce a perfect gasket seal and that the fluid only flows through the screen and not across the screen surface. However, for thin film analysis, *Wu's* [79] work into porous squeeze films stated that when the film thickness was large, the fluid flowed in a radial direction in relation to the porous substrate. Whereas, when the fluid film was thin, the resistance to radial flow was large and the fluid flowed through the porous media rather than across its surface. Therefore, for this particular analysis it can be assumed that flow across the screen surface is absent.

$$f(v) = -\frac{dp}{dy}\frac{\alpha\phi}{\mu} \qquad \text{Equation 5.27}$$

Where;

$$\phi = \frac{\pi r^2}{8} \qquad \text{Equation 5.28}$$

In order to calculate the thickness of the ink deposit on the substrate, the mean ink flow velocity through the screen needs to be calculated;

$$\bar{v} = \frac{1}{B_h}\int_0^{B_h} v dx \qquad \text{Equation 5.29}$$

The time for which the ink flows through the screen is given by;

$$\Delta t = \frac{B_h}{U_2} \qquad \text{Equation 5.30}$$

With *mr* representing the mesh ruling and *d* representing the mesh diameter, the percentage of open area within the mesh structure can be expressed as;

$$MOA = \frac{\left(\frac{1}{mr} - d\right)^2}{\left(\frac{1}{mr}\right)^2} x100 \qquad \text{Equation 5.31}$$

Therefore, the actual percentage of open area within the printing screen becomes;

$$\beta = \alpha MOA \qquad \text{Equation 5.32}$$

Thus, the quantity of in flow through the screen can be expressed as;

$$\bar{Q} = \bar{v}\Delta t B_h \beta \frac{1}{mr} \qquad \text{Equation 5.33}$$

Assuming that the ink is not absorbed by the substrate and neglecting any evaporation of the ink, two models can be developed that express the thickness of the ink deposited onto the substrate. The first expression assumes that the ink remains in a column as originally printed and the second model assumes that the ink spreads across the surface of the substrate.

$$Column\ model\ thickness = \frac{\bar{Q} mr}{\alpha B_h} \qquad \text{Equation 5.34}$$

$$Spread\ model\ thickness = \frac{\overline{Q}mr}{B_h} \qquad \text{Equation 5.35}$$

The solution to the specified generalised pressure equation necessitates a description of the viscosity variation through the fluid film, where numerous equations can be used to describe the behaviour of the ink when subject to different shear rates. Three of the more commonly used numerical models are the power law model of Ostwald-de Waele, the Sisko model and the Cross model [82]. Within this work, due to its relatively simple format, the power law will be developed into a function to describe the characteristics of the printing ink. Firstly, an expression for the shear stress is given in Equation 5.36 [83].

$$\tau = k\left|\dot{\gamma}\right|^{n-1}\dot{\gamma} \qquad \text{Equation 5.36}$$

Where;

$$\dot{\gamma} = \frac{\partial u}{\partial y} \qquad \text{Equation 5.37}$$

This develops into the power law equation, Equation 5.38.

$$\tau = m\left|\frac{du}{dy}\right|^{n-1}\frac{du}{dy} \qquad \text{Equation 5.38}$$

Where the term $m\left|\frac{du}{dy}\right|^{n-1}$ represents the viscosity coefficient and for a Newtonian fluid $n=1$. Values of n less than one indicates a pseudoplastic fluid, values of n greater than one indicates a dilatant fluid. The apparent viscosity is then equivalent to;

$$\mu = m\left|\frac{\partial u}{\partial y}\right|^{n-1} \qquad \text{Equation 5.39}$$

In order to calculate the variation in viscosity through the ink film when using the power law, the local velocity gradient needs to be established and this can be achieved through numerical differentiation of the velocity profile. The velocity profile, derived by *Dowson* [42], takes into account the cross film viscosity variation and assumes that the fluid adheres to both surfaces moving at velocities of U_1 and U_2. This equation, Equation 5.40, is then solved iteratively as it includes the variation in fluid viscosity.

$$v(z) = U_1 + \frac{dp}{dx}\int_0^z \frac{y}{\mu}dy + \left(\frac{U_2 - U_1}{F_0} - \frac{F_1}{F_0}\frac{dp}{dx}\right)\int_0^z \frac{dy}{\mu} \qquad \text{Equation 5.40}$$

For the solution to the generalised pressure equation to be calculated, a set of boundary conditions need to be specified. If the pressure in the bow wave is noticeable, then clearly, the pressure at the ink inlet will not be atmospheric. However, as stated in Chapter 3, the pressure generated within the bow wave is negligible. Therefore, the ink at the entrance to the nip junction can be assumed to be atmospheric and the pressure set to zero appropriately. Additionally, the pressure at the outlet was also assumed to be under atmospheric conditions, where the pressure was also set to zero accordingly. To eliminate the possibility of a sub-ambient pressure within the ink film during the expansion of the film profile, and to satisfy flow continuity through the nip, negative pressures were set to zero as they occurred. This implicitly satisfies a zero gradient condition as well as the *Swift-Stieber* prescription. This has been chosen for convenience, but it should be noted that alternative prescriptions could apply, such as a viscopillary model [84] and the *Landau Levich* film rupture model [85]. Summarising the corresponding boundary conditions;

$P_{in}=0$	$x=x_{in}$
$P_{out}=0$	$x=x_{out}$
dp/dx	$x=x_{out}$

The disadvantage in using the power law is that it assumes infinite viscosity at very low shear rates, producing numerical difficulties. Therefore, to prevent unrealistically high viscosity and to reduce the computational time, a lower limit of 250sec^{-1} was set. This limits the viscosity to a maximum value determined by the shear rate of 250sec^{-1}.

Additionally, to prevent the viscosity from falling below a set level, an upper shear limit was set. This value was set to $3000sec^{-1}$, therefore, disregarding any changes in viscosity that may occur above this value. These values were chosen by running a number of different configurations and observing the alteration in the viscosity array. If the upper limit was set too low, then the viscosity array exhibited a minimal change. Whereas, if this limit was set too high, then the calculation took excessive computational time while having a minimal effect on the final result. A limit below $250secs^{-1}$ was not deemed necessary due to the shearing action within the screen-printing process, therefore this value was chosen for each calculation.

5.4 Overall Solution Strategy

The solution to the governing equations was obtained using the BEM and the FDM techniques as previously described for the rubber covered squeegee model and the hydrodynamic model respectively. The results from the two sets of governing equations were then combined through an iterative process set through the following routine.

1. Appoint an initial engagement value for h_0. From this, the Hertzian pressure and the resultant indentation can be calculated, which will reduce computational errors, as the initial pressure is not set to zero.
2. The film thickness is calculated for the nip junction.
3. The pressure within the ink film is calculated.
4. Establish the elastomer deformation corresponding to the pressure.
5. If the elastomer deformation has failed to meet the convergence criteria, repeat section 2 with a new deformation value.
6. Once the convergence criteria has been obtained, examine the squeegee load equilibrium, which is calculated from the integral of the pressure profile. If the squeegee load and squeegee deformation equilibrium has not been achieved within 0.1%, appoint a new deformation value and go to section 1.

5.5 Impermeable Model

The numerical model can be used to calculate the effect of the press parameters and the screen open area upon the changes in rheological properties within the nip contact region. However, this section will utilise an impermeable screen to gain an initial understanding of the characteristics expected, with the permeable screen investigated in the next section. This will allow the direct effect of the press parameters to be studied and will also establish a datum that can be used for the permeable screen numerical models.

5.5.1 Validation Study

For the numerical model to be used to calculate the rheological properties within the nip contact region, it is necessary to carry out a validation study in order to confirm the models applicability.

Due to the nature of the numerical model, there has been no other published work that the model can be compared to, due to the previous models using Newtonian fluids or the width of contact being pre-determined. However, the numerical model that has been developed within this work has been used to investigate elastohydrodynamic lubrication within a roller train in coating applications [86]. Therefore, to validate the numerical model, the current model was run using identical settings that were used within the journal publication. This would then allow a comparison to be made between the two studies. The settings used in [86] are itemised in Table 5.1, with the viscosity for the Newtonian model set to 12.57Pas and the screen backpressure set to zero in accordance with the findings in Appendix C.

Load (Nm^{-1})	Roller Radius (m)	Elastic Modulus (Pa)	Rubber Thickness (mm)	Viscosity Coefficient	Viscosity Index	Speed (ms^{-1})
7000	0.15	2.0E6	15	50	0.75	2.5

Table 5.1 Published Numerical Model Settings [86]

The pressure profiles and the corresponding ink film thickness results can be seen in Figure 5.4. The results obtained from the numerical model that was developed within

this study can be seen in Figure 5.5. As can be seen from these figures, the pressure and the ink film profiles, for both ink types are identical. This confirms the accuracy of the model.

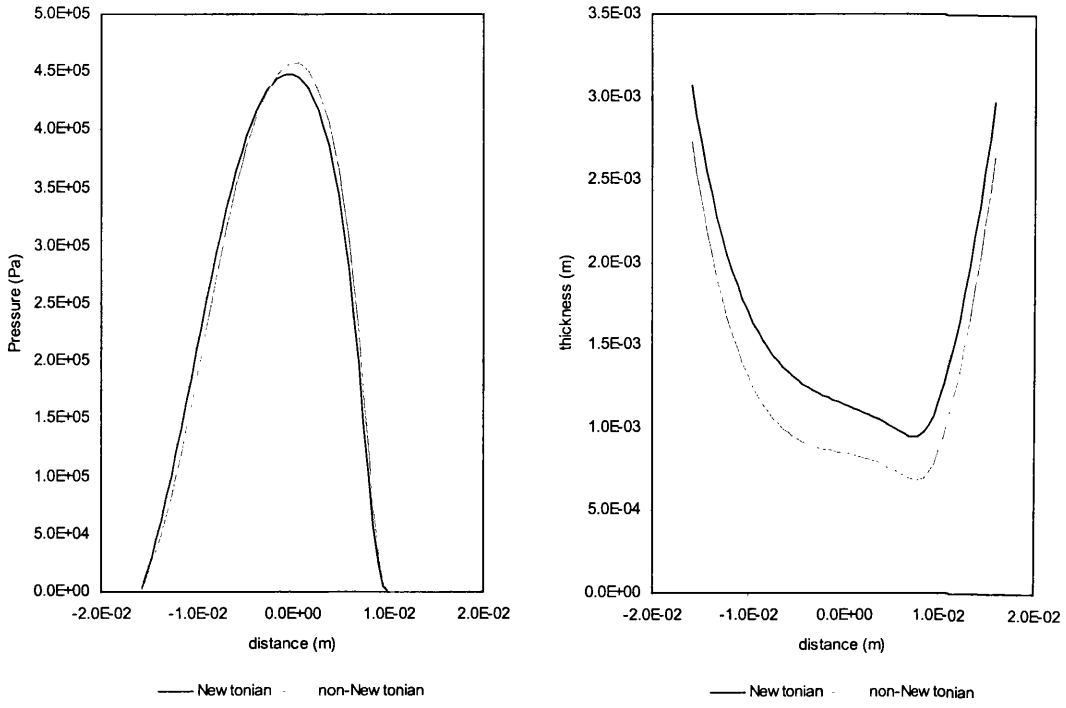

Figure 5.4 Published Numerical Model Results

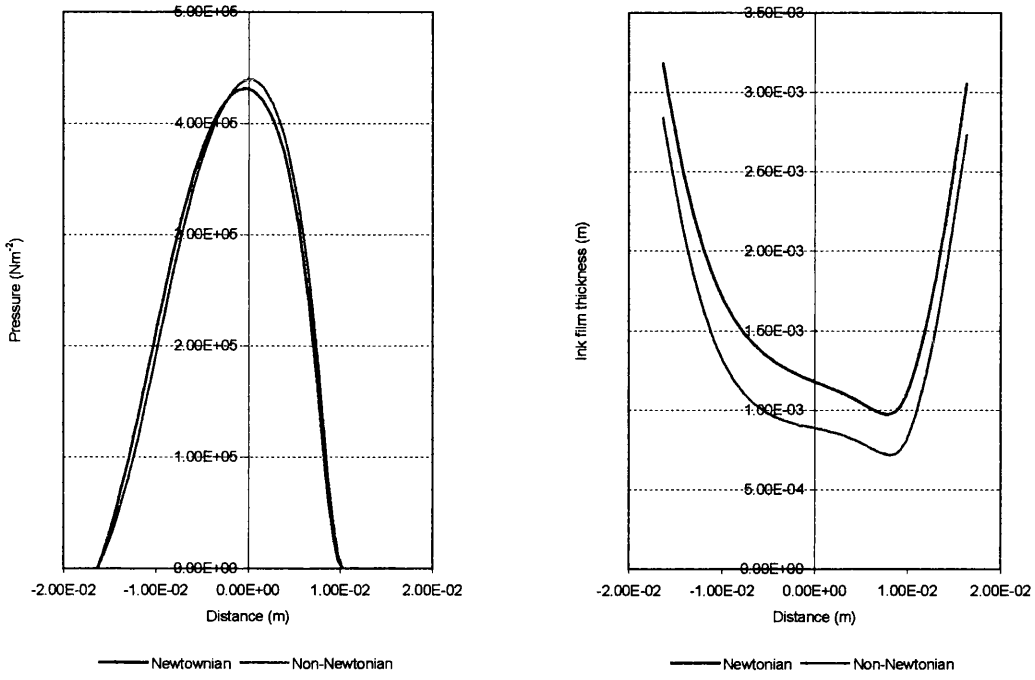

Figure 5.5 Predicted Results From the Current Model

5.5.2 Summary Comments

The validation study has shown that the numerical model produces results that correspond well with previously published work for Newtonian and non-Newtonian fluids. This will be developed further in the following sections to account for ink flow though the screen under the roller squeegee junction

5.6 Impermeable Model Numerical Investigation

It has been proven that the numerical model can accurately produce the pressure profiles and the ink film thickness values within the nip junction of a roller squeegee. The aim of this next section is to simulate the parameters that were utilised in the experimental studies, in order to recreate the characteristics within the nip junction. This will then allow a greater understanding of the ink transfer mechanisms within the screen-printing process.

The squeegee pressure was set to 4.5bar, which, for the numerical model, correlated to a squeegee reaction force of $750Nm^{-1}$ and $700Nm^{-1}$ for the 30mm and the 50mm diameter squeegees respectively (Appendix C). The contact width is assumed to be

zero for the initial calculation, as the squeegee is not yet in contact with the press bed. When the squeegee is brought into contact with the press bed at the next iteration, the subsequent contact width is calculated. The alteration of the squeegee pressure was not investigated as this proved to have a negligible effect upon printed results (Chapter 4). The ink characteristics were set to the appropriate values to characterise the power-law (Appendix B), with the material properties for the roller squeegee itemised in Table 5.2.

	Poisson's ratio	Elastic modulus	Rubber thickness
Roller squeegee surface	0.5	2.0×10^6	6.0mm

Table 5.2 Squeegee Material Properties

5.6.1 Results

The pressure profiles within the nip contact region, and the corresponding ink film thickness profiles, for the conventional UV ink, can be seen in Figure 5.6 for the rotating squeegee.

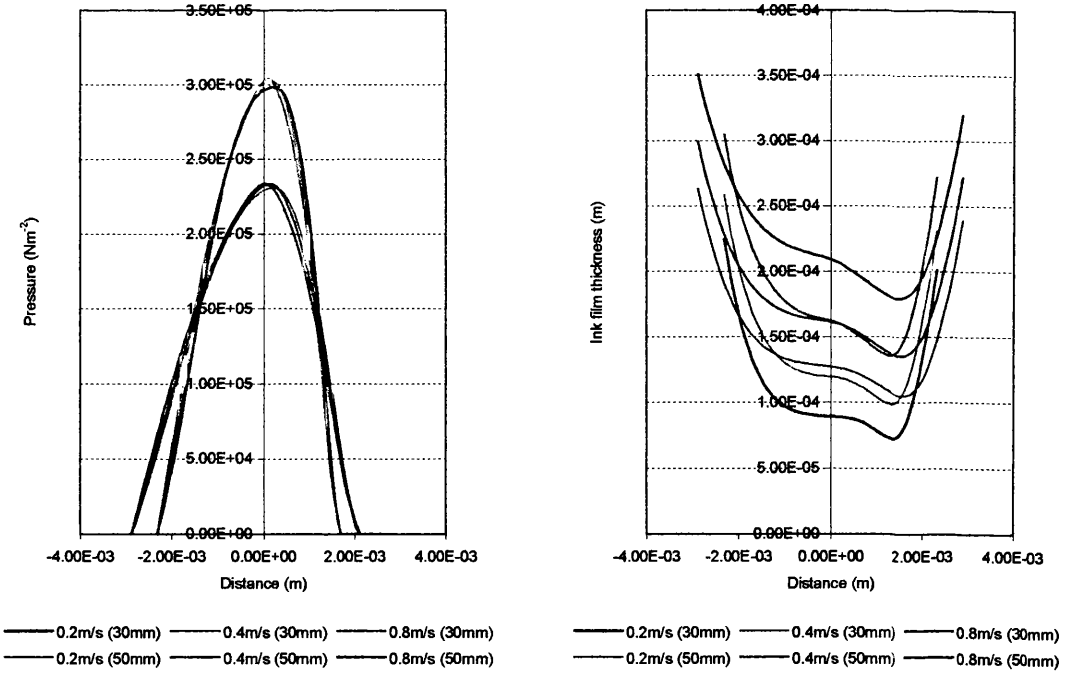

Figure 5.6 Film Pressure and Respective Ink Film Thickness for Rotating Roller Squeegee, Conventional UV Ink

An increase in the print speed has a slight effect of moving the pressure profile towards the inlet region of the contact, with minimal effect on the overall pressure distribution, in agreement with previously published data [75]. As expected, the pressure profiles for the 50mm diameter squeegee exhibit a greater contact width, with a peak value approximately 22% lower than the 30mm diameter squeegee. As the squeegee load is calculated from the integral of the pressure, a greater diameter squeegee would produce a greater contact width and would require a lower peak pressure value to obtain the same squeegee load.

Compared to the 30mm diameter squeegee, the 50mm diameter squeegee has produced a larger ink film thickness and an increased contact width, which has the effect of increasing the inking ability of the roller squeegee. Through the centre line of the point of contact, when the squeegee diameter is increased from 30mm to 50mm, the increase in ink film thickness is approximately 46μm when printing at $0.8ms^{-1}$ and approximately 38μm when printing at $0.2ms^{-1}$. This suggests that, at higher speeds, a change in squeegee diameter has a greater effect on the inking capacity of the squeegee than when printing at lower speeds. Additionally, the ink film thickness increases as the speed increases, to promote an increase in flow through the junction, which will further increase the inking ability of the squeegee. However, the increase in speed reduces the contact duration of the squeegee, which will be expected to reduce the squeegees inking efficiency.

To further investigate the behaviour details in the nip, Figure 5.7 and Figure 5.8 illustrate the velocity and the viscosity contours within the nip contact for the conventional UV ink, for the 30mm and the 50mm diameter squeegees at speeds of $0.2ms^{-1}$ and $0.8ms^{-1}$. The velocity and viscosity profiles both show lines of symmetry through the centre of the ink film indicating pure rolling contact. For each scenario, the ink velocity is at a minimum at the point of inlet where the pressure is ambient. As the pressure increases, the pressure gradient decays and the velocity of the ink flow increases. After the point of maximum pressure is reached, the fluid velocity increases at a greater rate, where it obtains a maximum value near to the outlet point. Near to the outlet point, the maximum fluid velocity exceeds the squeegee speed,

emphasising the pumping action of the nip contact. This has resulted in high levels of shear and therefore a reduction in ink viscosity, which is more noticeable near to the roller and press-bed surfaces, in agreement with previously published work [87] [88].

The results show that the different diameter rollers produce similar viscosity and velocity contours, indicating that the roller geometry has a minimal effect on the fluid properties. However, increasing the speed, increases the fluid velocity, with the resulting increase in shear reducing the fluid viscosity. Additionally, an increase in speed has reduced the contact time and resulted in the ink film thickness increasing, with the larger squeegee producing the greatest ink film thickness.

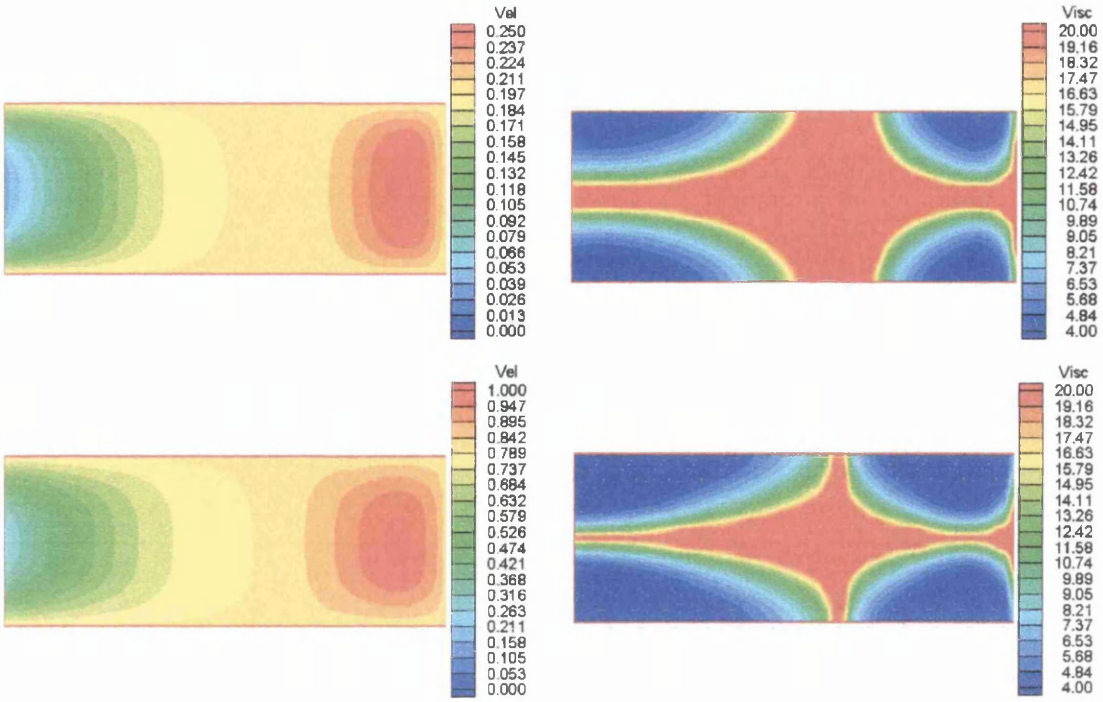

Figure 5.7 Velocity and Viscosity Contours for Conventional UV Ink With Rotating 30mm Squeegee at $0.2ms^{-1}$ and $0.8ms^{-1}$ Respectively

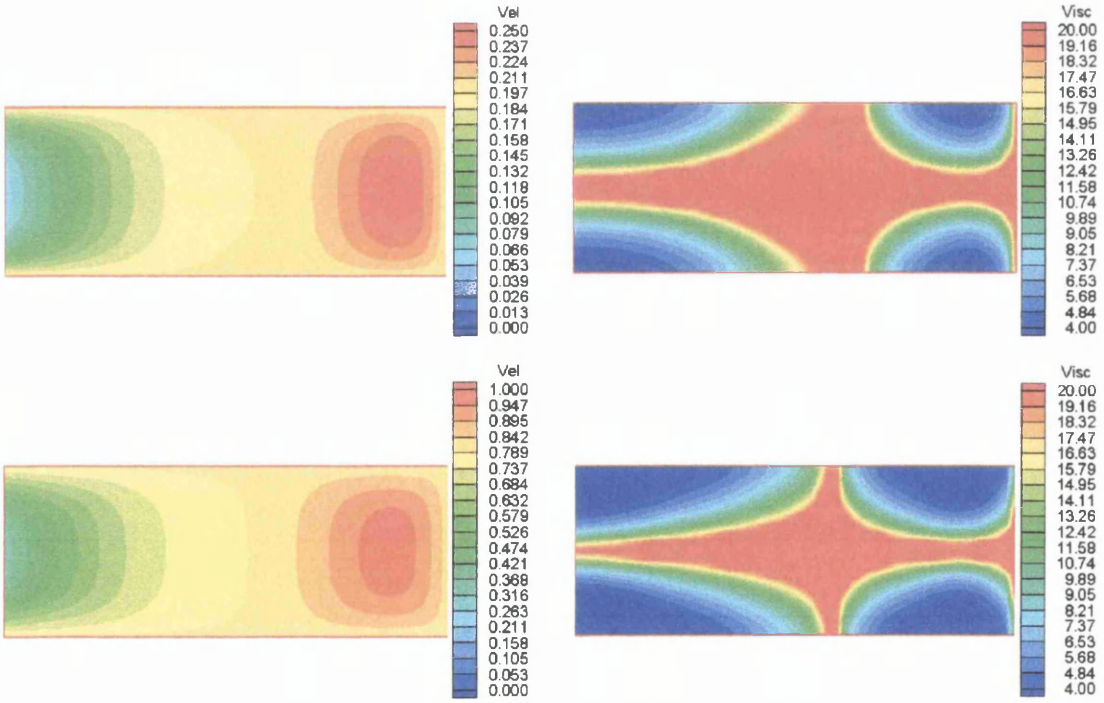

Figure 5.8 Velocity and Viscosity Contours for Conventional UV Ink With Rotating 50mm Squeegee at $0.2ms^{-1}$ and $0.8ms^{-1}$ Respectively

The pressure distributions and the ink film thickness profiles for the conventional UV ink, with the locked squeegee, can be seen in Figure 5.9, with corresponding selected velocity and viscosity contours in Figure 5.10 and Figure 5.11. Here, the pressure distributions and the contact widths are almost identical to those produced by the rotating squeegee, due to the hydrodynamic pressure being governed by the squeegee loading. Compared to the rotating squeegee, locking the squeegee has resulted in a reduction in the ink flow velocity through the nip contact gap, where the maximum velocity is the same as that of the squeegee. This has resulted in an overall reduction in the ink film thickness, which is further reduced as a result of the reduction in the inks viscosity, created by the increase in shear from the locking of the squeegee. Additionally, through the centre line of the point of contact, when the squeegee diameter is increased from 30mm to 50mm, the ink film thickness can be seen to increase by approximately 29μm at $0.8ms^{-1}$ and approximately 14μm at $0.2ms^{-1}$. These are considerably less than that observed with the rotating squeegee, indicating that the printing speed will effect the inking capacity of the rotating squeegee far greater than that with the locked squeegee.

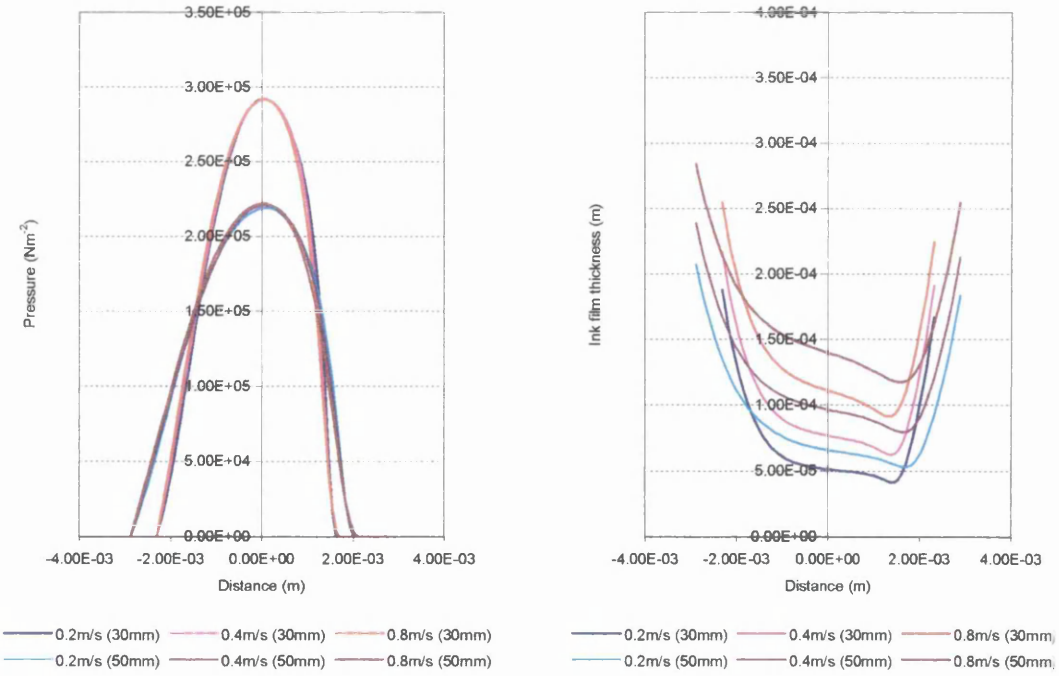

Figure 5.9 Film Pressure and Respective Ink Film Thickness for Locked Roller Squeegee, Conventional UV Ink

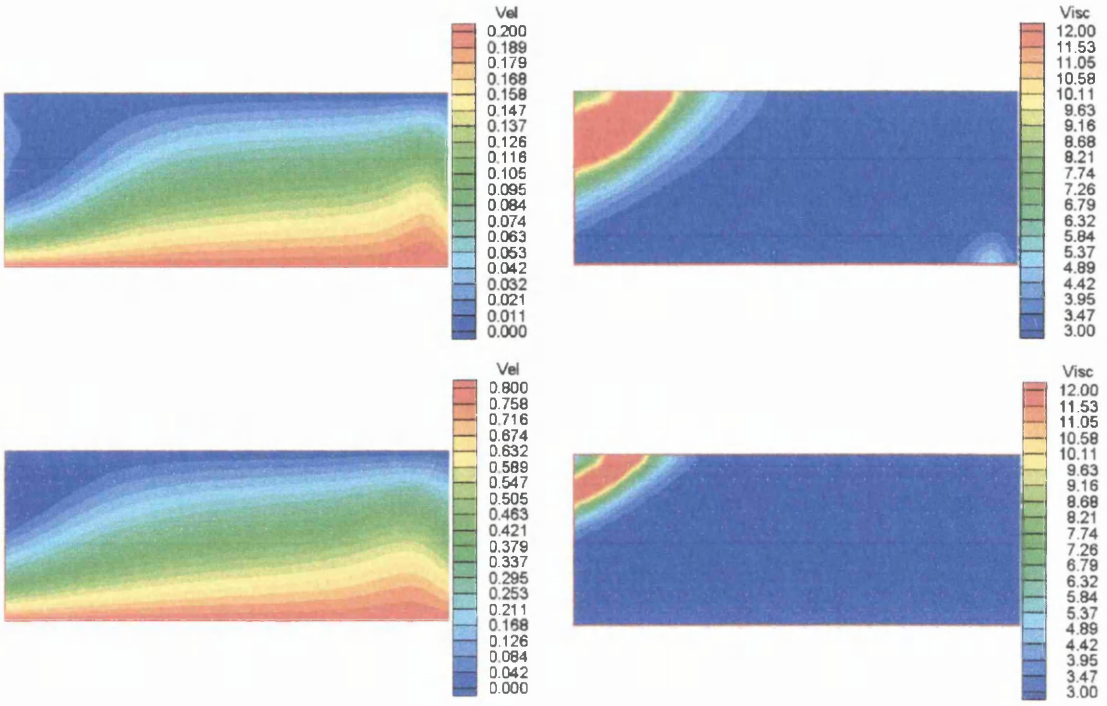

Figure 5.10 Velocity and Viscosity Contours for Conventional UV Ink With Locked 30mm Squeegee at $0.2ms^{-1}$ and $0.8ms^{-1}$ Respectively

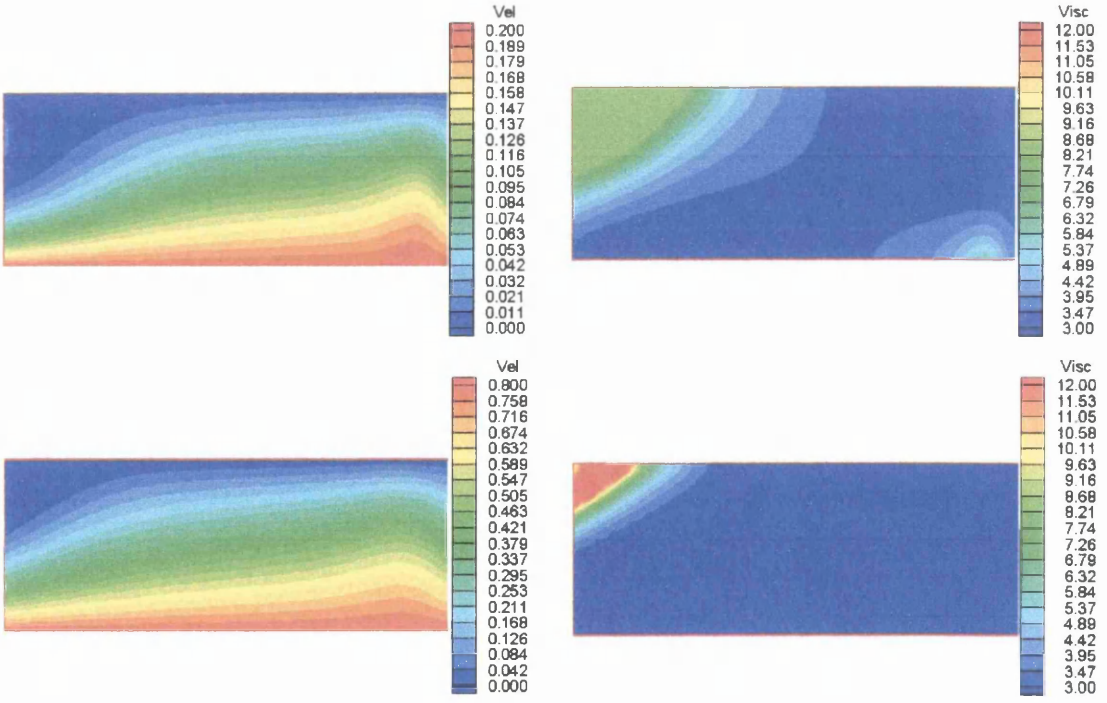

Figure 5.11 Velocity and Viscosity Contours for Conventional UV Ink With Locked 50mm Squeegee at $0.2ms^{-1}$ and $0.8ms^{-1}$ Respectively

The pressure profiles and the ink film thickness values for the rotating roller squeegees, printing the solvent-based ink, can be seen in Figure 5.12, with the velocity and viscosity contours shown in Figure 5.13 and Figure 5.14. As expected, the pressure profiles and the contact widths are similar to those observed with the conventional UV ink as the squeegee loading and dimensions remain the same. The velocity contours can also be seen as to be having the same trend as the conventional UV ink, but the solvent-based ink exhibits a much lower viscosity range. This reduction in ink viscosity has led to a lower ink film thickness, creating a reduced inking capacity to the screen. Additionally, the viscosity contours show that, although the viscosity varies throughout the entire nip contact region, the changes are relatively small compared to that observed with the conventional UV ink. This has resulted in the alteration in speed, and therefore an alteration in viscosity, having a smaller effect on ink film thickness for the solvent-based ink compared to the conventional UV ink.

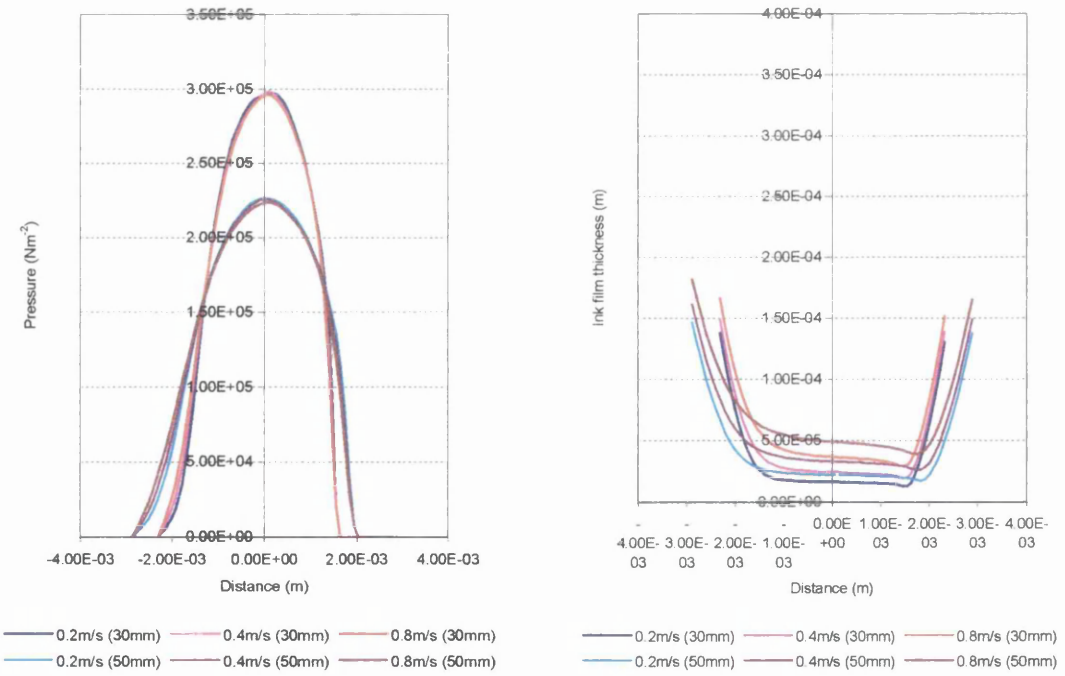

Figure 5.12 Film Pressure and Respective Ink Film Thickness for Rotating Roller Squeegee, Solvent-Based Ink

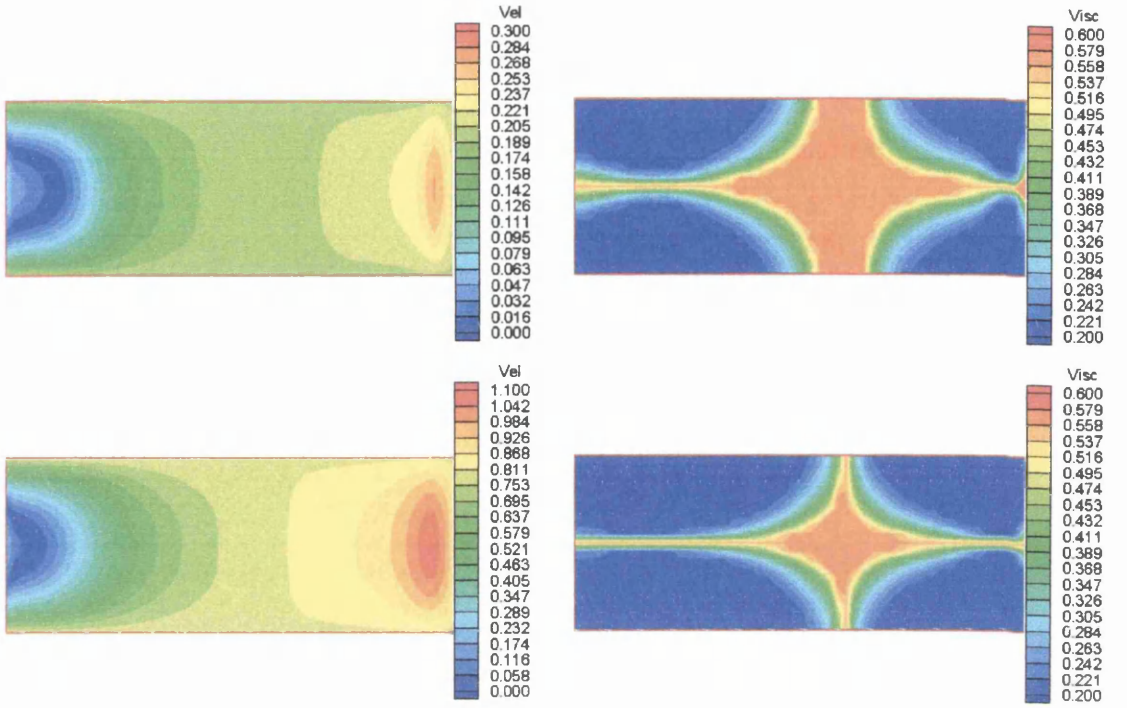

Figure 5.13 Velocity and Viscosity Contours for Solvent-Based Ink With Rotating 30mm Squeegee at $0.2ms^{-1}$ and $0.8ms^{-1}$ Respectively

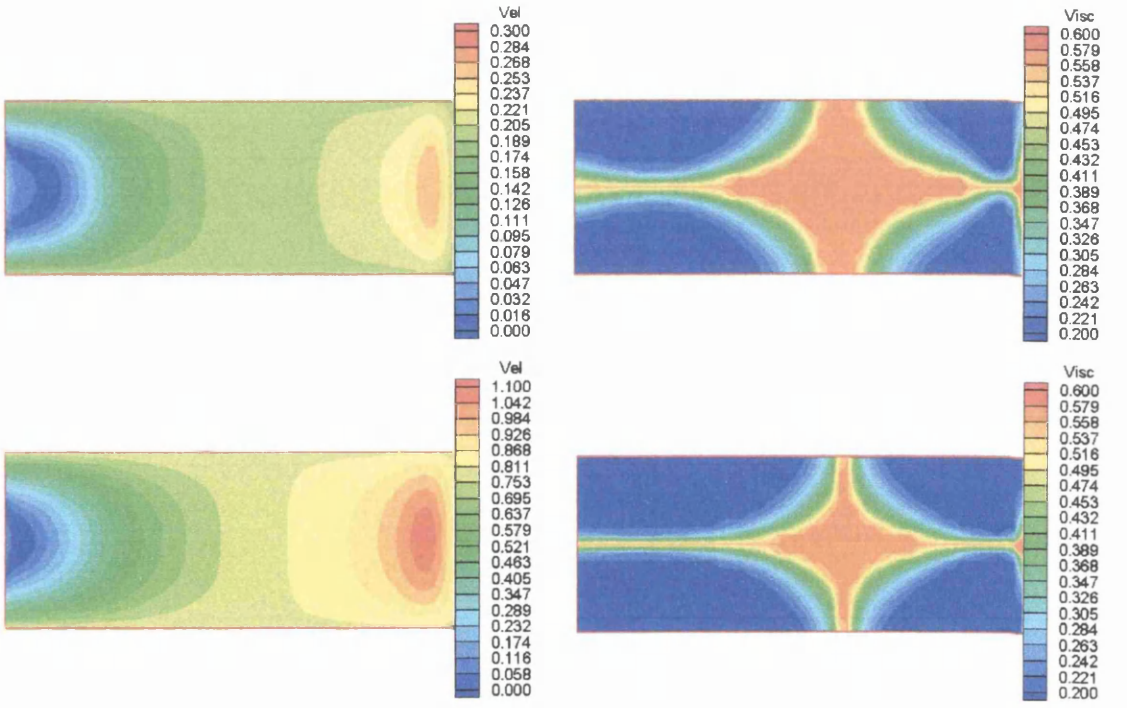

Figure 5.14 Velocity and Viscosity Contours for Solvent-Based Ink With Rotating 50mm Squeegee at $0.2ms^{-1}$ and $0.8ms^{-1}$ Respectively

With the squeegee locked, the pressure profiles and the contact widths for the solvent-based ink are similar to those observed with the squeegee rotating, with the ink film thickness at a reduced level, Figure 5.15. This reduction in ink film thickness is considerably lower than observed with the conventional UV ink and is primarily due to the lower viscosity ink, resulting in a much lower inking capacity. The lower viscosity solvent-based ink, Figure 5.16 and Figure 5.17, also results in the inking capacity being less affected by a change in print speed. However, the locked squeegee with the solvent-based ink produces the lowest film thickness, which will result in the lowest inking ability out of the squeegees and the inks that have been investigated.

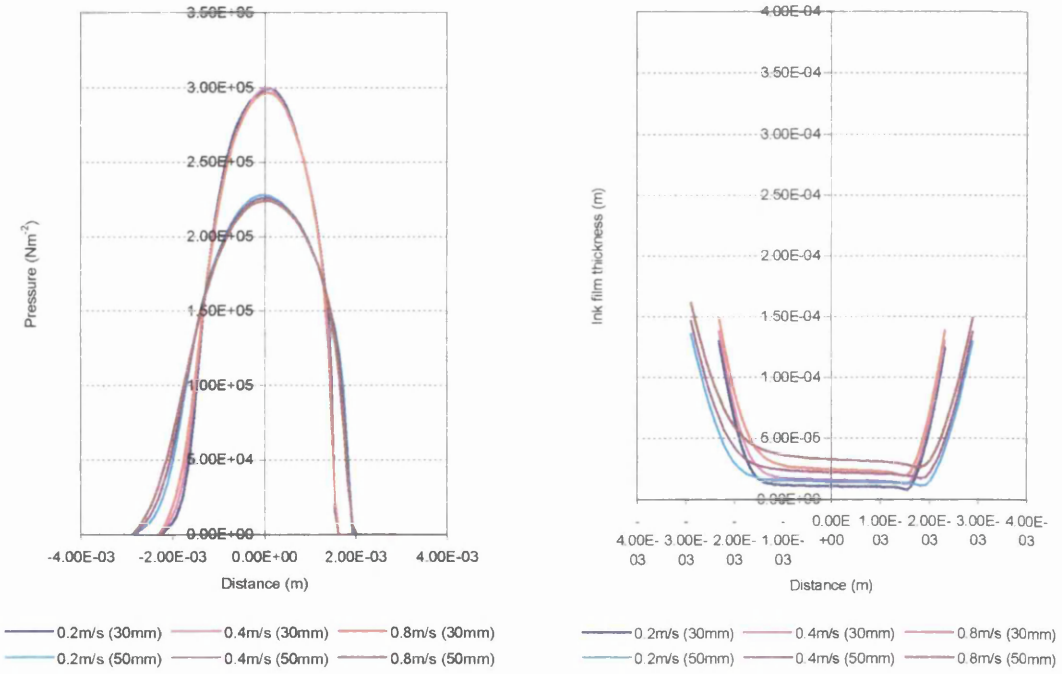

Figure 5.15 Film Pressure and Respective Ink Film Thickness for Locked Roller Squeegee, Solvent-Based Ink

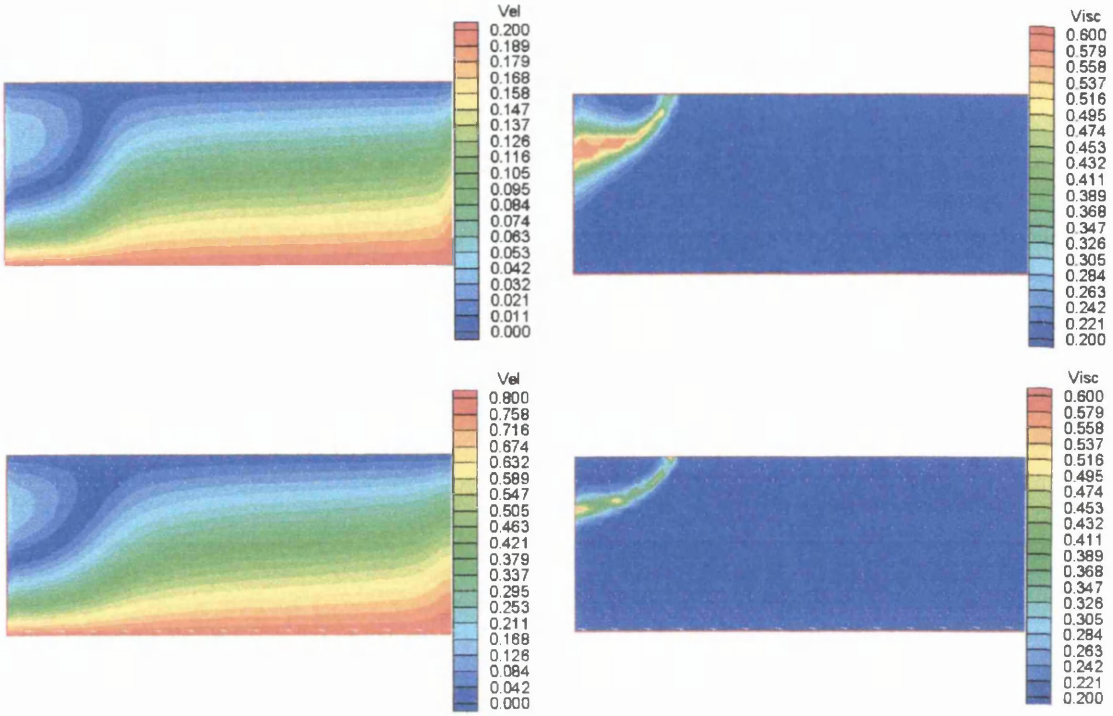

Figure 5.16 Velocity and Viscosity Contours for Solvent-Based Ink With Locked 30mm Squeegee at 0.2ms^{-1} and 0.8ms^{-1} Respectively

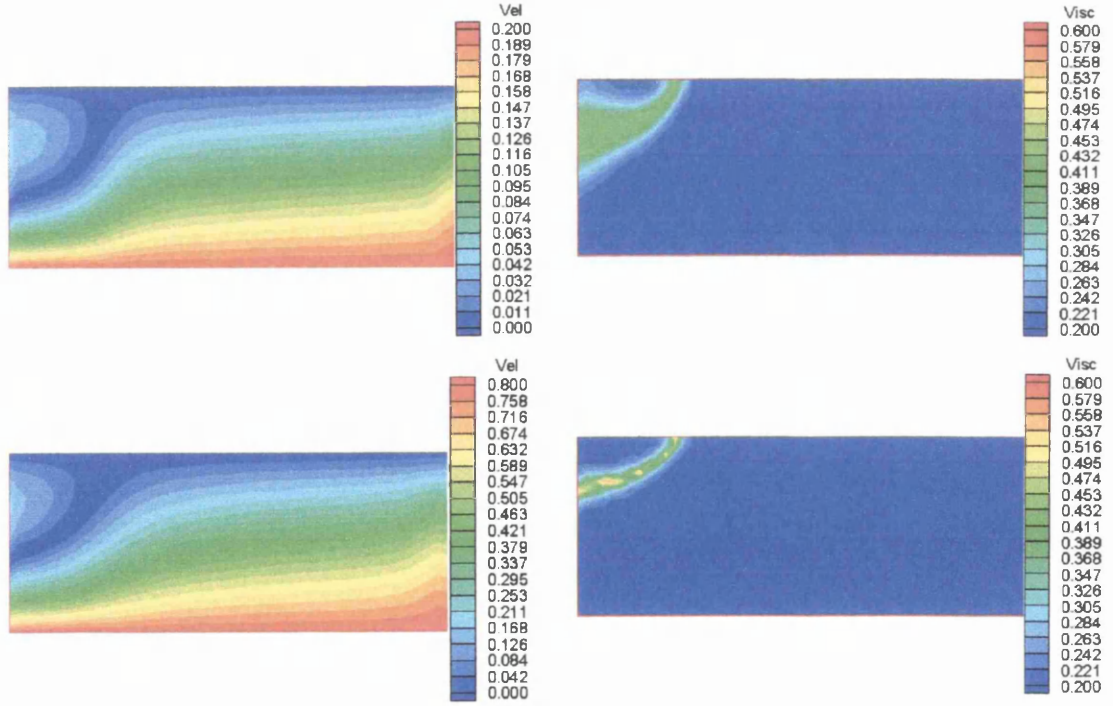

Figure 5.17 Velocity and Viscosity Contours for Solvent-Based Ink With Locked 50mm Squeegee at 0.2ms^{-1} and 0.8ms^{-1} Respectively

5.6.2 Summary Comments

The results obtained from the impermeable numerical model show that the printing speed and squeegee rotation both have a minimal effect on the pressure distribution and the contact width, although an increase in diameter will substantially increases the contact width. However, increasing the printing speed increases the ink film thickness resulting in a higher inking capacity in the nip, although this will subsequently reduce the contact duration. Additionally, increasing the squeegee diameter and rotating the squeegee both have the effect of increasing the ink film thickness and increasing the contact width. The alteration of the print speed can also be seen to influence the ink viscosity, which reduces as the shear rate increases with the print speed. This is more noticeable with the conventional UV ink, where the reduction in viscosity affects the ink film thickness by a greater amount than the solvent-based ink over the same range of print speeds.

5.7 Permeable Model

The preceding section investigated the rheological characteristics within the nip contact region when using an impermeable screen. This next section focuses upon the effect of the ink within the nip contact region when printing through screens of various open areas.

5.7.1 Validation Study

The primary aim for the simulation using the permeable screen was to use the same operating parameters as used in the impermeable model, but introducing open areas ranging from 0% to 100%. These results could then be compared directly with the experimental results obtained in the previous chapter. The screen backpressure was set to zero in accordance with the findings in Appendix C. Additionally, as the open area increases, more ink will be transferred through the screen and onto the substrate, resulting in a reduction in the ink film thickness in the nip contact region. Eventually, this will result in the squeegee coming into direct contact with the screen. When such a case arises, the governing equations for the numerical model will no longer be applicable in the absence of a thin film and the current model will be inappropriate.

From the impermeable numerical models, the lower viscosity of the solvent-based ink produced a significantly lower ink film thickness compared to that produced with the conventional UV ink. Introducing an open area to the solvent-based ink model resulted in sufficient ink to flow through the screen, causing the ink film to collapse, resulting in the squeegee coming into contact with the screen. This occurred for each setting with the solvent-based ink, but when the conventional UV ink was introduced, the modelling of the open area was achieved. However, for the rotating squeegee, this was only successful when the speed was set to the maximum printing speed of $0.8ms^{-1}$ with the 50mm diameter squeegee and with the open area set below 50%. When the squeegee was locked, this area reduced to 10%. Open areas greater than this and a reduction in speed, resulted in the ink film collapsing.

From the experimental studies, the corresponding settings for which the permeable model predicted a film on the screen surface are itemised in Table 5.3.

Ink	Squeegee	Speed	Percentage of Open Area					
Conventional UV	50mm (Rotating)	$0.8ms^{-1}$	0%	10%	20%	30%	40%	50%
Conventional UV	50mm (Locked)	$0.8ms^{-1}$	0%	5%	10%	-	-	-

Table 5.3 Solution Envelope

For each of these settings, the numerical model produced two values for the expected ink deposit. These are based on the column model and the ink spread model, described earlier in the chapter. To establish the accuracy and therefore identify the most appropriate of these deposit models, it was necessary to measure the height of the ink deposits that were produced in the experimental studies. This would then enable the predicted ink deposit to be compared to the actual printed height of the ink deposits that were produced using the same parameter settings. The heights of the ink deposits were measured using white light interferometry [57], where selected images obtained from the interferometer are shown in Figure 5.18 with their corresponding profiles. The profiles clearly illustrate that the dots are no longer columns of ink, but the ink has spread resulting in the individual dots slumping. Additionally, the images

for the 100% open area clearly show the interaction of the mesh fibres upon the printed image resulting in a series of peaks and troughs throughout the printed region.

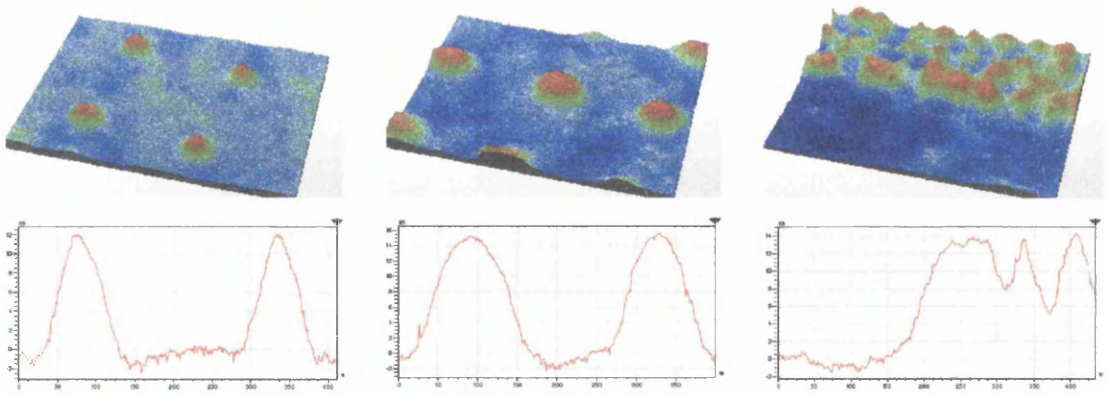

Figure 5.18 Selected Images and profiles of 20%, 50% and 100% Open Area Ink Deposits for Rotating 50mm Diameter Squeegee at 0.8ms^{-1}, 4.5bar

The actual measured heights for the ink deposits for the15% to100% open areas can be seen in Figure 5.19, along with the estimated ink deposits for the column model and the ink spread model for the 10% to 50% open areas. Additionally, the solid ink deposit predictions calculated with the ITM using a blade squeegee can also be seen in this figure. The column model produced results that decrease, with the spread model deposits increasing as the open area increases. This will be expected to occur until an open area of 100% is achieved, at which point the individual dots join to form a solid area. The actual heights of each of the printed deposits are in close agreement with the heights predicted with the ink spread model. An approximate constant value for the ink film thickness has also been added, after the 50% opening, where the squeegee rests on the screen and no additional ink transfer takes place. These heights range from approximately 9μm for the 15% coverage to approximately 15μm for the 50% coverage. The profiles of the ink deposit (Figure 5.18) also confirms that the individual ink deposits slump and spread across the substrate surface. Therefore, it can be stated that the ink spread numerical model can accurately predict the thickness of the expected ink deposit, neglecting any absorbency by the substrate.

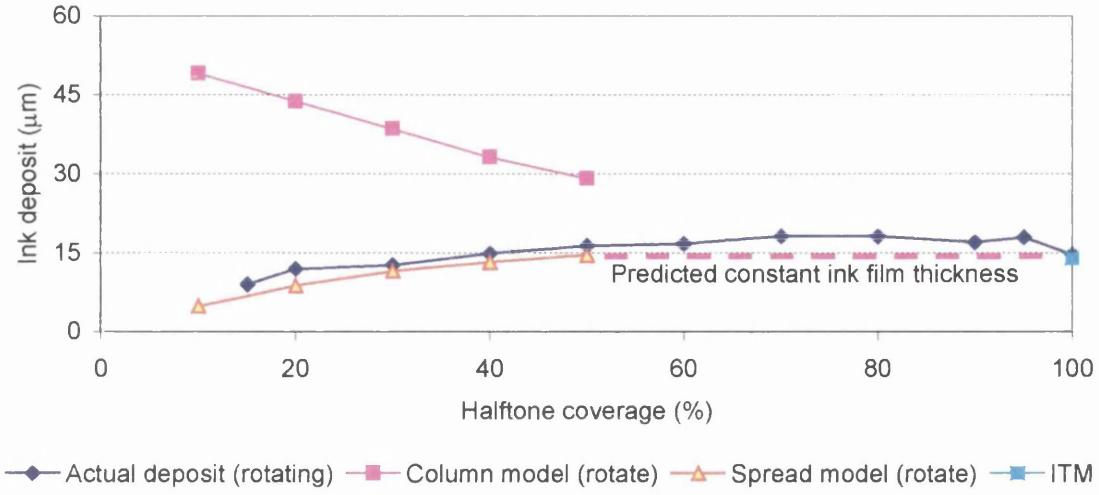

Figure 5.19 Actual Ink Deposit With Predicted Calculated Ink Deposit 50mmDiameter Squeegee at 0.8ms^{-1}, 4.5bar

5.7.2 Summary Comments

Using the ink spread model, the numerical model has been used to accurately calculate the expected ink deposit for a range of open areas. However, the success of the model is dependent upon an ink film being present underneath the squeegee. A large increase in open area has resulted in sufficient ink being transferred through the screen as cause the ink film underneath the squeegee to collapse. If this occurs, the model is no longer appropriate. The value of the open area for which this occurs is dependent upon many factors such as the ink viscosity, shear rate, squeegee diameter and the printing speed. Additionally, the ink spread model calculates the thickness of the ink deposit within close agreement to previous numerical models, which are only capable of calculating the height of the solid areas.

5.8 Permeable Model Numerical Investigation

The previous section has shown the ability of the numerical model to accurately predict the ink deposits throughout a number of different open areas. This next section discusses the rheological characteristics within the nip contact region using the same settings as described in the validation study for the permeable screen.

5.8.1 Results

The ink film pressure and the corresponding ink film thickness profiles for the 0% to 50% open areas (incrementing in 10% steps), can be seen in Figure 5.20, with selected velocity and viscosity contours in Figure 5.21 (0%, 10%, 30% and 50%). The effect of introducing a permeable screen has resulted in a slight alteration of the pressure profile, with the pressure profile moving slightly towards the inlet region with an increase in open area. The permeable nature of the screen has resulted in a reduction in the ink film thickness as the ink flows through the screen. This emphasises the fact that when printing higher open areas, an increasing quantity of ink flows through the screen, with less ink remaining on the screen after the print stroke. This has resulted in a gradual reduction in the ink flow velocity through the nip contact region. Additionally, this reduction in velocity has resulted in an increase in viscosity.

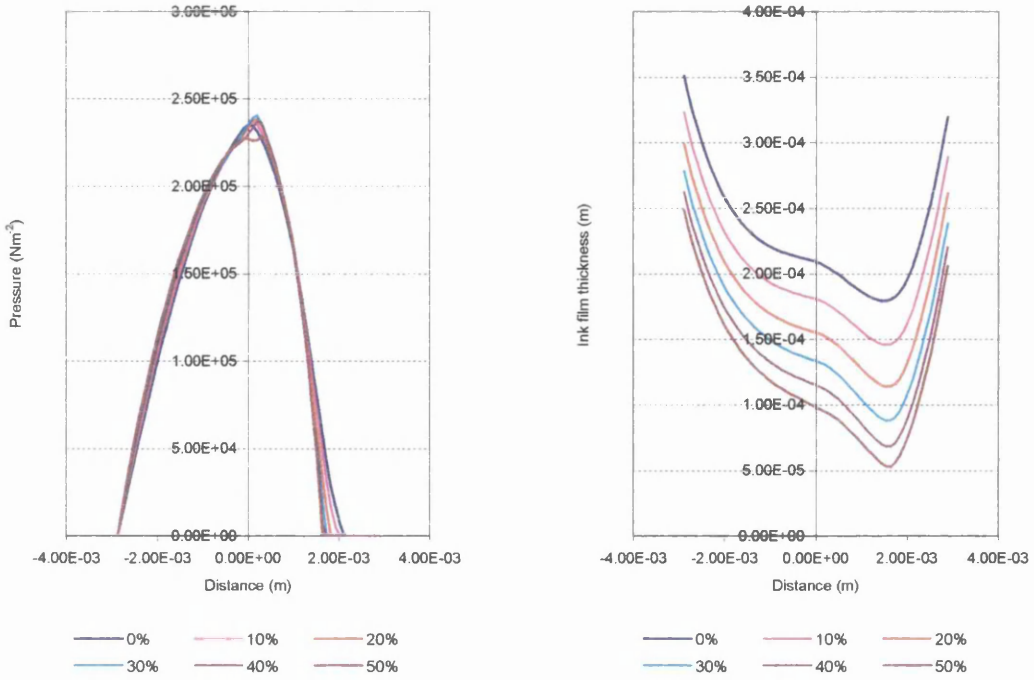

Figure 5.20 Film Pressure and Respective Ink Film Thickness for Rotating Roller Squeegee at 0.8ms^{-1}, Conventional UV Ink

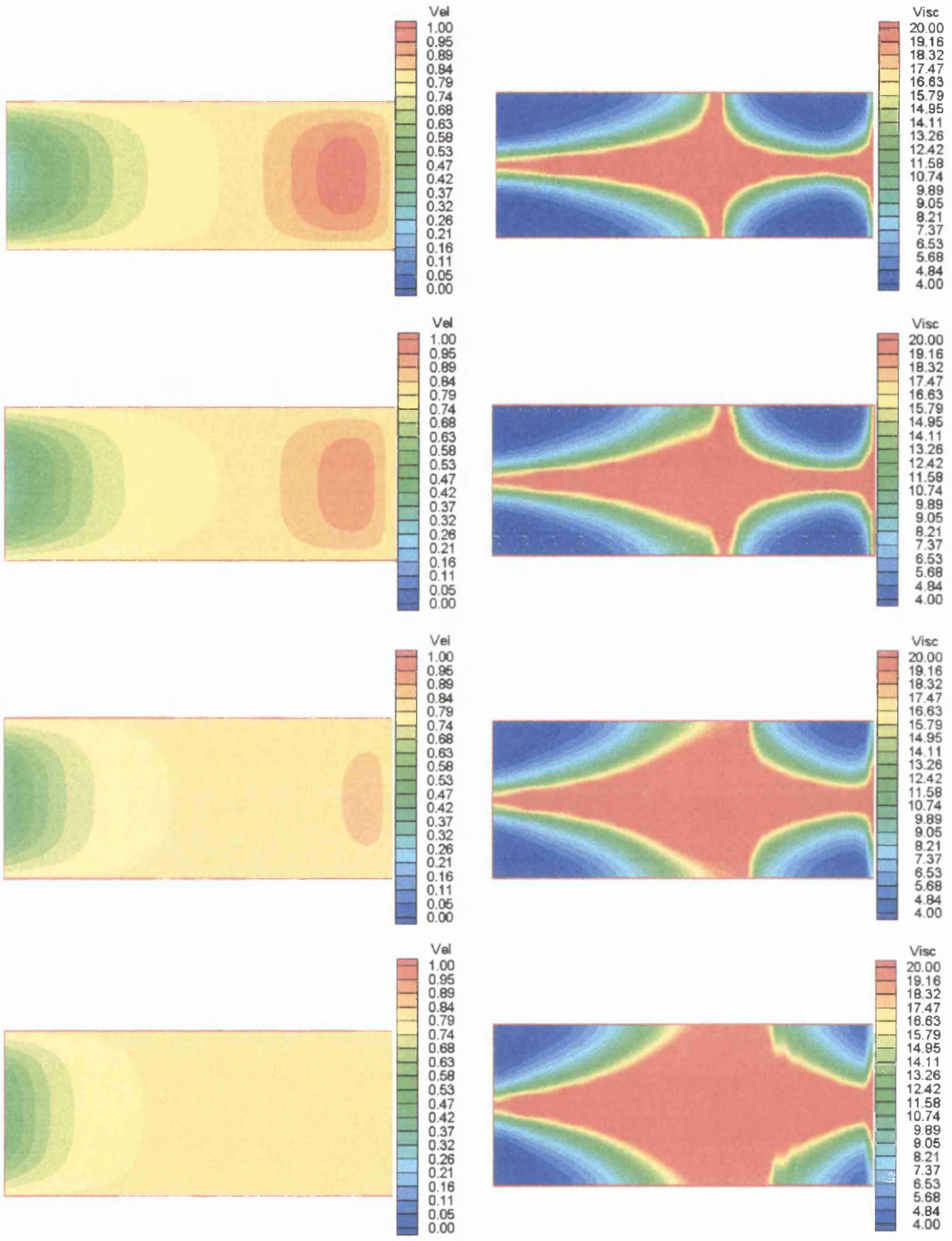

Figure 5.21 Velocity and Viscosity Contours for Conventional UV Ink With Rotating 50mm Squeegee at 0.8ms-1, for 0%, 10%, 30% and 50% Screen Open Area (Top Contours 0%, Bottom Contours 50%)

When an open area is introduced to the screen, the pressure profile for the locked squeegee moves towards the inlet region at a far greater rate than occurrs for the rotating squeegee, Figure 5.22. This suggests that the point of injection of the ink into the screen also moves towards the inlet region. Additionally, the ink film thickness significantly reduces with an increase in open area, where an open area of 10% or greater has resulted in the ink film collapsing, thus theoretically removing all of the ink from the screen surface. As a result of the ink flow through the screen, the velocity of the ink through the nip region reduces similar to that observed with the rotating squeegee, Figure 5.23.

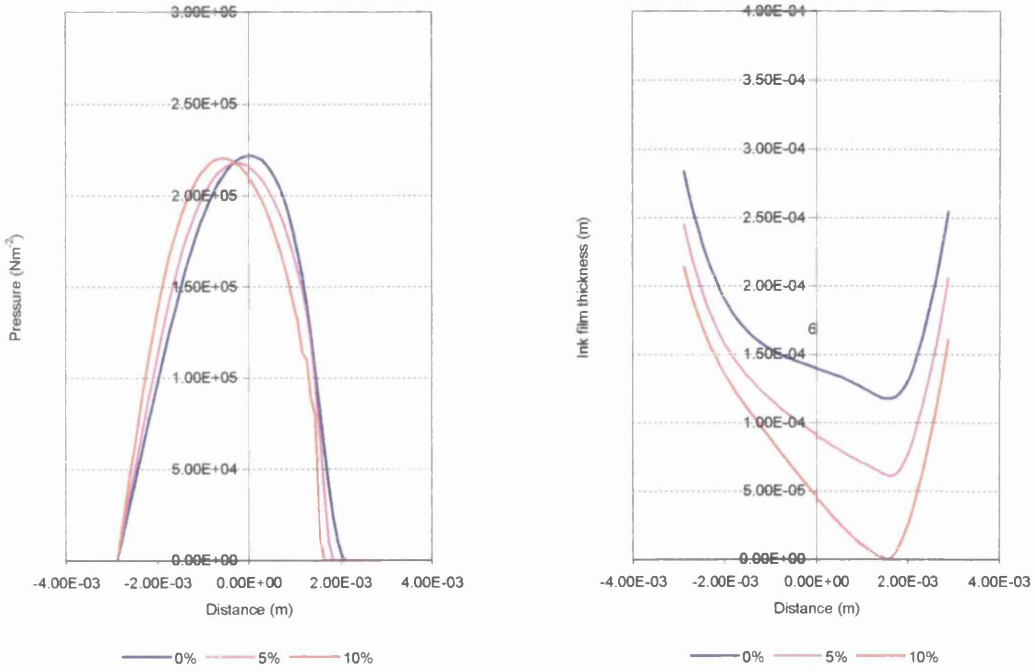

Figure 5.22 Film pressure and Respective Ink Film Thickness for Locked Roller Squeegee at 0.8ms^{-1}, Conventional UV Ink

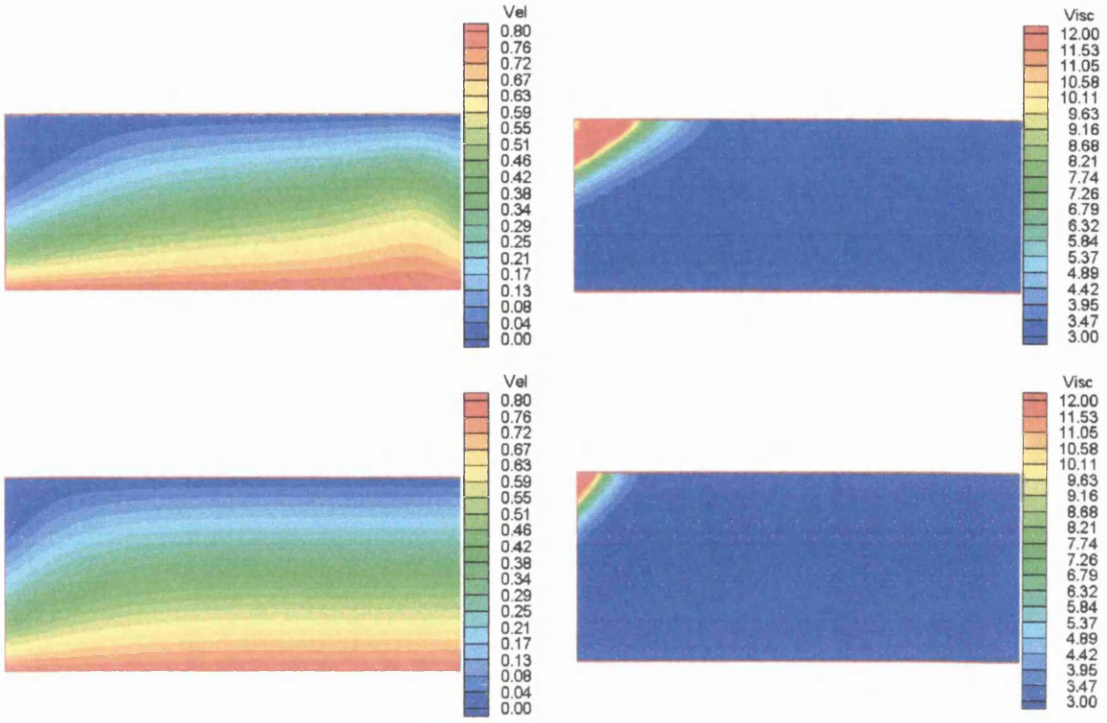

Figure 5.23 Velocity and Viscosity Contours for Conventional UV Ink With Locked 50mm Squeegee at 0.8ms^{-1}, for 0% and 10% Screen Open Area (Top Contours 0%, Bottom Contours 10%)

5.8.2 Summary Comments

Introducing a screen having an open area to the numerical model has resulted in a substantial reduction in the ink film thickness. This can be explained by the ink flowing though the screen and onto the substrate, which has resulted in a reduction in the ink velocity in the nip contact region. However, this introduces complications in running the model, as an ink film needs to be present for the model to run successfully. The models that have been run have produced ink deposits that correspond closely to the thickness of the actual ink deposits that were produced in the experimental chapter.

5.9 Conclusions

The experimental studies, in the previous chapter, highlighted the fact that the larger diameter roller squeegee produced higher ink coverage than the smaller diameter squeegee whilst printing at similar print speeds with the same pressure settings. Previously, this was believed to be resulting from a decrease in snap-off speed or an increase in the contact width. However, the numerical model has shown that a larger diameter roller squeegee produces a higher ink film thickness on the squeegee as well as an increased contact width. This has the effect of increasing the squeegees inking capacity and increasing the time during which ink can be transferred to the substrate, thus a greater quantity of ink can pass through the screen.

The results from the numerical models exhibited an increase in the ink film thickness with an increase in print speed. This will result in a higher inking capacity of the squeegee, resulting in a higher ink coverage. However, the experimental studies showed that an increase in speed would decrease the ink deposit. Previously this was believed to be because of an increase in snap-off speed or a reduction in the contact duration, or a combined mechanism. Therefore, it can be stated that the ink film thickness on the squeegee and the contact duration of the squeegee upon the screen both have a dominant effect upon the ink deposit that is generated.

With the squeegee locked, the experimental results produced lower ink deposits than if the squeegee were free to rotate. This was postulated to be as a result of the increase in the pressure generated by two moving surfaces. However, as the pressure

is governed by the squeegee loading, minimal difference in the pressure profiles was exhibited as the squeegee was free to rotate or when it was locked. However, the lower ink coverage for the locked squeegee can be explained by the reduction in the ink film thickness, created by the reduction in the viscosity of the ink, resulting in a reduction in the inking capacity of the squeegee to the screen.

To date, this is the first research that has focused on calculating the thickness of the ink deposits within a halftone gradation. This has resulted in a permeable model that produces two values for the estimated thickness of the ink deposit, one based on a column of ink and the other based upon the column of ink spreading across the substrate surface. However, introducing an open area into the printing screen resulted in numerical difficulties at slow speeds and for large open areas. This was due to the ink flowing through the screen and onto the substrate, resulting in a reduction in the ink film thickness causing the squeegee to come into direct contact with the screen. Based on the ink spread model, the numerical scheme produced estimated ink deposit results that were in close agreement with the actual thickness of the ink deposit that was measured with the white light interferometer. These values were also similar to those that were obtained in previous work into estimating solid ink deposits.

Chapter 6

High-Speed Belt Screen-Printing Press

6 High-Speed Belt Screen-Printing Press

6.1 Introduction

This chapter describes the design of the high-speed belt screen-printing press and highlights the relevant practical issues and design developments. Where appropriate, this draws upon the work that has been done in the preceding chapters, together with development of pertinent models for the belt component.

Before the design of such a press can be commenced, the press concept and design specification needs to be considered. These were discussed with the relevant members of the project and were finalised as follows;

- The concept of a stand-alone machine or one that can be integrated as part of another press needs to be considered.
- The belt system will be sprocket driven.
- Two main drive rollers will be used, each being 300mm in diameter. The space between these rollers will be sufficient as to accommodate the ink delivery and removal.
- The belt-screen will need to be able to withstand sufficient tensile load so as to ensure the correct biaxial tension is maintained to provide correct registration and snap-off throughout a print run.
- For high quality graphics, the belt will require an equivalent mesh count of at least 120 lines per inch.
- The screen will be produced either by coating the stencil onto the screen, as in traditional screen-printing, or it will be perforated directly to form the required image.
- The belt length will be approximately 3000mm, with a maximum permissible belt width of 508mm. The allowable thickness will be between 0.006mm and 0.25mm, with a typical thickness expected to be 0.07mm.
- The maximum image width is 200mm.
- The projected print speed is equivalent to 7000, B1 copies per hour, this being twice the speed of current cylinder presses.

- The range of speeds will be between $0.25ms^{-1}$ and $4ms^{-1}$ with an inching (jog) control facility. Additionally, very slow speeds must be achievable with a provision for crawl ($\sim 0.08ms^{-1}$).
- Provision must be made for belt removal.
- Two smaller tension rollers will be positioned in-between the two drive rollers and will move in the vertical field, coming into contact with the top side of the belt as to adjust the belt tension. This will have the additional benefit of allowing the belt to be removed and positioned with greater ease.
- To allow full adjustment of the snap-off angle, rollers will be positioned either side of the squeegee, which can be independently adjusted in the vertical direction to obtain full control of the belt approach and snap-off angle.
- The press will be able to accommodate squeegee diameters of between 25mm and 125mm
- A separate drive for the squeegee is required to allow for independent squeegee and belt speed.
- The ink delivery will need to ensure an adequate, distributed and timely supply to the printing head.
- Any ink remaining on the screen after the printing nip will need to be removed to minimise contamination, waste and clean-up time.
- Ink must be prevented from escaping over the sides of the belt.
- Clear access from the front and back of the system is required.

The main emphasis of this work has focused upon the specification and the implementation of the high-speed belt screen-printing press, with the physical design of the press being undertaken by AMTRI.

6.2 Press Design

Observing the press specification and configuration issues, the final design of the press was developed after a number of meetings and design sessions within the project industrial group. A schematic of the design can be seen in Figure 6.1, with the manufactured press in Figure 6.2.

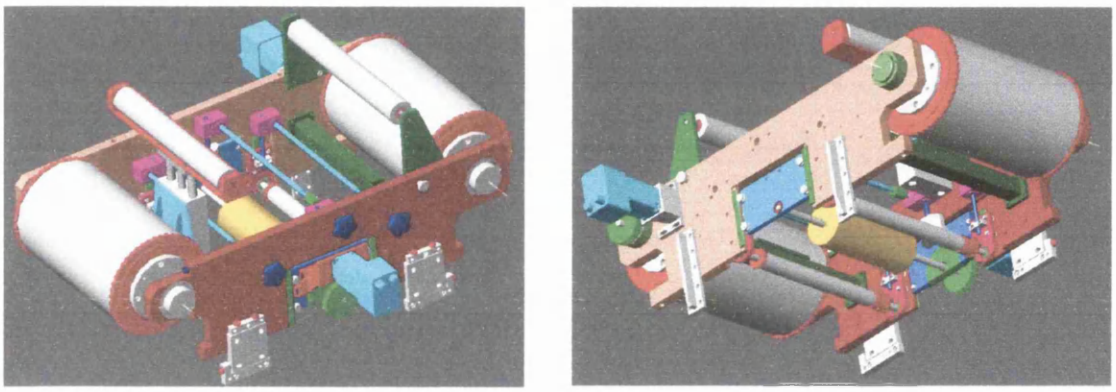

Figure 6.1 Final Design of The High-Speed Belt Screen-Printing Press

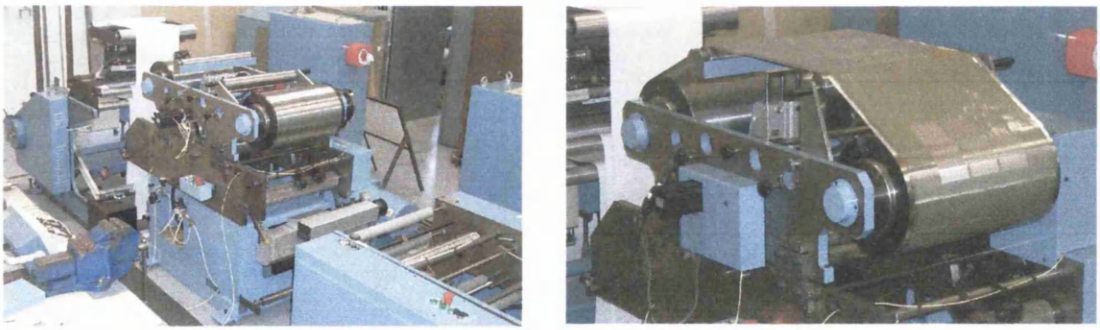

Figure 6.2 High-Speed Belt Screen-Printing Press

To adjust and maintain the correct belt tension, two rollers are situated at the topside of the press, one of which is controlled pneumatically to adjust the belt tension as appropriate, Figure 6.3. Additionally, the belt approach angle to the squeegee and the squeegee snap-off angle can also be adjusted with two rollers which are situated either side of the squeegee, Figure 6.4. The height of these can be independently adjusted, accurately controlling the angle of the belt in relation to the squeegee.

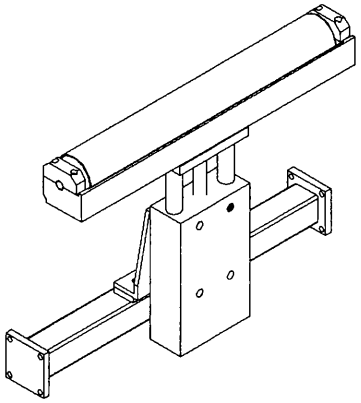

Figure 6.3 Pneumatic Belt Tension Roller

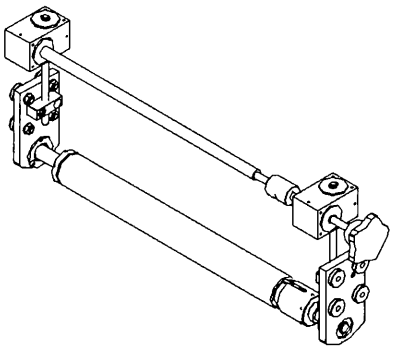

Figure 6.4 Belt Approach and Snap-off Angle Control Roller

As well as allowing the belt tension to be adjustable, the tension rollers also direct the belt away from the main body of the press, allowing easy access through the front and the back of the press, as defined in the specification. This will allow accessibility into the press for inspection and for any maintenance that may be required to the ink delivery and removal systems. A side view of the press showing the approximate path that the belt will follow over the two belt tension rollers on the topside of the press can be seen in Figure 6.5.

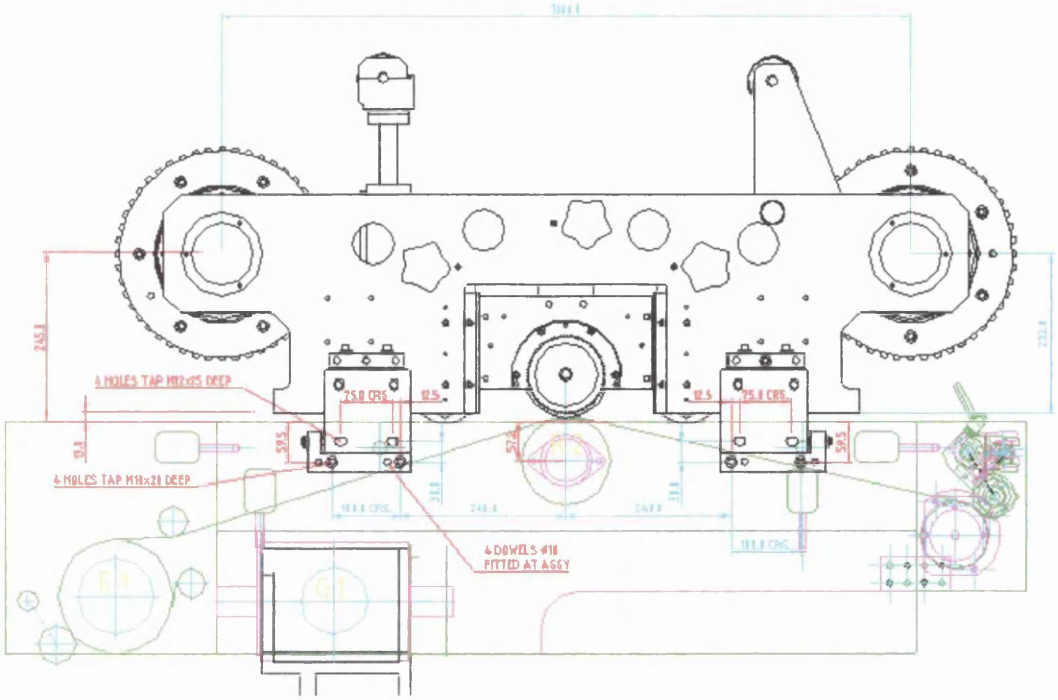

Figure 6.5 Side View of High-Speed Belt Screen-Printing Press

The removal of the belt from the press either requires the belt join to be separated, or a system incorporated into the press that will enable the removal of the joined belt. As the belt material has yet to be finalised, the method for joining the belt cannot be determined. Therefore, it is not known whether the belt can be re-joined. For this reason, it was decided that the press needed to be designed to accommodate the removal of a continuous belt. This was achieved by having two removable supports on one side of the press, connecting the press to the press stand, and two rigid permanent supports on the other side of the press. The removable supports are in the form of two plates that can be detached, with the two supports on the other side of the press maintaining the press position once the plates have been removed. This then allows a continuous belt to be removed or placed onto the press as required, Figure 6.6.

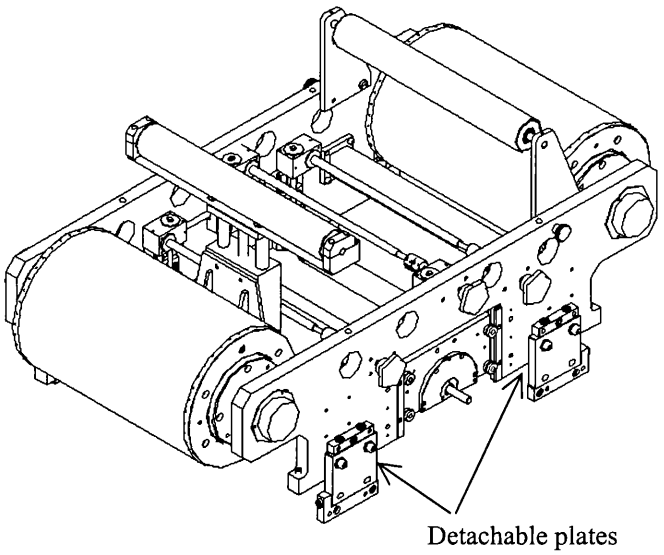

Figure 6.6 Detachable Plates for Belt Removal

6.3 Practical Issues and Development

Following on from the development and the manufacture of the press, a number of practical issues need to be resolved. These are the belt material and construction, along with the final squeegee specification that will be required for the high-speed application. Additionally, at this stage, there can only be a preliminary design of the ink delivery and removal system, as the exact quantity of ink cannot be established until printing commences. The next section investigates and analyses each of these areas in detail.

6.3.1 Belt Material and Construction

One of the most important aspects of the press design is the material and the construction of the belt-screen. The belt material will need to possess low elongation and high creep resistance characteristics, whilst maintaining the correct biaxial tension. A suitable material would be polyethylene terephthalate (PETP), where the mesh can be generated using laser ablation methods. The image area will be applied by perforating the image directly onto the screen or by producing a coated stencil over the perforated screen and exposing the stencil in the traditional way. As mentioned in the literature review, a patent for the use of a laser to ablate holes in a thin non-woven sheet of nylon or polyester to produce a screen was filed in 1992 [14], but the idea was never developed with its suitability remaining unknown. However, laser ablation has

been successfully achieved with relation to disposable and digital screens, although its printability was not thoroughly investigated [89]. If PETP is to be used for the belt, the effect of the ablation pattern will greatly influence the screen strength. Therefore, a number of ablation patterns have been investigated using Finite Element Analysis (see Appendix D) to find the most appropriate pattern to minimise stress concentration within the screen [90].

The analysis was established through micro and macro evaluation. The microanalysis involved modelling a symmetrical quarter section of a single hole formation and applying a load to the model to simulate the belt tension. Two thicknesses of PETP film were used, 0.1mm and 0.07mm, and these were subjected to a typical mesh tension of 15Ncm^{-1}. For analysis purposes the screen resolution was set to 65lpi, although the screen resolution in this type of analysis is insignificant as the loading is applied per unit length. Three holes were then modelled onto the film representing holes of sizes 3%, 40% and 70% area coverage and were produced in a square and a hexagonal formation, Figure 6.7. Regions of print that require area coverage of greater than 70% would need to rely on tone gain to increase the area coverage.

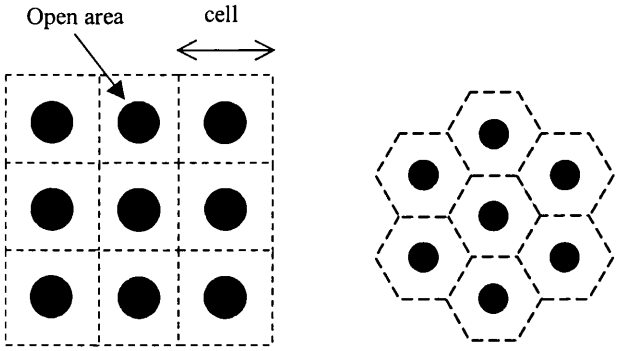

Figure 6.7 Square and Hexagonal Hole Formation

To simplify the modelling it is possible to only model a single symmetrical section, where the geometry, structure and loading are symmetric about the horizontal and vertical axis. The modelling of each of the formations was therefore simplified as quadrants, with the tension in the belt being converted into a face load. This face load

was then applied perpendicular to the edge of the cell area, with the axis of symmetry being formed through the horizontal and vertical axes of the formation, Figure 6.8.

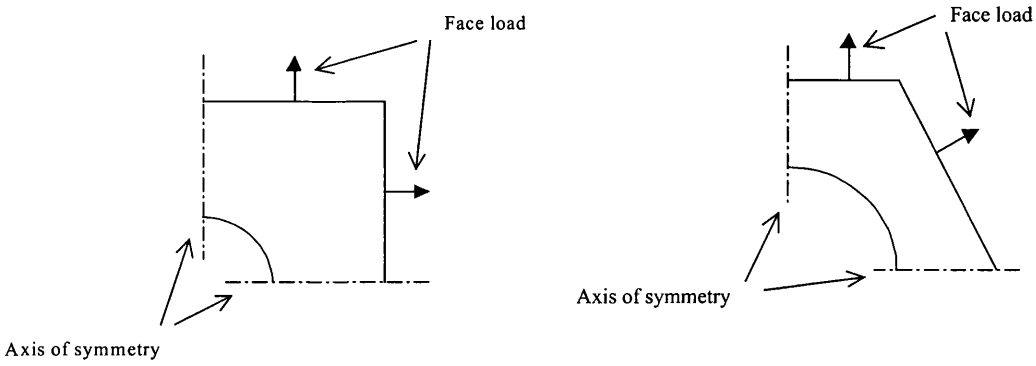

Figure 6.8 Square and Hexagonal Hole Formation Boundary Conditions

Stress concentration plots for the 0.1mm PETP film with 3% and 70% open areas in hexagonal and square formations can be seen in Figure 6.9 and Figure 6.10. Due to similar stress contours being produced for the rest of the results, the remaining contour plots are not presented. The stress distribution in each of the models followed similar patterns with the highest stresses generally being located at the periphery of the hole. As expected, the resultant stresses have proved to be largely dependent upon the film thickness, the hole formation and the percentage of open area. For the 70% open area in the hexagonal formation, a reduction from 0.1mm to 0.07mm film thickness resulted in the stress increasing from 152Nmm^{-2} to 217Nmm^{-2}, due to the reduction in cross-sectional area. For the square formation, this increase was even greater from 360Nmm^{-2} to 514Nmm^{-2}. However, a change in film thickness for the 3% open area saw a minimal change in stress distribution. The manufacturers of the PETP film state the maximum working stress of the PETP film as being 260N/mm^2. Therefore, for the PETP to be used as the belt for the press, the minimum thickness will need to be 0.1mm with the holes formed in a hexagonal formation, allowing a 1.7 safety factor before the screen fails.

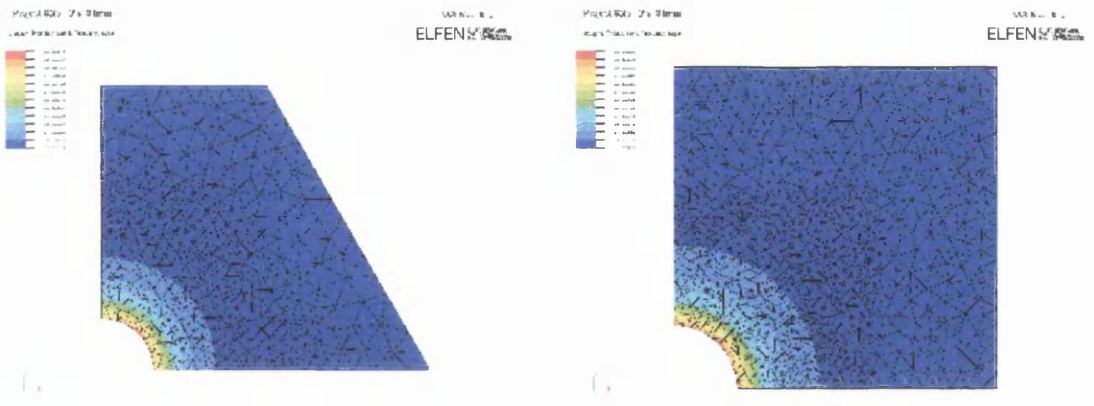

Figure 6.9 Effective Stress Plot of 0.1mm Thick PETP, 3% Open Area (Stress Range 15Nmm^{-2} to 31 Nmm^{-2} for both formations)

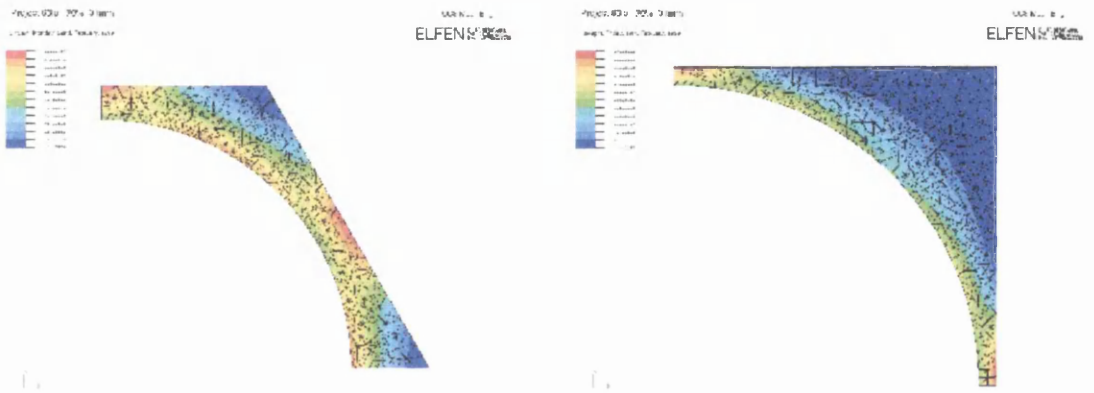

Figure 6.10 Effective Stress Plot of 0.1mm Thick PETP film, 70% Open Area (Stress Range 15Nmm^{-2} to 152 Nmm^{-2}, for hexagonal formation and 15Nmm^{-2} to 360 Nmm^{-2} for square formation)

The Finite Element Analysis of the ablated PETP film has shown that it is able to withstand the stresses induced as a result of the applied tension. However, when the downforce of the squeegee is applied to the screen, localised stresses will be induced in the film around the region of squeegee contact. For this reason, it is necessary to simulate the squeegee downforce to establish the resultant stresses within the PETP film. This was achieved using the same FEA method as used for the hole analysis.

The screen dimensions were set to the same dimensions as those that will be encountered between the two main drive rollers of the belt screen press, notably 508mm by 1000mm. A tension of 15Ncm^{-1} was then applied to the screen. It was

decided that an initial investigation was required modelling a screen that was not ablated. If this proved to be successful, then the ablated screen would be modelled. Applying the correct material properties, the 30mm diameter roller squeegee was then forced onto the screen, deflecting the screen a distance of 5mm, thus, producing a 5mm snap-off gap. The results can be seen in Figure 6.11, showing the maximum stress being almost 210Nmm^{-2}, located at the region of contact at the ends of the roller squeegee. Clearly, these results are greater than that which the PETP can withstand, suggesting failure of the screen.

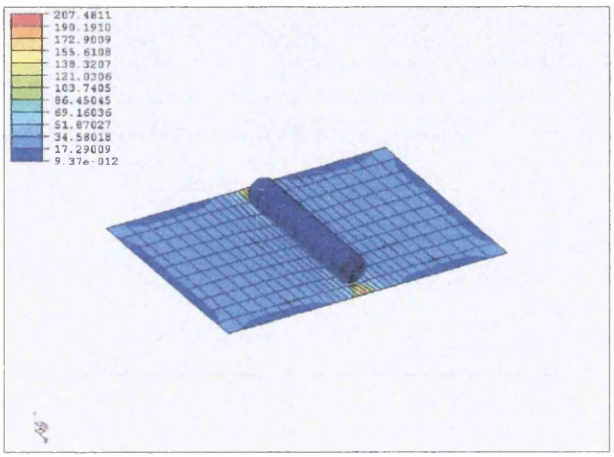

Figure 6.11 Effective Stress Distribution Within PETP Film When Displaced with Roller Squeegee

These results have highlighted that the PETP film cannot withstand the stresses that will be expected within the press design, without increasing the belt thickness which will be detrimental to print quality. However, other options exist, including the use of traditional polyester mesh, which is tensioned with the aid of cross members positioned across the width of the belt. Additionally, the belt can be constructed from thin stainless steel sheeting, which can either be chemically etched or laser ablated.

6.3.1.1 Summary Comments

At this stage in the project, the material used to construct the belt-screen has yet to be finalised. However, this work has highlighted the ability to predict the stresses that will be encountered in such a belt. Therefore, a range of material can be investigated in further studies to ensure an appropriate material is chosen.

6.3.2 Squeegee Design

The design of the high-speed belt screen-printing press has been developed to incorporate a system so that the squeegee can be removed from the press via a cassette mechanism, Figure 6.12. This mechanism allows the squeegee to be easily removed from the press for cleaning purposes and for changing squeegee types.

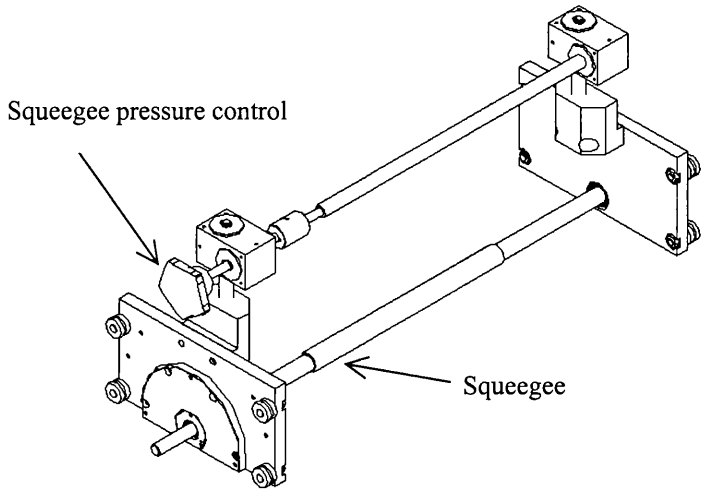

Figure 6.12 Squeegee Cassette Mechanism

The design specification for the press stated that the press would need to accommodate a squeegee of between 25mm and 125mm in diameter. However, the experimental and the numerical models demonstrated the different printing characteristics that will be experienced with different diameters of squeegees. Therefore, using the numerical model that was utilised in the previous chapter, this section covers an investigation into a number of different squeegee diameters and highlights their predicted characteristics for the belt screen press.

When using non-Newtonian inks in Chapter 5, the numerical model experienced difficulties when modelling open areas, as the ink was forced through the open areas of the screen and the squeegee came into contact with the screen. Thus, the governing equations within the numerical model were no longer valid. This was partly due to the ink shear thinning, resulting in the ink film thickness reducing further. To overcome this problem, this section of work focuses upon a Newtonian ink with a dynamic viscosity coefficient of 10Pas. This prevents the ink film from collapsing, enabling a broader range of open areas to be investigated. To study the effect of the

squeegee diameter minimum and the maximum squeegee diameters of 25mm and 125mm were investigated, along with an intermediate diameter of 75mm. The squeegee loading for each squeegee was set to $700Nm^{-1}$. Although the specification states the maximum speed to be $4ms^{-1}$, a medium linear speed of $2ms^{-1}$ was chosen as the effect of the speed was investigated in the previous chapter. The effect of printing open areas of 5%, 30%, 60% and 100% were then investigated. The results of which can be seen in Figure 6.13 to Figure 6.15 for the three squeegee diameters.

As with the non-Newtonian ink, a change in open area using a Newtonian ink has a minimal effect on the pressure distribution, with an increase in open area moving the point of maximum pressure slightly towards the inlet region. However, a change in the squeegee diameter from 25mm to 125mm produces a considerable reduction in pressure, producing an increase in the contact width. As seen in the experimental comparison of the two diameters, this increase in contact width will have a substantial impact upon the ink deposit, thus enabling the different diameters of available squeegees to predetermine the quantity of the ink deposited. Additionally, the increase in squeegee diameter has produced an increase in ink film thickness, which will further increase the ink deposit.

Observing the alteration in the ink film thickness, it can also be stated that as the open area increases, the ink film thickness reduces at a greater rate for an increased squeegee diameter. This is likely to result in a higher tone gain for the larger squeegee diameter as the pumping capacity of the squeegee is increased by a greater amount with an increase in squeegee diameter. This effect was observed within the experimental studies where the 50mm diameter squeegee produced a higher tone gain than the 30mm diameter squeegee for each open area. However, this was not stated within the numerical modelling chapter due to the inability to successfully model a full range of open areas with different squeegee diameters, whilst using non-Newtonian inks.

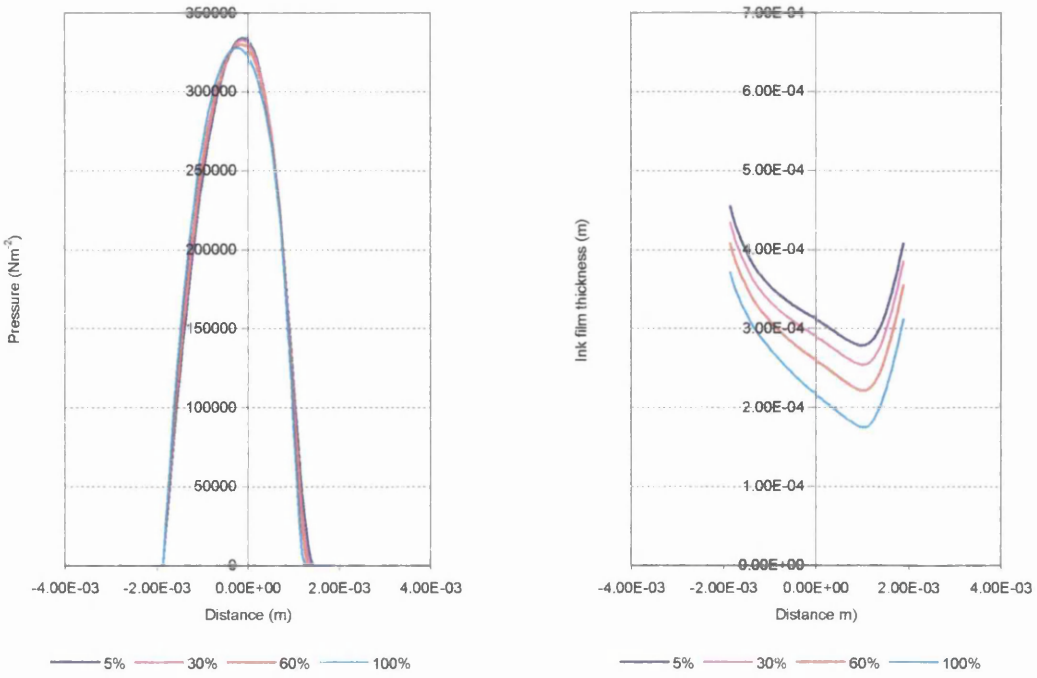

Figure 6.13 Film Pressure and Respective Ink Film Thickness for 25mm Diameter Squeegee

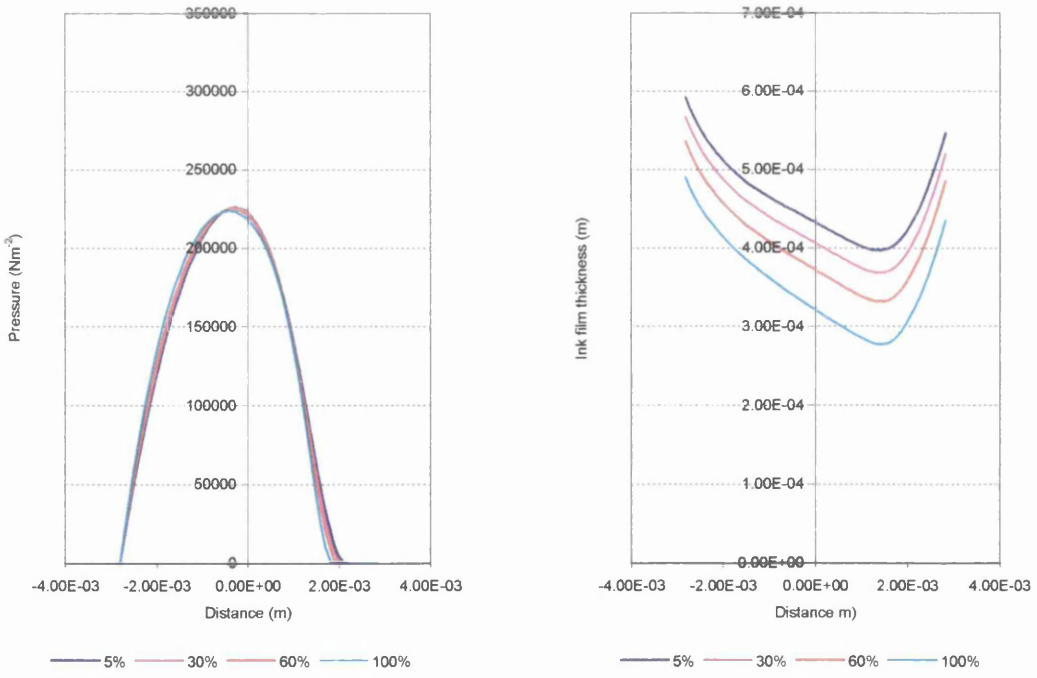

Figure 6.14 Film Pressure and Respective Ink Film Thickness for 75mm Diameter Squeegee

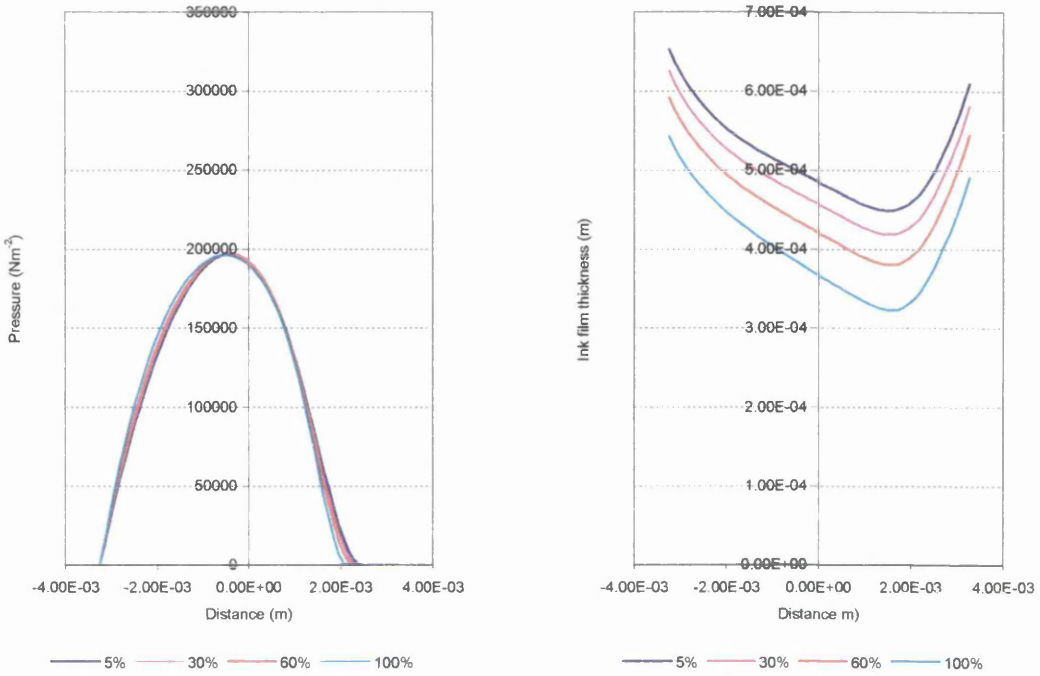

Figure 6.15 Film Pressure and Respective Ink Film Thickness for 125mm Diameter Squeegee

6.3.2.1 Summary Comments

Although the numerical models used Newtonian inks, the ink film thickness and the contact width varied dramatically with an alteration in the squeegee diameter. These results highlight the fact that it is possible to use squeegees from 25mm to 125mm in diameter, depending upon the ink deposit that is required. However, to minimise the tone gain, it is necessary to use a smaller diameter squeegee as the ink film thickness reduces to a lesser extent compared with that observed with the larger squeegees.

6.3.3 Ink Delivery and Removal

As print trials have yet to be carried on the belt press, the exact quantity of ink needed to print at high speed, and the quantity of ink that will remain on the screen after printing, cannot be established. Therefore, the details for the ink delivery and removal system cannot be decided upon until these trials are undertaken. For this reason, the press has been designed to allow for the accommodation of an ink delivery and removal system either side of the squeegee.

Depending upon the ink usage and inking requirement, there are a number of potential solutions available for the ink delivery system. Traditionally, screen-printers have *'guessed'* the amount of ink that is required for the particular print job and this has then been manually placed onto the print screen at regular intervals whilst the print job is in progress. However, the enclosed design of the high-speed belt screen-printing press means that this is no longer acceptable.

The method used to deliver ink in printing processes such as letterpress and lithographic, is with an ink train. In an ink train, ink is stored in an ink duct or a reservoir and the delivery of ink can be metered and transferred with the use of ink keys across the width of the roller. This allows the ink film thickness to be varied across the width of the printing unit, therefore allowing the ink flow to be focused upon the image area. A range of different rollers are then used to reduce the ink film thickness and to minimise print defects before it is transferred to the blanket roller to be printed onto the substrate.

Using a similar arrangement, an ink train can be incorporated onto the roller squeegee mechanism for the ink delivery. The ink train will not need to be as complex as those used in other printing process as the ink is not applied directly to the substrate, but is transferred onto the substrate through a printing screen. Additionally, the more rollers in the ink train, the thinner the ink film becomes, therefore if there are too many rollers then the ink film on the squeegee will be too thin for screen-printing. Figure 6.16 shows two schematics of an ink train that could prove to be suitable for the roller squeegee on the high-speed belt press.

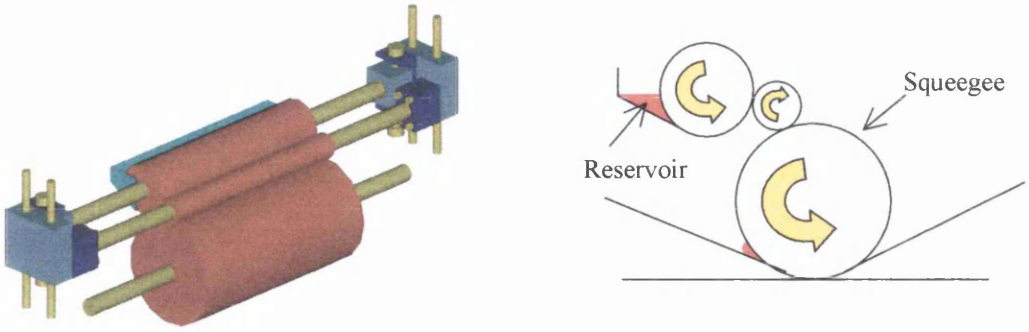

Figure 6.16 Ink Delivery Via Ink Train

The system comprises an ink reservoir formed by a duct roll, along with a single intermediate roller to further distribute the ink before it is applied to the roller squeegee. With the adjustment of the ink keys, the ink flow onto the roller squeegee can be monitored and adjusted as appropriate. The advantages of this system are that ink trains are well developed and have been successfully used for many years and the ink flow can be closely controlled. The disadvantages are that the system may prove to be complex and will need to be easily accessible for cleaning and maintenance purposes.

An alternative solution, where the press operator would not be required to gain access into the machine, would be to deliver the ink onto the press using a pipe system. The pipe will have a series of holes across its length and will be positioned above the belt screen and upstream of the squeegee. Ink is then pumped through the pipe and onto the press, Figure 6.17. The disadvantage to this system is that, due to the internal friction within the pipe, the ink flow will not be uniform across the press width and ink delivery cannot be easily directed to zones across the width of the screen.

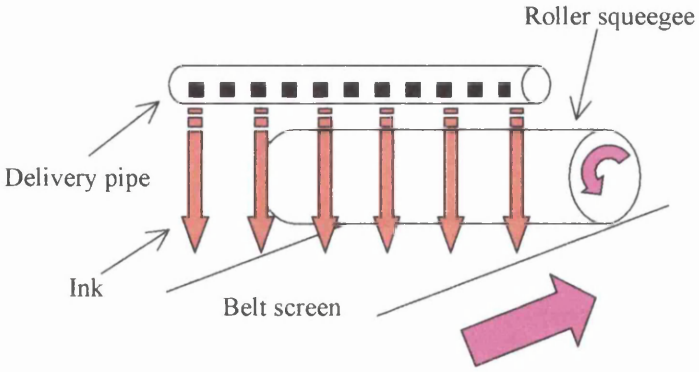

Figure 6.17 Ink Delivery Via Pipe

The ink can also be deposited onto the belt via a bank of ink droppers. Each dropper has the advantage that it can be individually controlled as to direct the ink onto the image areas of the screen.

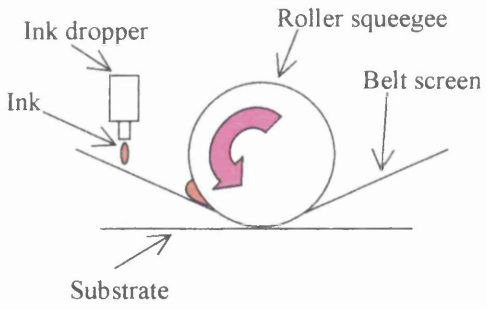

Figure 6.18 Ink Delivery Via Ink Dropper

The previous print trials with the roller squeegee on the flat-bed press have highlighted the fact that the roller squeegee fails to remove all of the ink from the screen immediately after the print stroke. Therefore, there will be a requirement to remove this ink from the screen in order to keep the press free from an excessive build up of ink and to minimise ink wastage.

There are a number of different options available to remove this ink. A simple method would be to use a vacuum to remove the ink from the screen surface. This ink could then be circulated back through the system to be used again. Problems may

arise with this solution depending upon the rheology and the tack of the ink and whether it would adhere to the screen or be successfully vacuumed from the surface.

A more appropriate solution would be to remove the ink by scraping it from the surface with a doctor blade, similar to that of a squeegee blade. However, the pressure generated by this blade will force a quantity of ink through to the underside of the screen. This ink on the underside of the screen will need to be collected by another blade, which will be positioned directly underneath the top blade. The angle of these blades could be set at an offset angle as to force the ink to the edge of the screen where it can be collected and reused.

6.3.3.1 Summary Comments

At present, the required quantity of ink needed to successfully print on the belt press is unknown. Therefore, it is impossible to design an ink delivery and removal system at this time. However, this section has presented a number of solutions that can be further considered and explored once the print trials have commenced and the ink quantities are known.

6.4 Closure

The high-speed belt screen-printing press has now been constructed, although there are several outstanding issues that still need to be resolved. However, this chapter has highlighted these issues and where appropriate, solutions and recommendations have been suggested. The main issue is that of the belt material and construction, as this will govern the success of the press. Although the belt material has yet to be finalised, it has been shown that it is possible to predict the stresses that will be encountered during the printing run. Therefore, appropriate material selection can be made without the cost of experimental trials. This chapter has also highlighted that a broad range of roller squeegees can be utilised, depending upon the required ink coverage. Additionally, the ink delivery and removal designs cannot be finalised until the required quantity of ink is known, although several preliminary designs have been presented.

The next chapter concludes this work, summarising the main findings and where appropriate, recommendations for future work are presented.

Chapter 7

Conclusions and Recommendations

7 Conclusions and Recommendations

7.1 Introduction

Screen-printing offers many advantages over the other printing processes. These advantages include producing the largest colour gamut and the thickest ink film deposit of the other available processes, as well as it being the only process that is used to produce electronic circuits and sensors. However, the main disadvantage to screen-printing is the limited printing speed. This work has focused on the design and development of a high-speed belt screen-printing press that is capable of printing high resolution graphics at a far greater speed. This will enable screen-printing to become more competitive and will also allow a stand-alone screen-printing press to be accommodated within different types of printing processes.

One of the fundamental issues was the inability for a traditional blade squeegee to withstand the increased wear and friction that will be present within such a printing system. For this reason, the use of a rotating roller squeegee was investigated, which will eliminate the problems expected from a blade squeegee. The literature review highlighted the fact that very little is known about roller squeegee screen-printing, as previous trials of printing graphic arts with a roller squeegee has proven to be largely unsuccessful. Additionally, the underlying physics and process mechanics of the ink transfer through the printing screen remains an important area, but has received minimal work, making the process less predictable with a need for a greater understanding.

Following this, the ability to screen-print with a roller squeegee has been studied both numerically and experimentally. This work has greatly increased the understanding of screen-printing, making it a more predictable process. This chapter presents conclusions from this work, with recommendations for further work into this field.

7.2 Conclusions

The main focus of the work was studying the applicability of a roller squeegee in screen-printing. The format of this fell into two categories. These were experimental and numerical studies. Concluding the experimental studies it was discovered that;

- Printing with a roller squeegee proved to be successful and could be achieved with the squeegee rotating at the printing speed or locked, preventing rotation. The printed images were crisp, sharp and were absent from excessive ink coverage. These prints were comparable to those produced with a blade squeegee in terms of visual quality, density and tone gain.
- As the speed is increased, there was a tendency for the ink deposit to reduce.
- Contrary to original thoughts, the initial experimental trials produced higher ink deposits for the locked squeegee than the rotating squeegee. However, this was later attributed to the screen adhering to the substrate when the squeegee was locked. Allowing the squeegee to rotate, effectively 'peeled' the screen from the substrate. This had the effect of increasing the snap-off speed, thus reducing the ink deposit. This was later resolved by increasing the snap-off gap, which effectively increased the mesh tension, preventing it from adhering to the substrate. Once this had been achieved, the locked squeegee produced a lower ink coverage than the rotating squeegee.
- A process parameter investigation was carried out where it was discovered that, using the range of settings that were chosen, the change in pressure level had a minimal effect on tonal reproduction. However, the rotation of the squeegee had the greatest effect on tonal reproduction, which had a strong interaction with the print speed.
- After the printing stroke, the roller squeegee failed to remove all of the ink from the surface of the printing screen. However, this can be advantageous, as this will enable solvent-based inks to be used with higher mesh counts. This is because the remaining ink on the screen surface will prevent the ink from drying in the screen, as can be seen to occur when a blade squeegee is used, which removes all of the ink from the screen.

From the numerical investigations, it can be concluded that;

- The larger the squeegee diameter, the higher the ink film thickness is on the roller squeegee. This will have the effect of increasing the pumping capacity of the squeegee, resulting in an increase in ink supply to the screen. Additionally, the increase in squeegee diameter will also increase the contact width, thus increasing the contact time of the screen upon the substrate, therefore further increasing the ink deposit.
- An increase in speed increases the ink film thickness, which would be expected to increase the ink deposit. However, the increase in speed results in a reduction in the contact time, thus a reduction in ink deposit is observed.
- The locking of the squeegee was seen to increase the shear rate within the ink film. This had the effect of reducing its viscosity. As a result, the ink film thickness and therefore the ink supply to the screen was reduced. This had the effect of reducing the ink deposit, which was previously believed to be due to a reduction in the pressure profile. However, the numerical model highlighted that, when a non-Newtonian fluid is used and the pressure profile is dictated by the squeegee loading, locking the squeegee has a minimal effect on the pressure profile.
- Two different models were used to predict the thickness of the ink deposit upon the substrate. One model assumed that the ink remained in the column in which it was deposited onto the substrate, with the other model assuming that the ink spreads across the substrate. The ink spread model produced results that were in very close agreement with the actual printed images for a number of open areas. This is the first occasion that this has been predicted.

A number of experimental and numerical investigations have been carried out within this work to develop a further understanding of screen-printing with a roller squeegee. When the process parameters were adjusted, the characteristics of the printed samples varied in accordance with previous investigations. However, comparing these to the results obtained from the numerical model highlighted other factors that are dominant in the ink transfer mechanism. This new information has been used to further the understanding of the process where the numerical and the experimental studies are in

strong agreement, gaining a further, better understanding of the screen-printing process.

Additionally, the work carried out for the high-speed belt screen-printing press has identified a gap in the printing machinery market and this has led to the design, manufacture and development of a suitable prototype press to fill this gap. More importantly, it has been proven that it is possible to produce high resolution graphic images using a roller squeegee. Ultimately, this will have advantages within the screen-printing industry as it will all but eliminate squeegee wear and drag, which will also result in less wear on the screen.

7.3 Recommendations

A new model has been developed and tested to further the understanding of the screen-printing process and initial exploration suggests that it is capable of producing reliable and accurate results. Also, a new concept of printing press has been manufactured. However, a further insight into the screen-printing process, with both traditional screen-printing and the high-speed belt screen-printing press, can be obtained with the following recommendations.

- Further investigations into the belt material need to be carried in order to obtain a suitable material for the high-speed belt screen-printing press.
- The ink delivery and removal mechanisms need to be finalised once the required quantity of ink is known.
- Once the press trials have commenced for the high-speed belt screen-printing press, a number of numerical models can be run to predict further characteristics.
- A development of the numerical model to accommodate traditional blade squeegees. This can then be used to calculate the effect of different squeegee properties upon the printed image without the expense of costly print trials.
- The numerical model can be modified so that it can accommodate the collapsing of the ink film underneath the squeegee.
- A full exploration of printing characteristics using the new model and to compare findings with experiments to further validate the model and to gain a further insight to the screen-printing process.

Appendix A

Permeability Experiments

A.1 Permeability Experiments

The rotating action of the roller squeegee will generate a higher pressure within the bow-wave of the ink than a traditional blade squeegee, due to the movement of two surfaces. The preliminary roller squeegee trials suggested that this increase in pressure may be pre-printing in the bow wave, a contributing factor into the observed increase in ink deposit. The aim of this section is to obtain a physical value for the pressure required to force the ink through the printing screen. Additionally, this study will allow the flow characteristic of the ink through a porous system to be calculated. This will then indicate the correct models that can be used to simulate the ink flow through the screen in the numerical model in Chapter 5.

The first experimental work into permeability was carried out by *Darcy* in 1830 [91]. Here, it was shown that the average velocity of water through a bed of sand was directly proportional to the driving pressure and inversely proportional to the thickness of the bed. More recently, this work has been applied to mathematical models for the permeability of printing screens [19] [92]. Although the printing industry has no standards or guidelines for the permeance values of printing screens and ink combinations, there are several methods to establish the air permeance values of paper and board. Two of these methods are the Schopper method [93] and the Bendsten method [94]. The pressure needed to force ink through the screen will be substantially higher than that required to force air through a similar substance. Therefore, new equipment and a new method was explored that could measure the pressure required to force a quantity of ink through the mesh of a printing screen.

The equipment was devised using the principles of the Bendsten gauge. The cell consists of four components, a precision machined, hardened steel piston and cylinder with two open ends of diameter 14mm, and an aluminium front and back plate, Figure A.1. The cylinder and piston were precision machined to obtain an ink seal to prevent ink from escaping through the top of the cylinder when the piston is inserted. The aluminium front and back plate is used to clamp the screen securely over the end of the piston assembly.

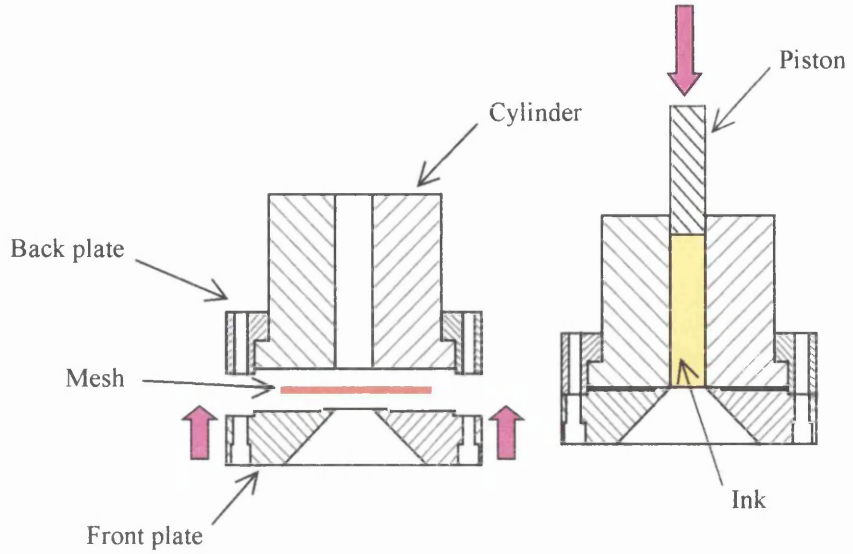

Figure A.1 Permeability Measurement Cell

The cell was then mounted in a Hounsfield Material Tester, Figure A.2, that is capable of accurate stroke speed, up to 500mm/min, and measures the force required to displace the piston in the cell. The cell pressure was then derived from a knowledge of the piston area. In this cell, sealing between the piston and cylinder was assumed to be due to fit proximity; no seals were inserted since they will induce a parasytic force. However, since drag may be induced by any thin ink film that exists between the piston and cylinder, the impact of this was explored during the development of the experimental procedure and this will be discussed later.

Figure A.2 Hounsfield H10K-S Material Testing Machine With Permeability Rig

To explore the experimental technique and to establish a procedure, screen samples of 20%, 50%, 80% and 100% open areas were cut from a gradation within a 150-34 printing screen. A sample of mesh was placed over the bottom end of the cylinder, where the front and back plates were clamped together with four bolts, securing the mesh to the cylinder. The compressibility of air, if contained in the cylinder, will lead to experimental error and for this reason, a syringe was used to introduce ink into the bottom of the cylinder during the filling process. The piston was then positioned into the cylinder a distance of 15mm to ensure alignment. Tests were then carried out with the piston being forced into the cylinder for a further 25mm at a speed of 400mm/min, with the reaction force being measured. This was then repeated at an increased speed of 500mm/min. To eliminate the friction on the cylinder wall, runs took place where a thin layer of ink was smeared onto the surface of the piston, without any ink being present in the cylinder and without mesh in place. This value was then subtracted from the value obtained when ink was present. To eliminate experimental error, each of the experiments was carried out three times and an average obtained.

A.2 Permeability Results

Figure A.3 depicts a characteristic curve, obtained directly from the material tester, displaying a dry run containing a smear of ink on the cylinder surface and a run with the cylinder containing ink, for a 20% open area at a speed of 400mm/min.

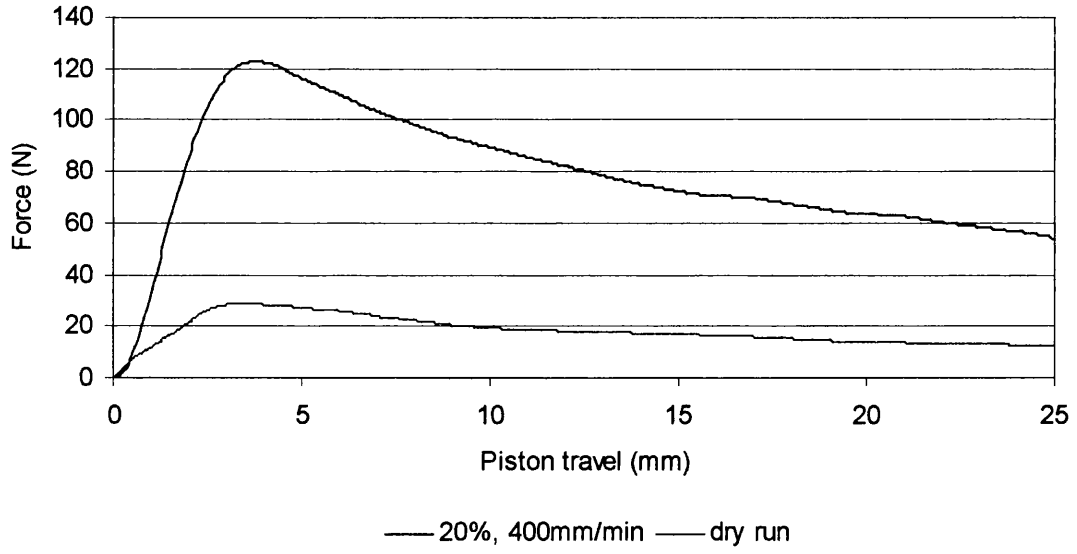

Figure A.3 Solvent-based Ink Permeability Plot

To ensure that stability had been achieved after the initial friction had been overcome, the pressure within the ink was calculated from the average reaction force over the last five millimetres of piston travel into the cylinder.

The experimental results can be seen in Figure A.4, where, due to the higher viscosity of the conventional UV ink, a far greater pressure is required to drive the ink through the mesh than with the solvent-based ink. However, both ink types follow the same trend pattern, with the pressure decreasing as the open area increases, due to the flow resistance decreasing.

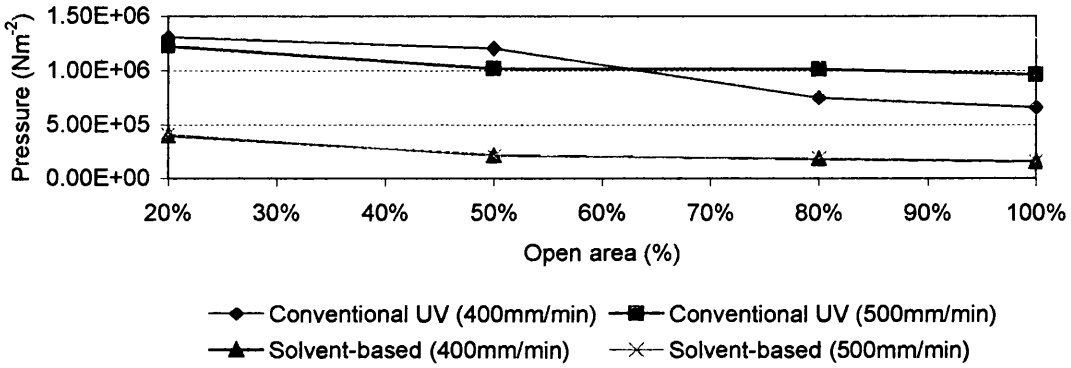

Figure A.4 Pressure Required to Force Ink Through 150-34 Mesh

In order to explore different models to simulate the ink flow through the screen, initially it is appropriate to neglect entrance effects of the ink flow into the screen and to examine the pressure drop. Additionally, the screen can be modelled as a series of cylinders where the flow is laminar. According to simple pipe flow [95];

$$\Delta p = f\left(\mu, u^n, t\right) \qquad \text{Equation A.1}$$

Therefore, the ink velocity through the screen may be derived from mass flow rate conservation, results for which are shown in Figure A.5.

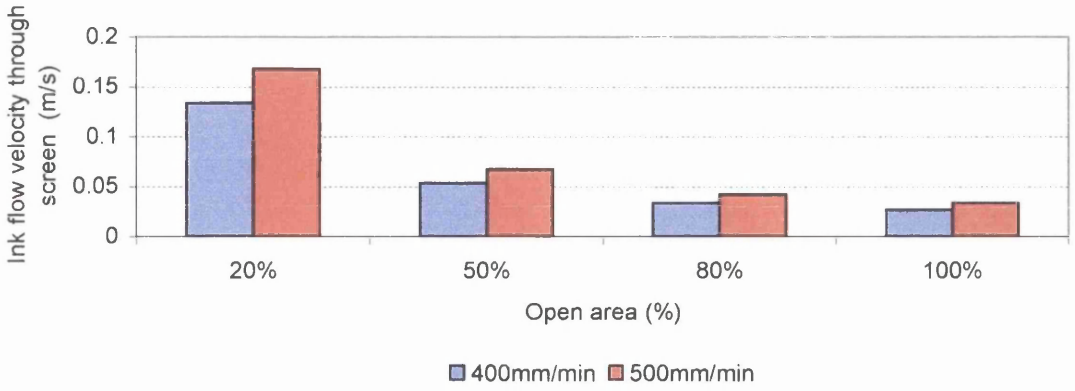

Figure A.5 Ink Velocity Through Screen

An additional reason for the increase in force within the lower open area coverages can be explained by the variation in stencil geometry when printing the different tonal areas. Figure A.6 shows a schematic of a 40% and a 10% open area stencil on a sample of mesh. As can be seen from this figure, as the open area decreases, the ratio of the restricted mesh open area, to that of the free mesh open area increases. Therefore, the increase in restricted mesh open area will limit the flow of ink through the print screen, thus, a greater force will be required.

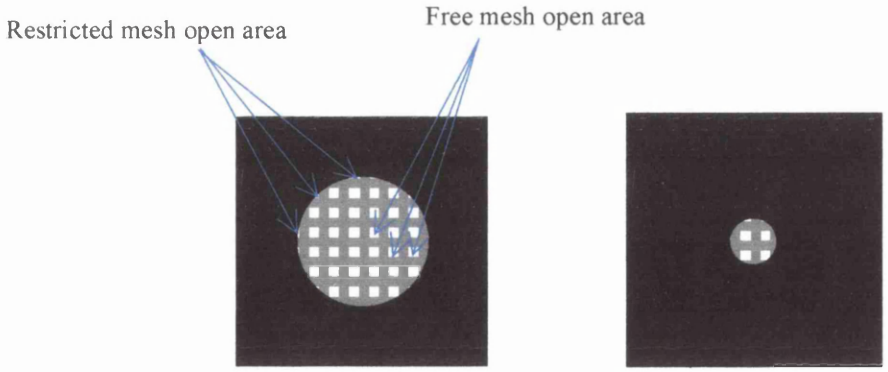

Figure A.6 Schematic of 40% and 10% Mesh Open Area

To further establish the applicability of a suitable model to predict the ink flow through the screen, requires a calculation of mesh Reynolds number to ensure the correct flow regime. Using the ink flow velocity through the mesh open areas, the appropriate Reynolds number can be calculated to establish whether the flow is laminar or turbulent. This will then help to obtain the correct criteria for the development of the numerical model to simulate the ink flow. The Reynolds number

with a value greater than 2000 indicates turbulent flow, and below this value indicates laminar flow. This is calculated by representing the mesh open area as a series of small cylinders, Figure A.7.

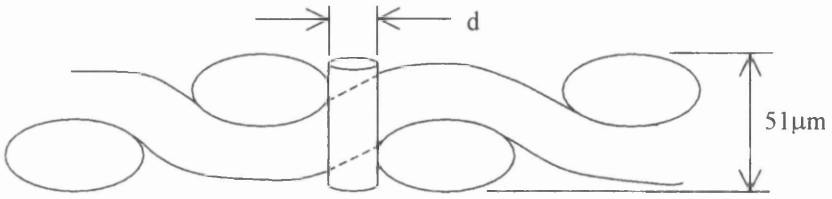

Figure A.7 Schematic of Mesh Cross-sectional Area

Using the equivalent cylinder diameter, the ink properties and the flow velocity through the screen, the Reynolds number can be calculated via Equation A.2, whilst assuming that the ink flow remains free from blockages.

$$Re = \frac{\rho v d}{\mu} \qquad \text{Equation A.2}$$

Figure A.8 shows the appropriate Reynolds number for the solvent-based and the conventional UV ink. This can be seen to be varying considerably throughout the variation in open area, due to the velocity of the ink flow increasing as the open area reduces. Creeping flow mechanisms dominate as the Reynolds numbers are consistently lower than 0.2 [96]. It can also be stated that, due to the Reynolds number being lower than 20, vortices and flow separation are absent downstream of the mesh [97].

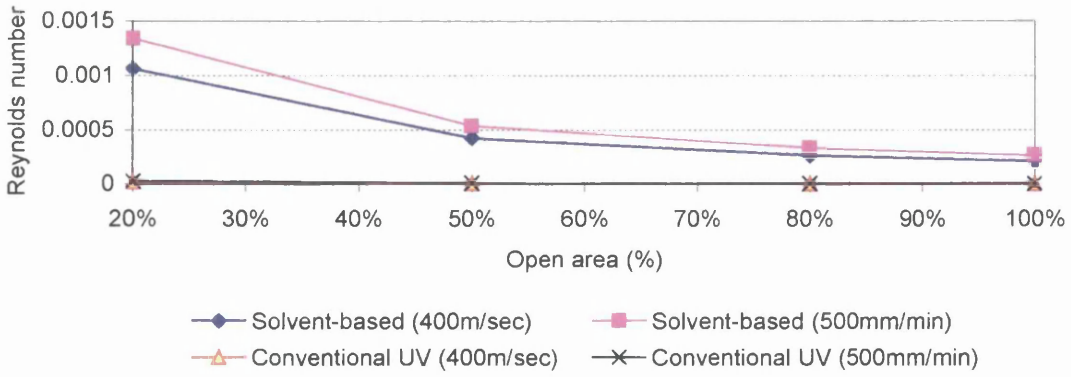

Figure A.8 Reynolds Number For Ink Flow Through Screen

To determine if the flow is developed or developing, the inlet length, or the entry length, of the mesh opening (L_e) needs to be established, with the assumption of the mesh opening being modelled as a capillary tube as previously mentioned. If the inlet length is greater than the length of the mesh hole, then the flow is developing, if it is less than the hole length, then the flow is developed, Figure A.9. For developed flow, the velocity across the opening is constant, with the velocity along the axis increasing in the direction of flow. This occurs until the flow reaches a maximum speed when the boundary layers join. Beyond this point, the velocity profile of the flow will remain consistent.

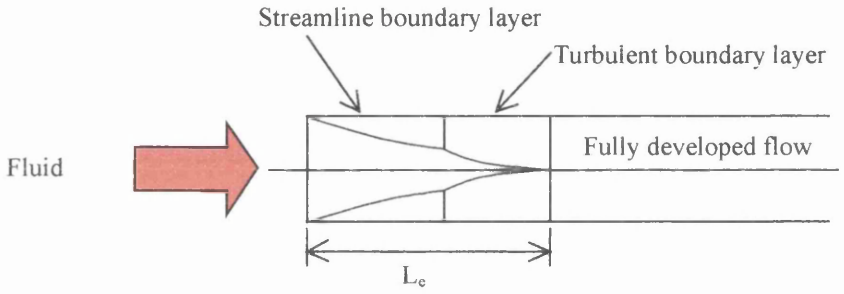

Figure A.9 Conditions at Entry to Pipe [103]

There have been many different predictions for the calculation of the inlet length of a capillary tube. *Philipoff and Gaskins* [98] and *Boger and Ramamurphy* [99] both stated that a shorter inlet length was required for a power-law inelastic liquid, than what was required for a Newtonian liquid. *Han and Charles* [100] predicted that 20 diameters were required for certain polymer melts, whilst *Kowalski* [101] increased this length to 40-60 diameters for polyethylene. An inlet length of 40 diameters was also concluded by *Middleman* [102] for a polyisobutylene solution in tetralin. However, all of these predictions have been based upon the flow from a reservoir into a capillary tube, where the ratio of the reservoir diameter to the capillary diameter can affect the results. In addition, all of these inlet length approximations are dependent upon the specific rheology of the fluid, whilst not taking into account the velocity of the fluid. Additionally, all of the models assume that the ratio of the reservoir diameter to the capillary diameter is much greater than 1. To establish the inlet length of the mesh openings, Equation A.3 [103] will be applied. This approximation was used as it

utilises the Reynolds number of the fluid and is therefore particular to the capillary diameter, fluid velocity and the rheology of the fluid.

$$L_e = 0.0288\,Re\,d \qquad \text{Equation A.3}$$

The inlet length required for fully developed flow to occur within the printing screen ranges from approximately $5x10^{-12}$m to $1.4x10^{-9}$m, depending upon the printing conditions, Figure A.10. The thickness of the printing screen is $5.1x10^{-5}$m, considerably greater than the inlet length, thus, signifying developed flow through the printing screen.

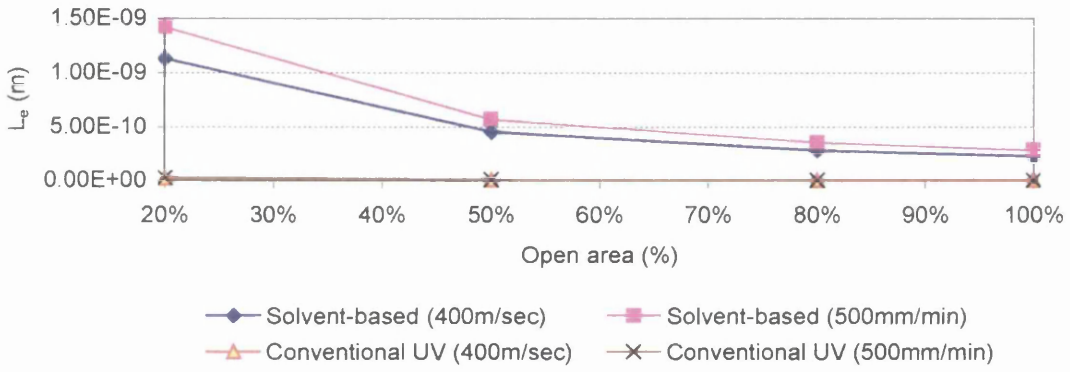

Figure A.10 Inlet length (L_e) of Mesh for Conventional UV and Solvent-based Ink

It can also be noted that it is possible to obtain physical permeability values for the different ink types and screen properties to give a more in depth understanding of the ink flow though the screen. However, the permeability values for the numerical model will be calculated through a numerical procedure as mentioned in Chapter 5, in line with the numerical process.

A.3 Closure

This section has discussed an experimental investigation into the ink transfer through a screen in the screen-printing process. It has been shown that the non-Newtonian ink flow is laminar, fully developed and creeping. Therefore, the numerical model can assume that this type of flow through the screen exists.

Appendix B

Ink Rheology

B.1 Viscosity Measurement

The viscosity of a fluid can be described as the resistance to the movement of one layer of fluid over an adjoining layer of fluid [95], or the measure of fluid internal friction. Fluid viscosity falls into two main categories, these are Newtonian and non-Newtonian. The majority of non-Newtonian fluids can be described as either dilatant (shear thickening) or pseudoplastic (shear thinning), Figure B.1.

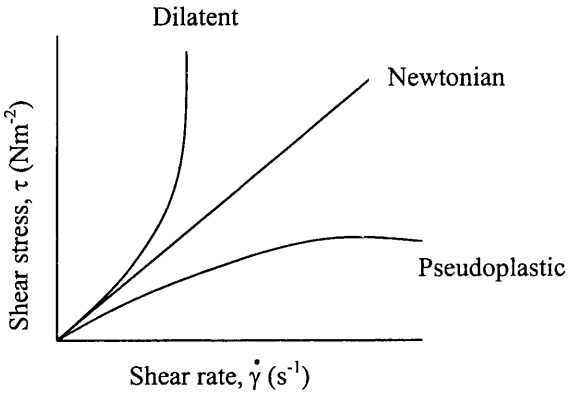

Figure B.1 Fluid Behaviour

The most common type of ink used in the screen-printing process is pseudoplastic, where direct and shear stresses induced at various points in the process causes a reduction in ink viscosity. A fast recovery time for the ink then ensures that there will not be excessive subsequent spreading of the ink on the substrate.

There are a number of techniques for determining ink viscosity, and of these, cone and plate rheometry offers several advantages, notably;

- Cone and plate instruments allow the velocity gradient to be kept constant throughout the sample measurement.
- The technique is particularly useful for the measurement of recovery of structure with time, such as thixotropic inks.
- Rheological properties at high shear rates can be recorded.
- Measurements on high viscosity inks are possible.

- In screen-printing, shear mechanisms exist at most stages of the process. Therefore, using a shear based viscosity measurement system is highly appropriate.

For these reasons, a Contraves CP400 cone and plate rheometer was used to measure the viscosity of the ink. A cone and plate rheometer work by rotating a cone above a fixed plate, with a volume of ink in-between the cone and plate, Figure B.2. The rotating action of the cone causes the ink to shear and the resultant torque on the cone is measured.

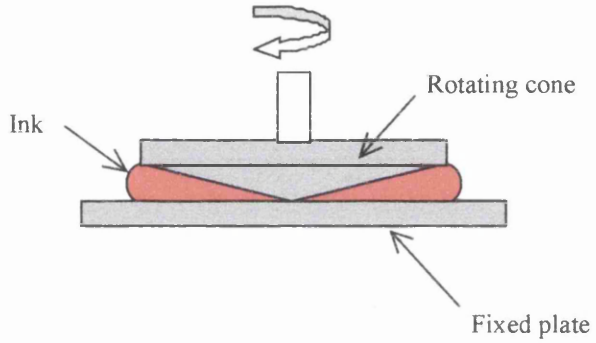

Figure B.2 Schematic of Cone and Plate Rheometer

Using the angular velocity of the cone, the shear rate of the ink at each speed can be calculated using Equation B.1.

$$\dot{\gamma} = \frac{\omega}{\sin\theta} \qquad \text{Equation B.1}$$

Where the resultant torque at each speed setting is used to calculate the shear stress, Equation B.2.

$$\tau = \frac{3T}{2\pi r^3} \qquad \text{Equation B.2}$$

Combining Equation B.1 and B.2, an expression for viscosity can be obtained, Equation B.3.

$$\mu = \frac{\tau}{\dot{\gamma}}$$ Equation B.3

B.2 Results

The individual shear rate plots for the solvent-based *(Mattplast ink containing 20% thinning retarder)* and a conventional UV ink *(UVspeed ink)* can be seen in Figure B.3. Here, the viscosity of the conventional UV ink can be seen to be considerably higher than that of the solvent-based ink, due to the addition of the thinning retarder and the different rheological properties of the ink.

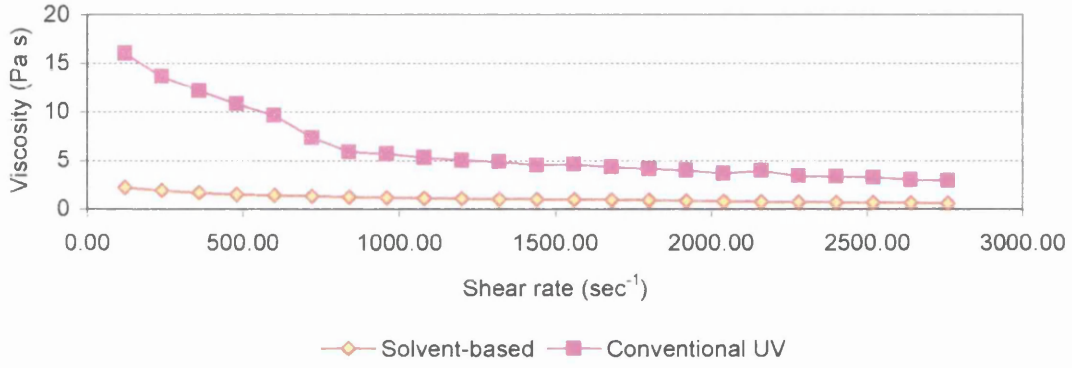

Figure B.3 Viscosity Profile Plots for Mattplast and UVspeed Inks

For the power law to be able to be used in the numerical model to describe the behaviour of the ink, the values of k and n need to be identified. This is achievable by measuring the viscosity of the ink and applying a best-fit approximation from the power law model through the measured viscosity profile. The results of which can be seen in Figure B.4, indicating the power law as a true representation of the viscosity of the fluid when under shear, with the appropriate values of k and n indicated in Table B.1.

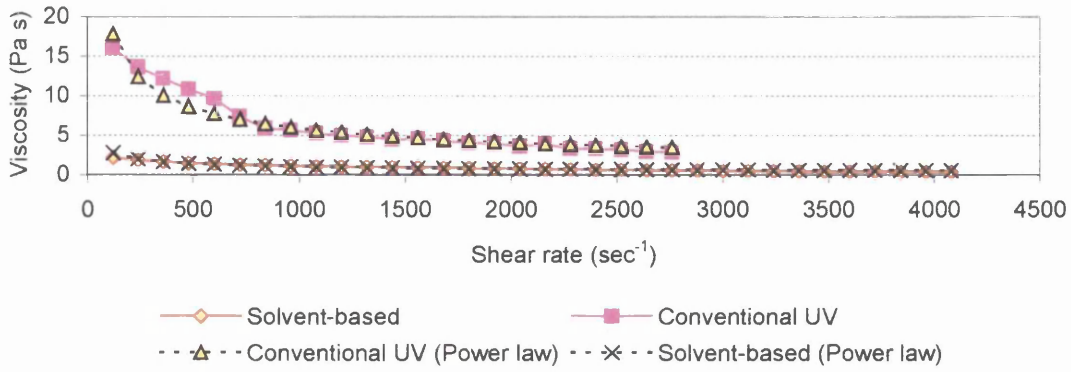

Figure B.4 Viscosity Profile Plots For Solvent-based and Conventional UV Inks With Power Law Approximations

Ink	*n*	*k*
UVspeed	0.482	215
Mattplast	0.618	4.62

Table B.1 Values of *k* and *n* for power law model

B.3 Closure

This section has discussed the relevant merits of measuring rheometry with a cone and plate rheometer. The viscosity of two ink types has been measured. These are a solvent-based and a conventional UV ink, which gave viscosity profiles that could be successfully represented with a power law approximation. This approximation can then be used for the development of a numerical model to simulate the different ink types.

Appendix C

Press Instrumentation

C.1 Press Instrumentation

This section describes the press calibration and instrumentation procedure that was carried out to ensure that the press conditions were closely controlled and monitored. Additionally, this will allow further information regarding the press set-up to be obtained, which is required for the numerical model.

C.2 Squeegee Downforce

The squeegee downforce is pneumatically controlled and is manually adjusted to obtain the correct squeegee pressure. However, due to the friction that exists between the piston and the cylinder within this air system, it cannot be used as an accurate measure of the downforce on the squeegee. For this reason, the vertical downforce on the squeegee was measured using two load cells positioned at either end of the squeegee, Figure C.1. Each cell is constructed as a thin walled ring. The dimensions were chosen to induce a typically 1000με under full load. This was measured by the means of a full bridge to maximise its sensitivity. The signal was monitored with a data acquisition unit connected to a computer allowing the squeegee pressure to be converted into force per unit length for use within the numerical model.

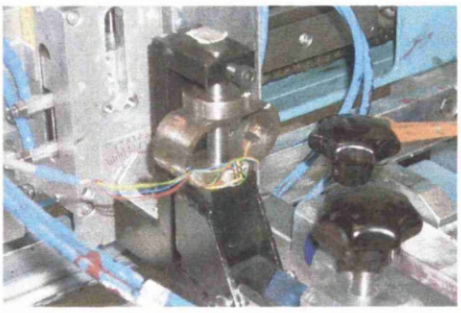

Figure C.1 Load Cell Measuring Squeegee Reaction Force

As the output signal from the load cells is in the form of volts, it is necessary to calibrate the load cells. This was achieved by incrementally applying 1kg masses to the load cells and recording the change in voltage. This was carried out for both load cells to a maximum mass of 4kg. The results of which can be seen in Figure C.2.

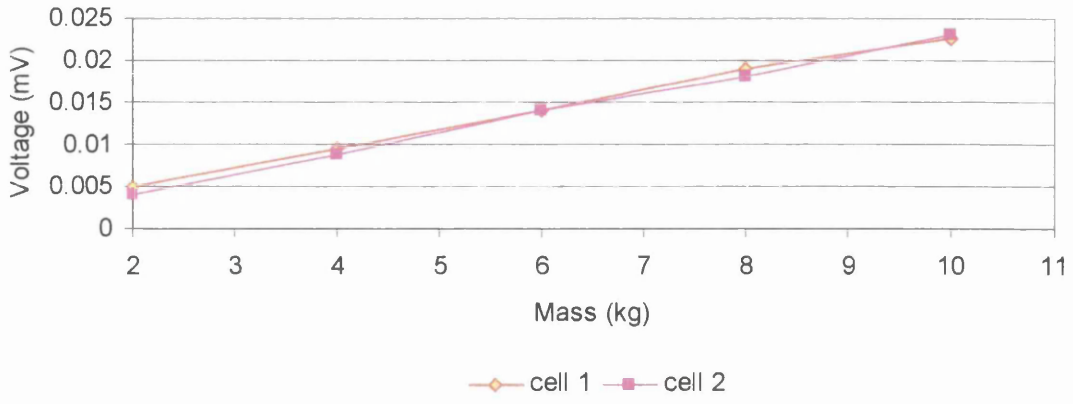

Figure C.2 Load Cell Calibration

The squeegee force was set to 3.5bar and the corresponding change in voltage was recorded for the 30mm and the 50mm diameter squeegees. This was than repeated at a squeegee pressure of 4.5bar. The change in voltage was then interpreted through to the calibrated values and converted into force per unit length, Figure C.3. These values of force per unit length are then input into the numerical model for the squeegee loading, where the contact width is subsequently calculated.

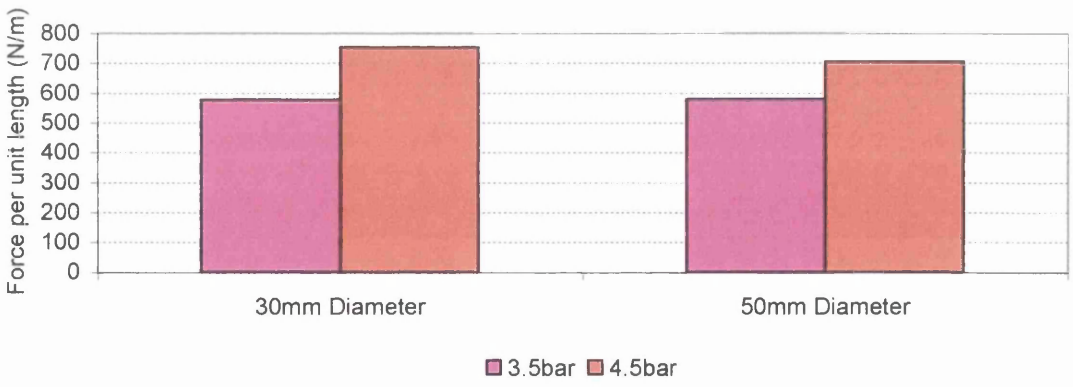

Figure C.3 Roller Squeegee Reaction Force For 30mm and 50mm Diameter RollerSqueegees at 3.5bar and 4.5bar

C.3 Back Pressure

When the squeegee traverses the printing screen, pressure is generated within the ink film. The resultant pressure differential forces the ink through the screen. However, the reactive force of the print bed upon the squeegee tip will be affected by the mesh tension and the resultant pressure differential will therefore influence the ink flow through the screen. For this reason, the pressure on the print bed needs to be measured and compared to the downforce of the squeegee. Subtracting the pressure on the print bed from the squeegee downforce will then give a value of the backpressure and the subsequent affect of the mesh tension..

The force was measured with a Flexiforce ELF Thin Film Transducer. This was calibrated by applying a single known load over the measurement area of the load cell. Once calibrated the load cell is placed in-between the substrate and the print bed, Figure C.4. During trials, the transducer was located in a gap in a paper substrate of identical thickness to the transducer to minimise any local loading effects.

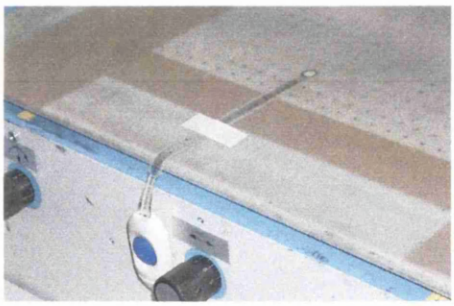

Figure C.4 Thin Film Transducer Used to Measure Backpressure

The transducer used a resistance change principal and when the squeegee passes over this transducer the resistance at the junction is affected. When this signal is subject to conditioning it produces a change in voltage, which is then referenced to the calibration voltage and subsequently data logged. This allows the force exerted on the substrate to be measured. The thin film transducer requires the load to be applied to the whole of the measurement area. However, due to the circular nature of the roller squeegee, a thin metal circular disc was applied onto the top of the transducer to spread the squeegee load across the required area.

The transducers sensitivity was insufficient as to register the load and this resulted in a sharp peak unless the speed was reduced to a very slow creep speed. This produced the results in Figure C.5, for squeegee pressures of 3.5b and 4.5b and the two roller squeegees, when traversing across the 10mm wide transducer.

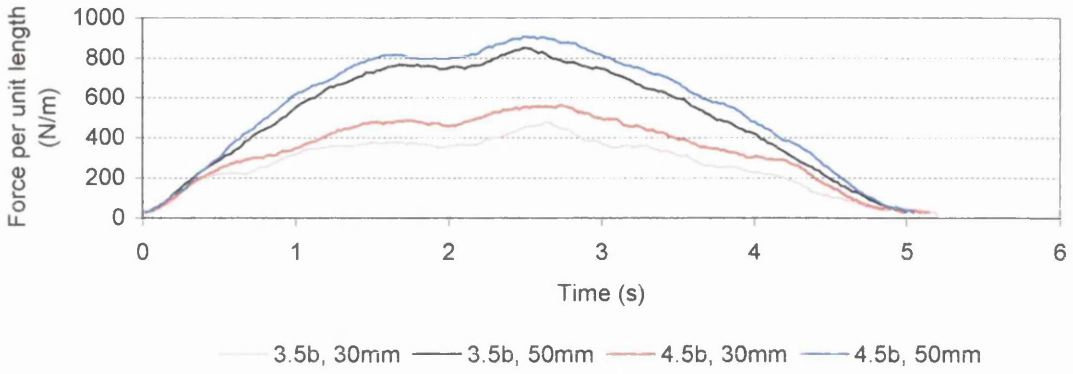

Figure C.5 Print Bed Force for 30mm and 50mm Diameter Roller Squeegees at 3.5bar and 4.5bar

As expected, the results show the force increases as the squeegee pressure increases. As seen from this figure, an increase in squeegee diameter has produced an increase in the reactive force due to the larger contact width. This phenomenon could be because of the local squeegee deformation being dependent upon the specific squeegee geometry. This is verified by the squeegee speed needing to be significantly reduced in order to produce a uniform load due to the circular nature of the squeegee.

C.4 Conclusions

Comparing the squeegee reactive force with the print bed force, it can be seen that within certain scenarios, there is little difference between these values. This suggests that the mesh has no affect on the squeegee pressure and the backpressure is minimal. Therefore, for completeness within the numerical model in Chapter 5, the backpressure can be assumed to negligible for each situation.

Appendix D

Finite Element Analysis

D.1 Finite Element Analysis

Finite element analysis is based on solving partial differential equations and can be performed either with a source code that is written for the specific application, or by using a computer modelling system where only the model geometry is input and then the loading conditions applied. The analysis is carried out over a series of small, simple shapes, called elements that combine to form the region that is to be analysed and are bounded by nodes on their perimeter [90]. The result of this is a series of matrix equations that relate the input at specified points in the element, to the output at these same points. The strains within the region to be analysed are expressed in differential form in terms of displacement, where the stresses are related to this strain. For linear analysis, in three-dimensions, the strain components can be written in vector form as [104];

$$\varepsilon = \left[\varepsilon_x, \varepsilon_y, \varepsilon_z, \gamma_{xy}, \gamma_{yz}, \gamma_{zx}\right]^T \qquad \text{Equation D.1}$$

Where for small displacements the normal strains are given as;

$$\varepsilon_x = \frac{\partial u}{\partial x} \qquad \varepsilon_y = \frac{\partial v}{\partial y} \qquad \varepsilon_z = \frac{\partial w}{\partial z} \qquad \text{Equation D.2}$$

And the shear strain written as;

$$\gamma_{xy} = \frac{\partial u}{\partial y} + \frac{\partial v}{\partial x} \qquad \gamma_{yz} = \frac{\partial v}{\partial z} + \frac{\partial w}{\partial y} \qquad \gamma_{xy} = \frac{\partial u}{\partial z} + \frac{\partial w}{\partial x} \qquad \text{Equation D.3}$$

The relevant stress-strain relationship can be written as;

$$\sigma = D\varepsilon \qquad \text{Equation D.4}$$

Where;

$$\sigma = \left[\sigma_x, \sigma_y, \sigma_z, \tau_{xy}, \tau_{yz}, \tau_{zx}\right]^T \qquad \text{Equation D.5}$$

In which $\sigma_x, \sigma_y, \sigma_z$ are the normal stresses and $\tau_{xy}, \tau_{yz}, \tau_{zx}$ are the shear stresses. For linear elastic situations, the stress-strain matrix is given as;

$$D = \frac{E(1-\upsilon)}{(1+\upsilon)(1-2\upsilon)} \begin{bmatrix} 1 & \frac{\upsilon}{1-\upsilon} & \frac{\upsilon}{1-\upsilon} & 0 & 0 & 0 \\ \frac{\upsilon}{1-\upsilon} & 1 & \frac{\upsilon}{1-\upsilon} & 0 & 0 & 0 \\ \frac{\upsilon}{1-\upsilon} & \frac{\upsilon}{1-\upsilon} & 1 & 0 & 0 & 0 \\ 0 & 0 & 0 & \frac{1-2\upsilon}{2(1-\upsilon)} & 0 & 0 \\ 0 & 0 & 0 & 0 & \frac{1-2\upsilon}{2(1-\upsilon)} & 0 \\ 0 & 0 & 0 & 0 & 0 & \frac{1-2\upsilon}{2(1-\upsilon)} \end{bmatrix}$$

Equation D.6

In which E is the elastic modulus and υ is Poisson's ratio.

Using the principle of virtual work, it is possible to eliminate the stress $\{\sigma\}$ and the strain $\{\varepsilon\}$ vectors. Therefore, the solution is obtained using force and displacement;

$$[K]\{\delta\} = \{f\} \qquad \text{Equation D.7}$$

Where $\{f\}$ is the vector of forces;

$$[K] = \int_{\Omega} [B]^T [D][B] d\Omega \qquad \text{Equation 8}$$

And $[B]$ is the matrix of derivatives and $[D]$ is the stress-strain matrix.

The linear analysis can then be resolved in a single procedure by solving the governing equations for the respective conditions. However, for non-linear analysis, the solution becomes iterative due to contact development in the context of the present work. Therefore, the solution cannot be solved in a single step and needs to be solved

iteratively, converging to a predefined tolerance for each load increment application as the contact interfaces converge within the step.

References;

[1] U.K. Environmental Technology Best Practice Programme, 1998. (ETBPP).

[2] MacPhee J. *"Fundamentals of Lithographic Printing. Volume 1, Mechanics of Printing."* GATF Press. 1998.

[3] Hunt B. *"Rotary Screen's Flexible Face for Labels."* Screen and Digital Printer, pp48-pp50, Nov/Dec 1999.

[4] "Rotary Screen's Flexible Face For Labels." Screen & Digital Printer, November/December 1999.

[5] Hamblyn S. M. *"An Investigation into Ultra-Violet Cured Multi-Coloured Screen-Printing."* M.Sc. Thesis, Mechanical Engineering, University of Wales Swansea, 1999.

[6] *"Handbook for Screenprinters."* SEFAR Mesh and Technology 2/1999.

[7] Claypole T. C., Gethin D. T., Jewell E. H., Anderson J. T. *"Improving the Productivity of High Quality Screen-Printing."* EPSRC Final Report on Grant GR/J 62807.

[8] Gill J. *"Screen Fabric Construction and Stretching Methods."* Screen-Printing. September 1999.

[9] Anderson J. T., Claypole T. C., Gethin D. T. *"The Tensioning Characteristics of a Polymeric Screen-Printing Mesh Material."* Journal of Prepress and Printing Technology, Vol. 4, 1999.

[10] *"Printing Technology Module Notes."* Printing and Coating MSc. Department of Mechanical Engineering, University of Wales Swansea, 1999.

[11] Orr M. *"Stencil Selection."* Screen Graphics, Jan/Feb 1995.

[12] Roy B., Gohrke T. *"How to Make Perfect Film Positives Every Time."* Screen-Printing Magazine, pp190-pp194, October 1991

[13] Vassie S. *"Mesh- So often the Key."* Screen Process, pp32-pp33, February 2002.

[14] Pfirrmann W. *"Selecting and Implementing CTS Technologies."* Screen Printing magazine, June 2000

[15] *"What Every Printer Should Know About Squeegees."* Screen Process, Novenber 1991, pp27-pp29.

[16] Jewell E. H., Claypole T.C., Barden T. *"A Comprehensive Study of the Effect of Squeegee Parameters on Flat Bed Screen Printing."* Welsh Centre for Printing and Coating Technical Report, January 1998.

[17] Hoff S. *"Where the Action is !"* Screen Graphics, Sept/Oct 1995.

[18] Barden T. *"The Effect of Process Parameters on Ink Film Thickness and Fine Line Reproduction in the Flat-Bed Screen-Printing Process."* M.Sc. Thesis, University of Wales Swansea, 2000

[19] Anderson J. T. *"An Investigation into the Physical Aspects of the Screen Printing Process."* Ph.D. Thesis, University of Wales Swansea, 1997.

[20] Bhagawat R. S. *"Rotary Screen Printing Machinery."* Colourage Vol. 34, No. 6, August 1987.

[21] Lau F. K. H., Yeung V. W. S. *"A Hierarchical Evaluation of the Solder Paste Printing Process."* Journal of Materials Processing Technology, 69, pp79-pp89, 1997.

[22] Miles L. W. C. *"Textile Printing."* Bradford Dyers Company Publications Trust, 1981.

[23] Owczarek J. A., Howland F. L. *"A study of the Off-Contact Screen-Printing Process- Part I: Model of the Printing Process and Some Results Derived From Experiments."* IEEE Transactions on Components, Hybrids and Manufacturing Technology. Vol. 13, No. 2, June 1990, pp358-pp367.

[24] Owczarek J. A., Howland F. L. *"A study of the Off-Contact Screen-Printing Process- Part II: Analysis of the Model of the Printing Process."* IEEE Transactions on Components, Hybrids and Manufacturing Technology. Vol. 13, No. 2, June 1990, pp368-pp375.

[25] Nickel J. *"The Way to Measure the Effective Squeegee Attack Angle and its Significance for the Ink Stream."* Screen Process, pp25-pp27, February 1993.

[26] Riemer D. E. *"The Direct Emulsion Screen as a Tool For High Resolution Thick Film Printing."* Electronic Component Conference Proceedings. 1971, pp463-pp467.

[27] Messerschmitt E. *"Rheological Considerations for Screen-Printing Inks."* Screen-Printing. September 1982.

[28] Riemer D. E. *"The Function and Performance of the Stainless Steel Screen During the Screen-Print Mechanism."* International Symposium on Microelectronics Proceedings. 1986, pp826-pp831.

[29] Riemer D. E. *"The Shear and Flow Experience of Ink During Screen Printing."* ISHM Proc., 1987, pp335-pp340.

[30] Riemer D. E. *"Analytical Engineering Model of the Screen-Printing Process: Part 1."* Solid State Technology. August 1988, pp107-pp111.

[31] Riemer D. E. *"Ink Hydrodynamics of Screen Printing."* Proceedings of the International Symposium on Microelectronics. 1985, pp52-pp58.

[32] Huner B. *"A Simplified Analysis of Blade Coating with Applications to the Theory of Screen-Printing."* The International Society for Hybrid Microelectroncs. Vol. 12, No. 2, June 1989.

[33] Glinski G. P., Bailey C., Pericleous K. A. *"A Non-Newtonian Computational Fluid Dynamics Study of the Stencil Printing Process."* Proceedings of the Institute of Mechanical Engineers, Journal of Mechanical Engineering Science, Part C, 2001, Vol. 215, No. C4.

[34] Kevra J. *"Estimation of Shear Rates During 'Rolling' in the Screening and Stencilling Process."* The International Society for Hybrid Microelectronics. Vol. 12, No. 4, December 1989.

[35] Jewell E. H., Claypole T. C. *"The Significance of the Ink Roll in Front of the Squeegee."* Welsh Centre for Printing and Coating, Report No: 04-01-SPTG, 2001.

[36] Huner B. *"A Stokes Flow Analysis of the Screen-Printing Process."* The International Journal of Microcircuits and Electronic Packaging. Vol. 17, No. 1, 1994, pp21-pp26.

[37] Banks W. H., Mills C. C. *"Tacky Adhesion- A Preliminary Study."* Journal of Colloid and Interface Science 8. 1953, pp137-pp147.

[38] Rangchi H., Huner B., Ajmera P. K. *"A Model for Deposition of Thick Films by the Screen-Printing Technique."* Proceedings of the International Symposium on Microelectronics. 1986, pp604-pp609.

[39] Huner B. *"A Second Look at the Printing Screen."* The International Journal for Hybrid Microelectronics. Vol. 12, No. 4, December 1989, pp181-pp187.

[40] Huner B. *"Effects of In-Plane Permeability in Printing Screens."* The International Journal of Hybrid Microelectronics. Vol. 13, No. 2, June 1990, pp35-pp40.

[41] Anderson J. T., Gethin D. T., Claypole T. C., Jewell E. H., Bohan M. F. J., Korochkina T. V. *"Hydrodynamic Interactions in the Screen-Printing Process."* Journal of Prepress and Printing Technology, Vol. 5, 1999.

[42] Dowson D. *"A Generalized Reynolds Equation for Fluid-Film Lubrication."* International Journal for Mechanical Sciences. Vol. 4, pp159-pp170, 1962

[43] Abbott S. J., Gaskell P. H., Kapur N. *"Screen-Printing: A Mathematical Model for Predicting Liquid Transfer."* Submitted to IEEE, June 2000

[44] Carvalho M. S., Scriven L. E. *"Deformable Roll Coating Flows: Steady State and Linear Perturbation Analysis."* J. Fluid Mech. (1997), Vol.339, pp143-pp172.

[45] Huner B. *"An Analysis of a Screen-Printing System Equipped with a Trailing Blade Squeegee."* The International Journal of Microcircuits and Electronic Packaging. Vol. 16, No. 1, 1993, pp31-pp40.

[46] Huner B. *"A Note on the Morgan-Cameron Approximation."* Wear, 140 (1990) pp383-pp385.

[47] Anderson J. T., Claypole T. C., Gethin D. T. *"Squeegee Behaviour Measurement and Modelling for Graphics Printing."* Journal of Prepress and Printing Technology, Vol. 4, 1999.

[48] Cudworth C. J. *"Finite Element Solution of the Elastohydrodynamic Lubrication of a Compliant Surface in Pure Sliding."* 5th Leeds-Leon Symp. On Tribology, Leeds, 1979.

[49] Xue Y-K., Gethin D. T., Lim C. H. *"Numerical Modelling of the Contact Between Lithographic Printing Press Rollers by Soft EHL Theory."* Proceedings of the Institute of Mechanical Engineers, Part J: Journal of Engineering Tribology, Vol. 208, 1994.

[50] Bohan M. F. J., Lim C. H., Korochkina T. V., Claypole T. C., Gethin D. T. *"An Investigation of the Hydrodynamic and Mechanical Behaviour of a Soft Nip Rolling Contact."* Proceedings of the Institute of Mechanical Engineers, Part J: Journal of Engineering Tribology, Vol. 211, 1997.

[51] Eschenbach W., Wagenbauer K. *"Impression Forces and Pressure Distribution in the Cylinder Contact Areas of a Sheet-Fed Offset Press."* Adv. In Printing Sci. Tech. Vol. 1, pp109-pp127, 1961

[52] Ilias S., Govind R. *"A Study on Concentration Polarization in Ultrafiltration."* Separation Science and Technology, 28(1-3), pp361-pp381, 1993.

[53] Ilias S., Schimmel K. A., Assey G. E. J. M. *"Effect of Viscosity on Membrane Fluxes in Cross-Flow Ultrafiltration."* Separation Science and Technology, 30(7-9), pp1669-pp1687.

[54] Bowen W. R., Williams P. M. *"Prediction of the Rate of Cross-Flow Ultra-filtration of Colloids with Concentration-Dependent Diffusion Coefficient and Viscosity- Theory and Experiment."* Chemical Engineering Science. Vol. 56, pp3083-pp3099, 2001.

[55] Hawkyard C. J., Miah A. S. *"The Parameters of Rotary Screen Printing."* Journal of the Society of Dyers and Colourists. Vol. 103, January 1987.

[56] Scott G. E. *"Rotary Screen Printing: A Revolution in Wallcovering Production."* Journal of the Oil and Colour Chemists Association. Vol. 72, No. 9, September 1989.

[57] WYKO Surface Profilers Technical Reference Manual, Vecco Metrology Group.

[58] Jewell E. H., Claypole T. C. *"The Role of Role of Flowcoat in Ink Transfer."* University of Wales Swansea, Screen Printing Technology Group, Report no: 02-01-SPTG.

[59] Fox I. J. *"Characterisation of Prints Using image Analysis Methods."* M.Phil. Thesis, University of Wales Swansea, 1999.

[60] Field G. G. *"Color and its Reproduction."* Second Edition, GATF Press, 1999.

[61] Bohan M. F. J. *"In Process Colour Module Notes."* Printing and Coating M.Sc. Notes, Department of Mechanical Engineering, University of Wales Swansea.

[62] Jewell E. H., Claypole T. C. *"The Effect of Ink Thinning on Solvent Ink Rheology and Tonal Reproduction."* Welsh Centre for Printing and Coating, Report no: 01-01-SPTG, Feb 2001.

[63] Jewell E. H. *"The Screen Printer's Press-side Companion. 1st Edition"* University of Wales Swansea, October 2000.

[64] Appleton W., Claypole T. C., Jewell E. H., "*Preliminary Findings of the Effects of Print Parameters on Dot Reproduction in Screen-Printing.*" WCPC, University of Wales Swansea January, 1995

[65] Anderson J., Appleton W., Claypole T. C., Jewell E. H., "*An Investigation into the Effect of Squeegee Design and Print Speed on Ink Transfer.*" WCPC, University of Wales Swansea March 1996.

[66] Appleton W., Claypole T. C., Jewell E. H., Kirwan A. *"An Investigation into the Effect of Flat Bed Screen-Printing Parameters on Tonal Reproduction.*" WCPC, University of Wales Swansea February 1996

[67] Jewell E. H., Claypole T. C. *"Snap Speed and its Effect on Ink Transfer in Screen-Printing."* 02-02-SPTG, WCPC, University of Wales Swansea, February 2002

[68] Hoff S. *"On The Edge"* Screen Graphics, Sept/Oct 1995.

[69] *"ScreenCalc Ink Mileage Predictor. Version 2:- Instruction Manual"* WCPC, University of Wales Swansea, June 2001.

[70] Phadke M. S. *"Quality Engineering Using Robust Design."* Prentice-Hall International Editions, 1989.

[71] Montgomery D. C. *"Design and Analysis of Experiments, Fourth Edition."* John Wiley & Sons, 1997.

[72] Bohan M. F. J. :- Welsh Centre for Printing and Coating. Private Communication

[73] Jewell E.H., Claypole T. C., Barden T. *"The Effect of Flat-Bed Screen-Printing Parameters on Ink Film Thickness."* 00-01-SPTG, WCPC, University of Wales Swansea.

[74] Xue Y. K., Gethin D. T., Lim C. H. *"Elastohydrodynamic Lubrication Analysis of Layered Line Contact by the Boundary Element Method."* International Journal for Numerical Methods in Engineering, Vol.39, 1996.

[75] Bohan M. F. J., Claypole T. C., Gethin D. T., Basri S. B. *"Application of Boundary Element Modelling to Soft Nips in Rolling Contact."* 49th Annual TAGA Tech. Conf., Quebec City, Canada, May 1997.

[76] Timoshenko S. P., Goodier J. N., *"Theory of Elasticity. Third Edition."* McGraw-Hill Book Company. 1970.

[77] Brebbia C. A., Walker S. *"Boundary Element Techniques in Engineering."* Newnes-Butterworths, 1980.

[78] Dowson D., Higginson G. R. *"A Numerical Solution of the Elastohydrodynamic Problem."* J. Mech. Eng. Sci., 1, 1959, pp6-pp15.

[79] Wu H., *"Squeeze Film Behaviour for Porous Annular Disks."* Trans. ASME, F92 (1970), pp593-pp596.

[80] Brebbia C. A., Dominguez J. *"Boundary Elements: An Introductory Course."* McGraw Hill, 1989.

[81] Banerjee P. K., Butterfield R. *"Boundary Element Method in Engineering Science."* McGraw Hill, 1981.

[82] Davey A, Guthrie J. T., Hall C. "*Flow Properties of Fluid Systems.*" Surface Coatings International, pp329-339, 1997-(7).

[83] Wilkinson W. L. *"Non-Newtonian Fluids:- Fluid Mechanics, Mixing and Heat Transfer."* Pergamon Press Ltd., 1960.

[84] Kubota, T., Scriven, L. E. *"Forward roll coating in the runback feed condition.*" Proc. IS& T Coating Conf., Boston, USA, p.309, 1993

[85] Landau L., Levich B. *"Dragging of a Liquid by a Moving Plate."* Acta Physicochim USSR, 17, 42, 1942

[86] Bohan M. F. J., Fox I. J., Claypole T. C., Gethin D. T. *"Numerical Modelling of Elastohydrodynamic Lubrication in Soft Contacts Using Non-Newtonian Fluids."* International Journal of Numerical Methods for Heat and Fluid Flow, Vol. 12, No. 4, pp494-pp511, 2002

[87] MacPhee J., Shieh J., Hamrock B. J., *"The Application of Elastohydrodynamic Lubrication Theory to the Prediction of Conditions Existing in Lithographic Printing Press Roller Nips."* Advances in Printing Science and Technology 21. Pp242-pp276, 1992

[88] Lim C. H., Bohan M. F. J., Claypole T. C., Gethin D. T., Roylance B. J., *"A Finite Element Investigation into a Soft Rolling Contact Supplied by a Non-Newtonian Ink."* J. Phys. D: Appl. Phys, Vol.29, pp1894-pp1903. 1996

[89] EPSRC Grant GR/K80785, Disposable and Electronic Screens for Screen-Printing

[90] Smith I. M., Griffiths D. V., *"Programming the Finite Element Method."* John Wiley & Sons, Third Edition, 1998.

[91] Coulson J. M., Richardson J. F., Backhurst J. R., Harker J. H. " *Chemical Engineering, Volume 2, Fourth Edition.*" Pergamon Press, 1991.

[92] Huner B. "*Effects on In-Plane Permeability in Printing Srcreens.*" The International Society for Hybrid Microelectronics. Volume 13, Number 2, June 1990.

[93] ISO 5636/2 *"Paper and Board: Determination of Air Permeance (medium range)- Part 2: Schopper Method."*

[94] ISO 5636/3 *"Paper and Board: Determination of Air Permeance (medium range)- Part 2: Bendsten Method."*

[95] Massey B. S. *"Mechanics of Fluids. Sixth Edition."* Chapman and Hall, 1992.

[96] *"Dictionary of Science and Technology."* Larouse 1995

[97] Coulson J. M., Richardson J. F., Backhurst J. R., Harker J. H. " *Chemical Engineering, Volume 2, Fourth Edition.*" Pergamon Press, 1991.

[98] Philipoff W., Gaskins F. H. *"Trans. Soc. Rheol."* 2, 263 1958

[99] Boger D. V., Ramamurphy A. V. *"A.I.Ch.E.J."* 16, 1089, 1970

[100] Han C. D., Charles M. *"A.I.Ch.E.J."* 16, 499, 1970

[101] Kowalski R. C. *"Proc. 4th Int. Cong. on Rheol. (Interscience)"* Part 3, 481, 1965.

[102] Middleman S. *"The Flow of High Polymers. (Interscience)"* 46, 1968

[103] Coulson J. M., Richardson J. F., Backhurst J. R., Harker J. H. " *Chemical Engineering, Volume 1, Fourth Edition.*" Pergamon Press, 1991.

[104] Hinton E., Owen D. R. J. *"An Introduction to Finite Element Computations."* Pineridge Press Limited, Swansea, U.K. 1985.